Tuning the Transport Properties of Layer-by-Layer Thin Films for Fuel Cell Applications

by

James Nathan Ashcraft

B.S. Chemical Engineering
University of Missouri (2004)

SUBMITTED TO THE DEPARTMENT OF CHEMICAL ENGINEERING IN PARTIAL FULFILLMENT OF THE REQUIREMENTS FOR THE DEGREE OF

DOCTOR OF PHILOSOPHY IN CHEMICAL ENGINEERING
AT THE
MASSACHUSETTS INSTITUTE OF TECHNOLOGY

AUGUST 2009

Signature of Author……...
James Nathan Ashcraft
Department of Chemical Engineering
August 31, 2009

Certified By……...
Paula T. Hammond
Professor of Chemical Engineering
Thesis Supervisor

Accepted By……..
William M. Deen
Professor of Chemical Engineering
Chairman, Committee for Graduate Students

Tuning the Transport Properties of Layer-by-Layer Thin Films for Fuel Cell Applications

by

James Nathan Ashcraft

Submitted to the Department of Chemical Engineering
On August 31, 2009, in partial fulfillment of the requirements for the degree of
Doctor of Philosophy in Chemical Engineering
at the Massachusetts Institute of Technology

Abstract

The increasing global focus on alternative energy sources has led to a renewed interest in fuel cells. For low power, portable applications, direct methanol fuel cells (DMFCs) are the most promising type of fuel cell. DMFCs can operate at ambient conditions and only require dilute methanol solutions and air to be input to the devices. At the core of these devices is a proton exchange membrane (PEM) that allows rapid proton transport through the polymer matrix while preventing fuel from permeating across. Additionally, PEMs must have long-term stability in the fuel cell environment, the ability to operate over a wide range of conditions (temperature and humidity), and be cost effective.

A promising, robust method for fabricating polymer films with tunable properties is layer-by-layer (LbL) assembly. This technique consists of building a polymer film by sequential dipping into polymer solutions with complementary interactions, such as opposite electrostatic charges. The LbL method allows the formation of thin films that have perm-selective properties and high ionic conductivity values. This work describes the optimization of multilayer systems for use as the PEM in DMFCs.

First, LbL assembled films of poly[bis(methoxyethoxyethoxy)-phosphazene] (MEEP) and poly (acrylic acid) (PAA) are demonstrated by utilizing the hydrogen bonding between these two polymers. These films show controlled thickness growth, high ionic conductivity, and excellent hydrolytic stability. The ionic conductivity of these films is optimized by tuning the assembly pH of initial polymer solutions and thereby controlling the hydrogen bonding characteristics. Despite similar film composition, MEEP/PAA LbL films assembled at higher pH values have enhanced water uptake and transport properties, which play a key role in increasing ion transport within the films. At fully humidified conditions, the ionic conductivity of MEEP/PAA is over one order of magnitude higher than previously studied hydrogen bonded LbL systems.

The next LbL systems studied consist of a highly sulfonated aromatic polyether (sPPO) paired with amine containing polycations. The best performing sPPO system has ionic conductivity values which are the same order of magnitude as commercially relevant PEMs and has the highest ionic conductivity ever obtained from a LbL assembled film. Additionally, these LbL systems have methanol permeability values over two orders of magnitude lower than traditional PEMs. Incorporating the sPPO systems into DMFCs results in a 53% improvement in power output as compared with DMFCs using traditional PEMs. In-depth structure property studies are performed to understand the nature of the high ionic conductivity of the sPPO LbL systems with respect to film growth, composition, water uptake, and ionic crosslink density.

Lastly, the mechanical properties of highly conducting LbL films are improved by forming the LbL matrix on highly tunable electrospun fiber mat (EFM) supports. Free-standing LbL films have moderate mechanical properties when dry, but are mechanically deficient when hydrated. Coating an EFM with the LbL dipping process produces composite membranes with interesting "bridged" morphologies, while still maintaining high ionic conductivity values. The spray LbL assembly is studied as a means for the rapid formation of LbL films on EFMs. At optimized conditions, the LbL materials conformally coat the individual fibers throughout the bulk of the EFM and have uniform surface coatings. The mechanical properties of the spray coated EMFs are shown to be superior to the pristine LbL systems.

Thesis Supervisor: Paula T. Hammond
Title: Bayer Chair Professor of Chemical Engineering and Executive Officer

Dedicated to my loving family:

Brea, Jim, Cathy, & Emily

Acknowledgements

I hope this section provides a glimpse of how thankful and fortunate I am to be where I am today.

I must first thank my advisor, Prof. Paula Hammond, for the opportunity to be a part of her group and investigate this research project. Paula brought a skillful balance of guidance and direction to my research, while still allowing me to explore my own interests and curiosities. In addition to her scientific expertise, she is probably one of the most energetic, compassionate, and sincere professors at MIT. I also thank my thesis committee members, Prof. Klavs Jensen, Prof. Yang Shao-Horn, and Prof. Jeff Tester, for their guidance over the last four years. It has been an honor to learn from this exceptional group of leaders in their respective research areas.

As for colleagues in the Hammond group, I must first and foremost thank Avni Argun for his help, guidance, teaching, and encouragement. More than anyone, I learned what it takes to be a successful researcher on a daily basis from Avni. I thank Jodie Lutkenhaus for welcoming me into the group and teaching me electrochemistry. I thank Shujun Chen and Jung Ah Lee for their help obtaining quality SEM and TEM images. I also thank my quality, dedicated colleagues in the Hammond group that I've had the pleasure of working with and alongside including: Kevin Krogman, Kris Wood, Nicole Zacharia, Ryan Waletzko, Kris Stokes, Seung Woo Lee, Kris Van Hege, Tarek Farhat, Andy Miller, Dan Schmidt, Dan Bonner, Josh Moskowitz, Helen Chuang, Byeong Su Kim, Fevzi Cebeci, Eric Verploegen, Juhyun Park, and Pil Yoo. I also thank the following incredible UROPs and undergraduates that I've been fortunate to work with and learn from: Alex Hsu, Chris Boyce, Ismael Gomez, Kris Jensen, Manuel Esquivel, Jeff Zhou, Marie Herring, and Nalan Korkmaz.

Outside of the Hammond group, I've been fortunate to collaborate with many researchers at MIT and beyond. I thank the late Allan Smith (Masscal Scientific Instruments) for all of his help understanding the QCM technique and his inspiration as a scientist and entrepreneur. I thank the members of the Shao-Horn group, especially Jungik Kim, for their willingness to help with electrochemistry and fuel cell issues. I would also like to thank Shuo Chen for help obtaining SEM images. I am particularly thankful for the help that Meredith Silberstein contributed to understanding the mechanical properties of materials discussed in this thesis. Several members of the Rutledge group including Joe Lowery, Minglin Ma, Liang Chen, and Chia-Ling Pai deserve thanks for their help teaching me the electrospinning process and allowing me to use their homemade equipment. I also thank Prof. Harry Allcock and David Kim Yong Lee of Penn State University for the collaboration on polyphosphazenes, which comprises Chapter 2 of this work. I thank Ilke Kalcioglu for her assistance with indentation measurements of the polyphosphazene materials. I also thank Raj Rajendran and his colleagues at DuPont who were willing to share their expertise on making accurate conductivity and fuel cell measurements.

I am very thankful for the quality people through the Department of Chemical Engineering – professors, lecturers, staff, graduate students, and undergraduate students – that make Building 66 (and beyond), such a wonderful, unique community. I also thank the kind people at the Institute for Soldier Nanotechnologies for use of facilities throughout my time at MIT.

Finally, and maybe most importantly, I owe thanks to several people outside of lab that have helped me get to this point. I thank my parents, Jim and Cathy, for all of their love and support and for providing me with every opportunity to be a success. I am also deeply thankful for the love and encouragement from my sister, Emily, and grandmother, EA. A special thanks goes to my beautiful wife, Brea, who made the last three years of graduate school more enjoyable on every level; thank you for your love, support, and patience during this awesome season of life. I thank my "family" at Hope Fellowship Church for support and encouragement over the last three years. Lastly, let me quote a wise man who once said, "Give thanks to the LORD, for he is good; his love endures forever."

Table of Contents

List of Figures

List of Tables

1. Introduction

Portions of this chapter are reproduced from Allan L. Smith, J. Nathan Ashcraft, Paula T. Hammond, *Thermochimica Acta*, 2006, vol. 450, pg. 118-125, with permission of Elsevier Limited.

1.1 Introductory Remarks

Fuel cells have received considerable interest in the past few decades as the demand for energy production that is efficient, environmentally-friendly, and generated from renewable resources increases. Although fuel cells can be used for a wide range of power requirements, the development of low-power, low-temperature, small, portable fuel cells is extremely important. Applications for these fuel cells include military use for portable soldier power, commercial products such as laptops and cell phones, and new power applications in textiles, plastic, and other non-traditional thin shapes. The two most promising types of fuel cells for portable use are standard proton exchange membrane fuel cells (PEMFCs), where the fuels are hydrogen and oxygen gases, and direct methanol fuel cells (DMFCs), where the fuels are liquid methanol and gaseous oxygen. At the core of both PEMFCs and DMFCs is a proton exchange membrane (PEM) that serves as a barrier to fuel and oxidant crossover or exchange, allows protons to easily permeate through, and prevents electrons from passing from the anode to the cathode. The current state-of-the-art PEMs are DuPont's Nafion family of perfluorosulfonic acid membranes, which have existed for over 40 years. However, Nafion membranes have two serious drawbacks that have prevented their widespread use: (i) high cost, both to produce and to process, and (ii) high methanol permeability for DMFC applications.

This thesis work focuses on using the recently developed materials chemistry tool of multilayer assembly to design and tune the transport properties of PEMs for use in portable PEMFCs and DMFCs, focusing on DMFCs operating at ambient and near-ambient conditions. Multilayer or layer-by-layer (LbL) assembly involves the formation of thin films through the alternating adsorption of positively and negatively charged polymer species from aqueous solutions at ambient conditions. Films can also be built up from polymers containing hydrogen-bonding pairs, which may be important for use in PEMs. The LbL assembly technique is robust, allowing the incorporation of a wide range of polyelectrolytes and polymer electrolytes, macromolecules, and nanoparticles; film thicknesses are easily tuned by the number of layers deposited and the pH or ionic strength (salt concentration) of the solutions used. Additionally, the LbL technique can conformally coat any geometry with pin-hole free, mechanically stable polymer films.

There are several advantages for using LbL assembly in the construction of PEMs for fuel cells. LbL assembly offers the ability to use inexpensive, commercially available polymers and simple, aqueous processing conditions. A second advantage multilayer films have over traditional PEMs is that extremely thin LbL films can effectively reduce the flow of specific gases, while maintaining a high flux for others.[1-3] Therefore, a thin film that can achieve power densities comparable to that of Nafion membranes, but at one or two orders of magnitude thinner, can result in fuel cells with higher volumetric power densities. Also, thinner films can have lower resistances than typical thicker PEMs. Thin, conformal films also give the ability to investigate less traditional fuel cell geometries. Also, the ability to form LbL films on functional or reinforcing substrates allows for the fabrication of composite materials with enhanced properties. Finally, the

most important advantage to LbL PEMs is the ability to create nanoscale, and often homogeneous, complex blends of polymers previously not achieved with conventional techniques. All of these advantages provide a rich and compelling range of new materials systems created one layer at a time that can be tuned for the desired properties of a fuel cell PEM.

1.2 Fuel Cells

Sir William Grove designed and built the first fuel cell in 1839, based on reversing the direction of the electrolysis reaction of water. He proved that hydrogen and oxygen could be combined to produce electrical current; however, fuel cells did not receive significant attention due to the advent of cheap fossil fuels and steam power. It was not until the 1960's, when NASA decided to use fuel cells to power systems on the first spacecraft, that fuel cells have developed commercial and research interest. While NASA's decision to implement fuel cells was based mainly on the relative small size and weight of fuel cells compared to batteries and low toxicity as compared to nuclear power, fuel cells are receiving widespread interest today because of the ability to efficiently produce safe, reliable and environmentally friendly power from renewable resources.

Although there are six main types of fuel cells, PEMFCs and DMFCs are the best candidates for providing portable power at ambient conditions based on power production and operating conditions.[1] A schematic of a typical hydrogen PEMFC is shown in Figure 1-1. The membrane electrode assembly (MEA) is the core of the fuel cell and consists of the PEM sandwiched between the anode and the cathode. Hydrogen is supplied to the anode where it is catalytically oxidized; protons are transported through

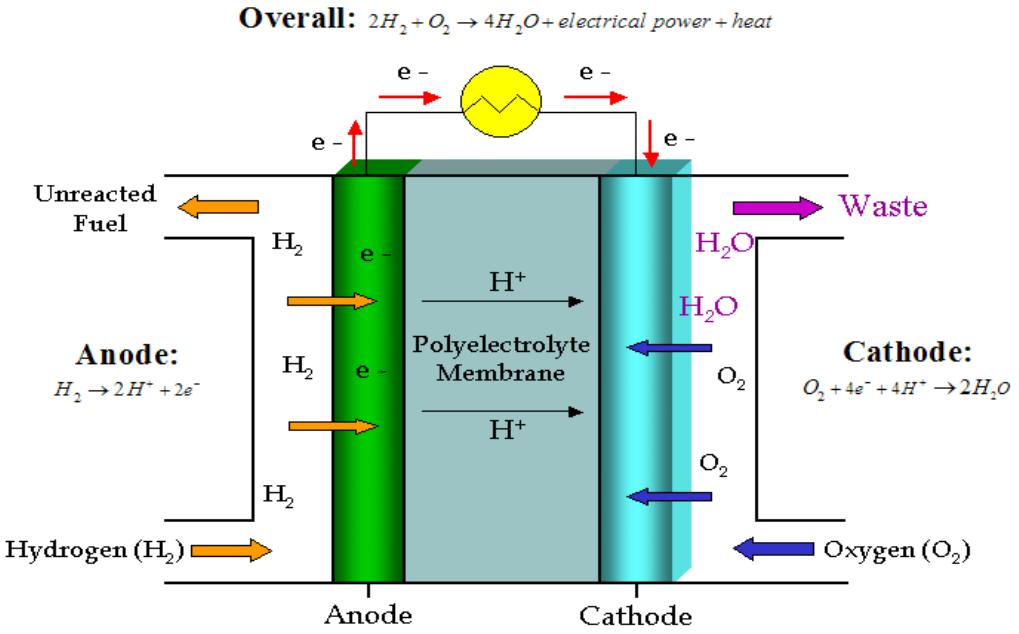

Figure 1-1. Schematic of an operating PEMFC with hydrogen as the fuel (adapted from Abruña).[2] The MEA is composed of the PEM, anode, and cathode. Hydrogen is oxidized at the anode, protons are transported through the PEM to the cathode, electrons travel through the external circuit, and oxygen is reduced at the cathode generating water.

the PEM to the cathode, and electrons travel through the external circuit. Due to the relative low operating temperature of PEMFCs, noble metal catalysts, such as platinum, are required at the anode and cathode. Oxygen, which is supplied to the cathode, is reduced to yield the only by-product of the fuel cell, water. Operation of DMFCs are very similar to hydrogen PEMFCs, except liquid or gaseous methanol is supplied as the fuel to the anode instead of hydrogen gas, and the by-products of the fuel cell reactions contain carbon dioxide in addition to water. DMFCs may be a more attractive option for portable applications due to their higher power densities. Recently, the idea of a

"passive" DMFC has been proposed.[3] As shown schematically in Figure 1-2, the "passive" or "air-breathing" DMFC eliminates so-called parasitic power losses, including pumps and fans, by simply letting methanol and air diffuse to the anode and cathode, respectively.[4]

The maximum work that can be obtained from a fuel cell is given by the following expression:

$$\Delta G_{\max} = -n \cdot F \cdot E^0 \qquad \text{Equation 1-1}$$

where $\Delta G_{\max}$ is the change in molar free energy, which corresponds to work, n is the number of electrons that balance the half-cell reactions, F is Faraday's constant, and E^0 is the reversible cell voltage, which is determined by the half reactions at the anode and cathode. A thermodynamic efficiency of the fuel cell reaction is then given by:

$$\xi_{th} = \frac{\Delta G}{\Delta H} \qquad \text{Equation 1-2}$$

where ΔH is the enthalpy of reaction. Fuel cells often have high thermodynamic efficiencies especially at low temperatures; although, these high efficiencies are never met owing to internal resistance losses, interfacial losses between the PEM and electrodes, overpotentials, mass transport limitations and fuel crossover.[5] In fact, even at zero current density, the reversible potential is not achieved because of competing anodic reactions.[6]

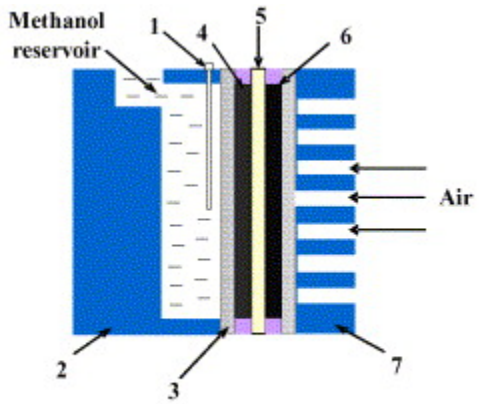

1. Thermocouple 2. Anode plate 3. Current collector 4. Anode 5. Membrane
6. Cathode 7. Cathode plate

Figure 1-2. A schematic representation of a passive or air-breathing DMFC (reproduced with permission from Journal of Power Sources, Elsevier Limited).[4] Methanol and air diffuse to the MEA, rather than being pumped, compressed, or circulated, which can reduce parasitic power losses.

An immense amount of research is currently ongoing worldwide related to PEMFC and DMFC technologies including, but not limited to the following: hydrogen production and distribution, development of new polymers for PEMs, development of new platinum alloy catalysts, catalyst poisoning, water management in the fuel cell, and fuel crossover. [1, 7] Since this thesis work will focus solely on the PEM, the remaining fuel cell review will focus on the PEM. The ideal PEM has all of the following properties:

- Completely prevents unreacted fuel from absorbing and diffusing to the opposite electrode, a phenomenon known as fuel crossover
- A very high ionic conductivity for protons and a very low electronic conductivity for electrons
- Long-term stability in the fuel cell environment (temperature, humidity, mechanical stress, electrical load)

- Ability to operate at ambient conditions, especially for portable applications
- Low material and processing costs

The current "gold standard" of PEMs is DuPont's perfluorinated polymer, Nafion, with the general chemical structure shown in Figure 1-3.[8] Nafion membranes have been around since the 1960s and have been extensively studied because of their superior properties, including ionic conductivities up to 0.1 S cm^{-1} in a 100% humidified environment.[5] The high ionic conductivities are a result of microphase separation that yields sulfonic acid "canals" that allow protons to easily travel through the membrane.[9] The perfluorinated backbone and side chains give the polymer excellent thermal and oxidative stability. The two downsides to Nafion are its high cost, both to produce and to process, and its high methanol permeability for DMFC applications. Currently, the cost of Nafion is prohibitive to widespread commercial use in PEMFCs and DMFCs, and efficiency losses from methanol crossover have prevented the fabrication of robust DMFCs. Again, there are large amounts of research on-going trying to overcome these obstacles by a variety of approaches, and many of these efforts will be discussed throughout this thesis.

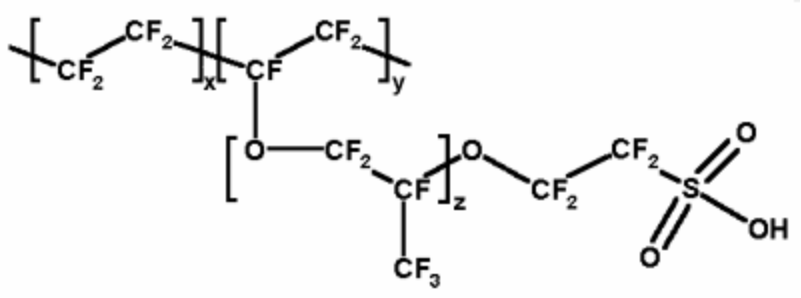

Figure 1-3. General chemical structure of Nafion (x~5-13.5, y~1000, z~1-3). The perfluorinated backbone and side chains give the polymer excellent stability, while the sulfonic acid groups form nanoscale channels for ions to rapidly transport throughout the membrane.

Lastly, to analyze the performance of a fuel cell, polarization curves are most commonly used. A representative polarization curve is shown in Figure 1-4 along with corresponding power density values. Current density (current normalized by the active area of the MEA) is used to make comparisons between devices easier. For the voltage versus current curve, there are four main regions to highlight:

1. Open Circuit Voltage (OCV). The OCV is the voltage when no current is drawn through the fuel cell. Although the theoretical OCV is defined by the anode and cathode half reactions, the OCV of actual devices is lower than theory due to fuel crossover, contact resistances, and irreversibilities.
2. Activation Losses. The sharp drop in voltage at low current densities is termed activation losses and is attributed to slow electrode kinetics.
3. Ohmic Losses. The linear drop in voltage seen after the activation losses is attributed to ohmic resistance losses from ion transport through the PEM.

4. Mass Transport Limitation. The sharp drop in voltage seen at high current densities is due to mass transport limitations, as the concentration of fuel and oxidant at the electrodes is too low to meet the demand placed on the fuel cell.

The power density curve is generated by simply multiplying the voltage and current density at each data point. While polarization curves make it easy to compare different devices' performance, other factors including, but not limited to the following: fuel and oxidant concentration or partial pressure, catalyst loading, MEA preparation, operating temperature, water management, and device history must be accounted for to make accurate comparisons.

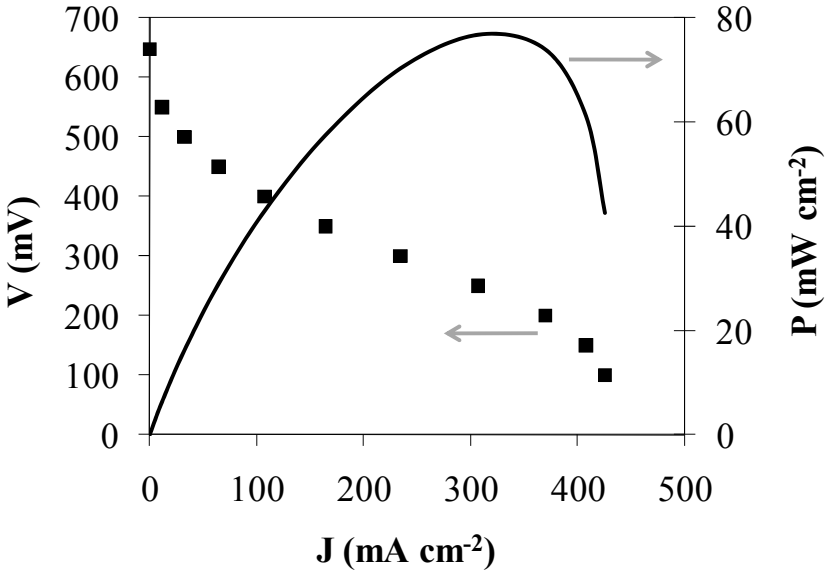

Figure 1-4. A representative fuel cell polarization curve with corresponding power density values. The key aspects of the polarization curve are the OCV, activation losses, ohmic losses, and mass transport limitations.

1.3 Layer-by-Layer Assembly

The multilayer assembly or LbL assembly process developed by Decher in the early 1990s consists of the building up of a polymer thin film in a step-wise fashion as illustrated in Figure 1-5.[10, 11] A substrate containing a surface charge is brought in contact with an aqueous polyelectrolyte solution of opposite charge, allowing the polyelectrolyte to diffuse and absorb to the substrate. Enough polymer absorbs to overcompensate the surface charge, which results in a reversal of the surface charge of the substrate [12]. The substrate is then dipped in a series of rinse baths to remove any polymer that is not tightly bound to the substrate. Next, the substrate is contacted with a polyelectrolyte solution of opposite charge to that of the surface, followed by dipping in a second series of rinse baths. The overall process can be repeated as many times as required to produce a film of desired thickness. Additionally, the thickness of each deposited polymer layer can be tuned, in the range of 1-100 nm, by adjusting the pH or ionic strength of the polyelectrolyte solution and rinse bath.[13, 14] Other key advantages of the LbL assembly technique include the following:

- The process is easily automated by use of a computer-controlled slide stainer
- The entire process can be performed at ambient conditions in aqueous solutions, i.e. no harsh solvents are generally required
- The ability to conformally coat substrates of complex geometry
- A low cost of materials, mainly because the required concentration of the polymer solutions is ~10^{-2} M
- New techniques, including spraying and roll-to-roll processing, can cut down the film deposition time by up to a factor of 100

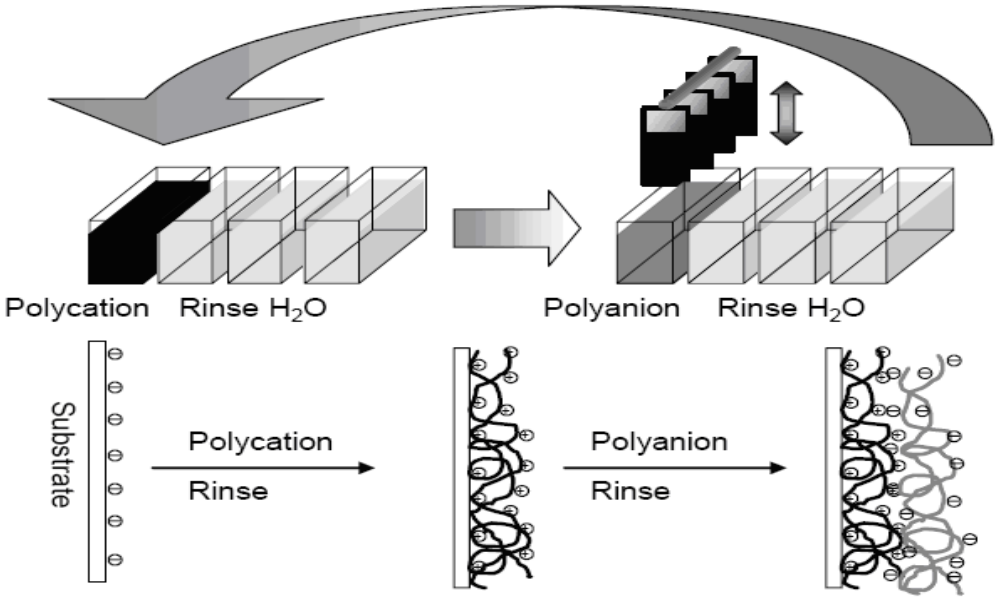

Figure 1-5. Schematic of the LbL assembly process (reproduced with permission and adapted from M.C. Berg, MIT).[15] A substrate containing a surface charge is brought in contact with an aqueous polyelectrolyte solution of opposite charge. Enough polymer absorbs to overcompensate the surface charge, and the substrate is contacted with a polyelectrolyte solution of opposite charge to that of the surface. The substrate is rinsed after each polymer layer is absorbed to remove any polymer not tightly bound into the LbL matrix. The overall process can be repeated as many times as required to produce a film of desired thickness.

Owing to these advantages for developing polymer thin films, research interest in multilayer films has grown extensively in recent years. LbL films have found use in applications such as light-emitting devices, sensors, electrochromics, conductive coatings, patterning, analytical separations, and gas separations.[16-21] Significant research

has also focused on incorporating a variety of materials besides standard polyelectrolytes into multilayer films, including small organic molecules or inorganic compounds, macromolecules, biomacromolecules such as DNA or proteins, and colloids.[22-25] Furthermore, mechanisms besides electrostatic attraction have been investigated as means to build up layers, including hydrogen bonding, covalent bonds, adsorption/drying cycles, and specific recognition.[26]

Hydrogen-bonded films may be particularly attractive for use as fuel cell PEMs, as will be discussed below. The concept was developed by Rubner and Zhang almost simultaneously in 1997.[27, 28] Instead of depositing alternately charged polyions, layers are built up by the alternating deposition of polymers that have hydrogen-bond-donating groups and hydrogen-bond-accepting groups. Subsequent studies have examined numerous hydrogen-bonding polymer pairs and have shown that these systems can be easily tuned by alterations in the temperature and pH of the processing conditions.[29, 30] Work by Delongchamp et al. showed that hydrogen-bonded systems show promise as solid state electrolytes.[31] Also, although the LbL technique traditionally uses only aqueous solutions, hydrogen-bonded films allow for new polymer systems to be explored. Polymers that are nonionic and/or water-insoluble can now be incorporated into multilayer films by using appropriate organic solvents during the deposition process.[32]

1.4 Layer-by-Layer Ion Exchange Membranes

Based on the required properties of PEMs, the LbL assembly of polyelectrolytes and polymer electrolytes is a promising technique for designing these systems. Although

the idea of using polyelectrolyte complexes in fuel cell membranes was proposed by Michaels in 1965, these systems were not feasible because of their high resistance to proton conduction.[33] Recent research, including work in the Hammond research group, has focused on the ion permeation and ion conductivity in multilayer films.[18, 31, 34-37] Specifically, our recent work has developed several multilayer systems of hydrophobic and hydrophilic polymers, utilizing both electrostatic and hydrogen-bonding assembly, which have room temperature ionic conductivities up to 10^{-4} to 10^{-5} S cm^{-1}.[31, 37] These ionic conductivity values are two orders of magnitude higher than previously reported in LbL film systems. Also, simple changes in the pH and ionic strength of the polymer deposition solutions can have large effects on the ionic conductivity. Ion transport occurs by intra-chain and inter-chain ion hopping or swinging through a polymer matrix.[38] Therefore, systems where the polyelectrolytes are charged and the polymer chains have greater mobility show the greatest increases in ionic conductivity.[37]

The first application of multilayer films as a PEM in fuel cells was recently reported by Farhat et al.[39] This study focused on applying electrodes to existing hydrogen bonded and electrostatically assembled films deposited on porous membranes to create MEAs. Electrodes were standard, commercially available C/Pt gas diffusion electrodes. These MEAs were tested in a home-built fuel cell device at 90-95% relative humidity (RH) and at ambient temperature. Among the polymer systems studied, the poly(ethylene oxide)/poly(acrylic acid) (PEO/PAA) system delivered the highest power, which was nearly 50% of the performance of the control Nafion fuel cell operated under the same conditions. The low open-circuit voltage (OCV) of this system is attributed to "activation losses and fuel crossover." [39] The multilayer PEM was approximately 5 times thinner

than traditional PEMFC membranes. Also, the ability of these LbL fuel cell systems to operate at lower humidity is an advantage over the Nafion membranes, which require conditions near 100% RH to perform. Unfortunately, the overall performance of the home-built hardware used in this study was inferior to commercial standards, and comparison studies used in standard hardware did not elucidate the same performance increases for PEO/PAA over Nafion.

1.5 Water Transport in Proton Exchange Membranes

Water uptake and transport in PEMs plays an important role in the development of highly conductive membrane materials, understanding structure property relationships, and for the reduction or elimination of balance of plant humidification systems in commercial fuel cell devices.[40] Commonly used sulfonic acid containing polymers have strong dependencies of ionic conductivity values on relative humidity.[41] In these systems, the Grotthuss "hopping" mechanism, shown in Figure 1-6b, best describes how protons move through the PEM. The Grotthuss mechanism consists of the 'hopping' of a proton between adjacent water molecules. Protons can also move through the PEM matrix by a vehicle mechanism, shown in Figure 1-6a, where protons simply diffuse through aqueous pathways. It is likely that proton transport in a PEM occurs by a combination of both mechanisms.

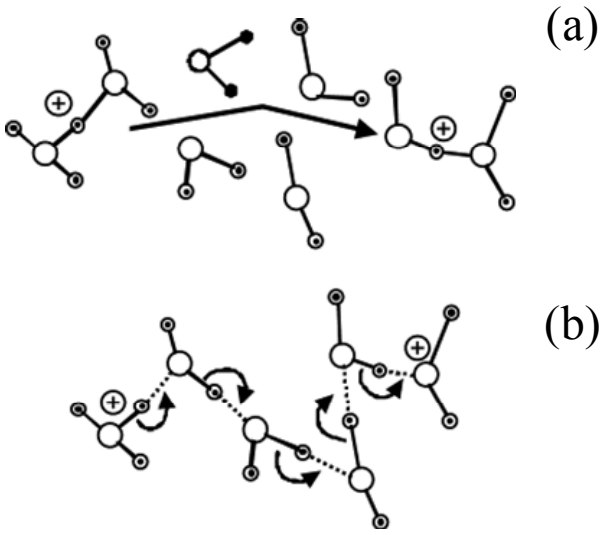

Figure 1-6. Schematic of proton transport mechanisms in hydrated PEMS (reproduced with permission from Polymer, Elsevier Limited).[40] The vehicle mechanism (a) consists of proton diffusion through aqueous pathways, while the Grotthuss mechanism (b) consists of protons 'hopping' between adjacent water molecules.

In addition to the important role that water plays in ion transport, understanding the overall water balance within the PEM is critical for successful device operation. Figure 1-7 shows the main ways water is supplied, generated, or transported in the PEM. Typically, humidified gases are fed to the MEA in PEMFCs to ensure the membrane stays hydrated. Maintaining membrane hydration is less of an issue in DMFCs, where the fuel is a methanol-water mixture. During fuel cell operation, electro-osmotic drag draws water molecules with protons to the cathode, where water is also generated as oxygen is reduced. Also, the concentration gradient across the membrane leads to back diffusion of water from cathode to anode. Due to the accumulation of water at the cathode, referred to as "cathode "flooding," fuel cell systems are designed to remove water from the cathode

side of the MEA. Flooding of the cathode prevents oxygen from reaching the catalyst sites and reduces device efficiency. The balance between maintaining membrane hydration and minimizing cathode flooding often necessitates complex external water management systems, causing parasitic power losses and lower fuel cell performance. Thus, membranes with optimal water uptake and transport properties could reduce or eliminate the need for these water management systems.

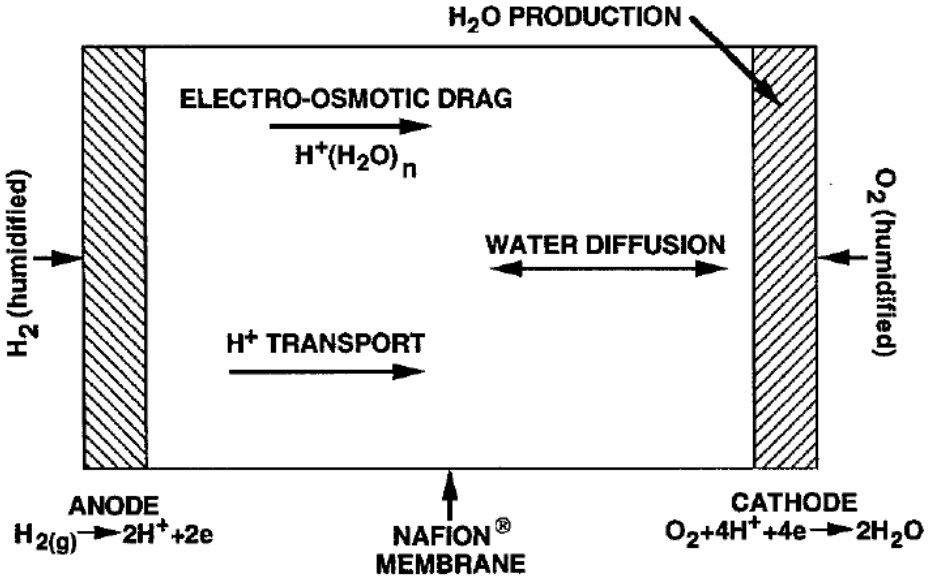

Figure 1-7. Schematic of the water uptake and transport in a PEMFC (reproduced with permission and adapted from Journal of The Electrochemical Society, The Electrochemical Society).[41] Humidified gases are often fed to the MEA. Electro-osmotic drag draws water to the cathode, where water is also generated as oxygen is reduced. The concentration gradient across the membrane leads to back diffusion of water from cathode to anode.

To measure the water uptake and transport of LbL films in this thesis, we utilize a new quartz crystal microbalance (QCM) technique.[42, 43] A schematic of the apparatus used is shown in Figure 1-8. This QCM method has been used to determine the permeability of various gases through polymer thin films, coatings and powders. QCMs measure the change in mass per unit area of a sample by measuring the variation in frequency of a quartz resonator due to absorption and diffusion of the permeating species, in this case water, in thin films. The governing equation for QCMs is the Sauerbrey equation,

$$\Delta f = \frac{-2 f_0 \Delta m}{A \rho_q \mu_q} = -C \cdot \frac{\Delta m}{A} \qquad \text{Equation 1-3}$$

where f_0 is the fundamental frequency of the crystal, Δm is the mass of the adsorbed gas, $\mu_q = 2.95 \times 10^{11}$ g cm^{-1} and $\rho_q = 2.65$ g cm^{-3} are the shear modulus and the density of quartz, respectively, and A is the area of a geometrically flat surface of an electrode on a major face of the crystal. Thus, the shift in the resonant frequency is directly proportional to mass uptake per unit area.

Permeability is defined as:

$$P = \frac{J \cdot l}{\Delta p} = S \cdot D \qquad \text{Equation 1-4}$$

where J, l, and Δp are the flux, film thickness, and partial pressure difference across the film, respectively. Analyzing water permeation through a film involves both an equilibrium thermodynamic property, solubility (S), and a kinetic property, the diffusion coefficient (D). Both parameters, S and D, can be obtained from mass uptake experiments using the QCM.

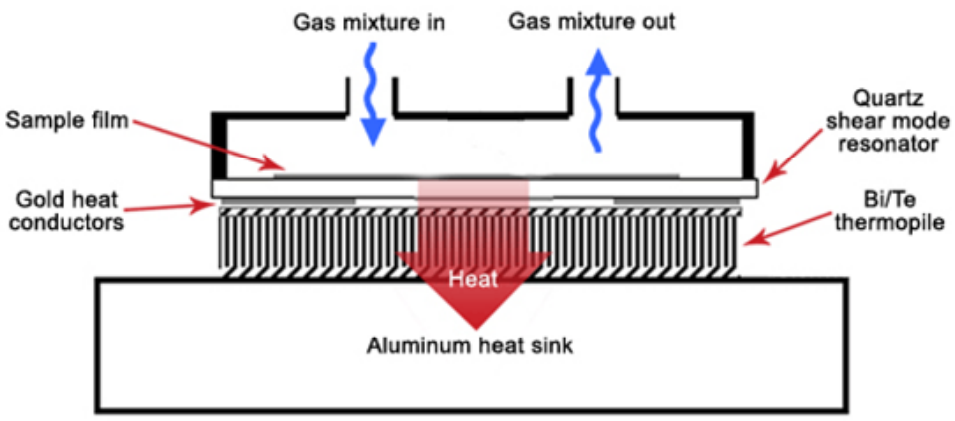

Figure 1-8. Schematic of the quartz crystal microbalance/heat conduction calorimeter (QCM/HCC), known as the Masscal G1 (reproduced with permission from Masscal Scientific Instruments). The ability to control the relative humidity of the sample chamber allows for the precise measurement of water uptake and transport in thin LbL films.

To analyze water uptake in LbL films, they are assembled on quartz crystals and equilibrated at 30 °C under a dry nitrogen atmosphere until there is no longer a loss in moisture from the film, as evidenced by a constant frequency response from the QCM. By varying the relative humidity of the sample chamber either as one step to 100% RH or multiple incremental steps up to 100% RH, water uptake and permeability is calculated. The linear sorption isotherm from the multi-step experiment yields the films' solubility. Diffusion coefficients are calculated by modeling the single-step experiments as the one-dimensional diffusion of water into a slab as described by the following simplified equation,

$$-\frac{1}{\pi^2}\ln\left[\frac{(m_\infty - m_t)\pi^2}{8(m_\infty - m_0)}\right] = \frac{D}{l^2}t \qquad \text{Equation 1-5}$$

where, m_∞, m_i and m_t are the mass of the film plus the sorbate (water) at time = ∞, 0 and t, respectively, and l and t are thickness of the LbL film and time, respectively.[44, 45] The permeability of the LbL film is simply calculated from Equation 1-4 as the product of solubility and the diffusion coefficient. It is important to note that while deviations from the Sauerbrey equation can exist for highly hydrated films, these deviations are minimal for thin films studied at the QCM's fundamental frequency (5 MHz).

1.6 Measuring Ion Transport in Proton Exchange Membranes

Measuring the ionic conductivity of new PEMs is the first way to characterize their promise; however this is a nontrivial measurement. For a given PEM, the ionic conductivity is related to number and type of charge carriers by the following equation:

$$\sigma = \sum_i n_i q \mu_i \qquad \text{Equation 1-6}$$

where n is the number of charge carriers of species i, q is the charge, and μ is the mobility of species i. Thus, the ionic conductivity of a material can be increased by increasing the number of charge carriers or the mobility of the charge carrying species within the PEM. The equation for determining conductivity in a PEM is the following:

$$\sigma = \frac{l}{R \cdot A} \qquad \text{Equation 1-7}$$

where l is the distance between the electrodes used, A is the cross-sectional area through which protons are moving, and R is the resistance measured. In a fuel cell, protons move

through the z-direction of the PEM from anode to cathode, yet measuring the through-plane conductivity of a PEM is difficult. In fact, the most common method for measuring through-plane conductivities is to assemble a full MEA and test the MEA inside fuel cell hardware while the device is not operating (i.e. no fuel is supplied). While this technique can lead to information about the through-plane membrane resistance, it is expensive, as noble metal catalyst must be used for every new membrane test, time intensive, as an MEA must be made from each PEM sample, and complex because of the resistances that must be taken into account (current collector and diffusion layer, diffusion layer and catalyst, catalyst and PEM, etc.). To illustrate the difficulty in making direct through-plane conductivity measurements on PEMs outside of a fuel cell, Figure 1-9 shows the resistance that would be measured for a set of hypothetical 1 μm thick PEMs having a range of ionic conductivities (assuming no contact resistances anywhere in the system). For example, the resistance measured for a 1 μm thick PEM having an ionic conductivity of 1 x 10^{-4} S cm^{-1} would be ~10 Ω. PEMs with higher conductivity values would give lower resistances, which become on the same order of magnitude or lower than the system/series resistances, and thus impossible to measure. The range of resistance values that can be accurately measured using standard impedance analyzers is shaded in Figure 1-9. While it is possible to measure through-plane resistances for some PEM materials, these are membranes with inherently low ionic conductivity values, and are therefore less interesting for study.

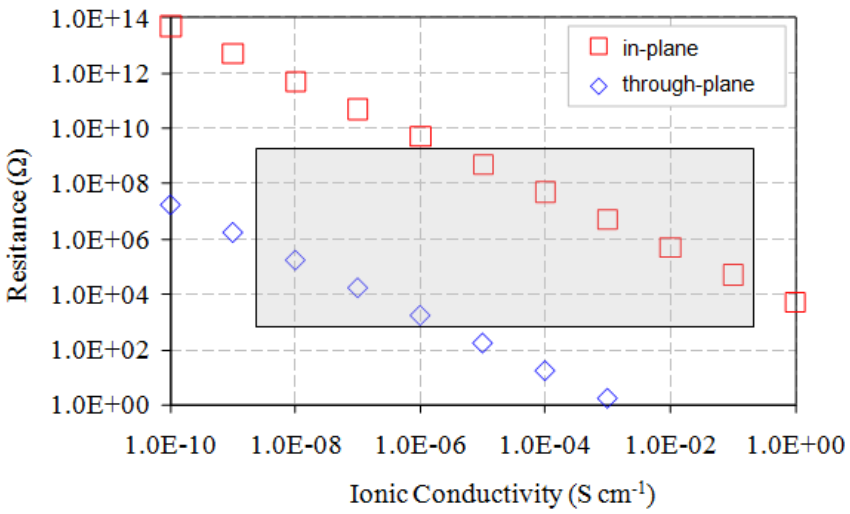

Figure 1-9. Comparison between through-plane and in-plane measurement techniques for a set of hypothetical 1 μm thick PEMs having a range of ionic conductivities. The shaded region bounds the region of resistance values that can be measured (y-axis) and the conductivity values relevant for PEMs (x-axis).

To measure the ionic conductivity of highly conductive PEMs, an in-plane measurement technique is utilized, as shown in Figure 1-10. Since the distance between the electrodes (l in Equation 1-7) is several orders of magnitude larger for in-place measurements, accurate impedance values can be determined, as seen in Figure 1-9. For in-plane measurements, the PEM is pressed against platinum wires that are 1 cm apart and two-probe AC electrochemical impedance spectroscopy is performed. It should be noted that the conductivity cell used (Figure 1-10) also allows for four-probe DC measurements to be performed.

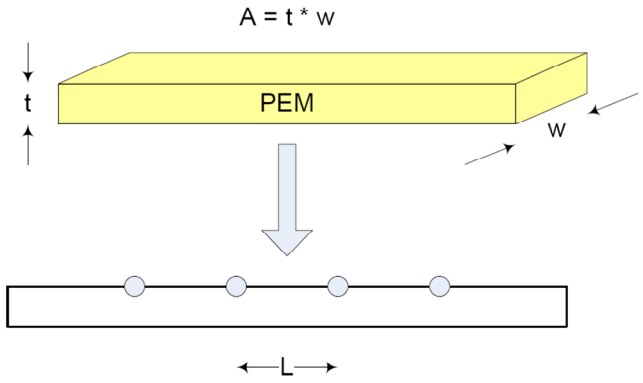

Figure 1-10. Schematic of the conductivity cell used to measure the in-plane resistance of PEMs by two-probe AC electrochemical impedance spectroscopy.

When performing in-plane conductivity measurements, it is important to be aware of potential anisotropy in the membrane. For most PEM systems, including polymeric LbL films, it is safe to assume that on a macroscopic scale ion transport is isotropic. However, if there is potential for anisotropy in the PEM, in-depth morphological characterization should be done and reporting in-plane conductivity values as bulk conductivities should be carefully described. Another concern with in-plane measurements is the potential for measuring only surface conductivity. To ensure accurate conductivity measurements, measuring the in-plane conductivity for the same PEM material at several thicknesses can confirm that bulk conductivity is observed. For a given PEM material the ratio of membrane thicknesses for two different samples should equal the inverse ratio of corresponding impedance values measured. If this ratio is observed, then bulk conductivity values are being measured.

A model Nyquist plot for a highly conductive PEM measured in-plane is shown in Figure 1-11, along with the corresponding equivalent circuit used to model the

impedance data. The details of electrochemical impedance spectroscopy are discussed elsewhere.[46] In the equivalent circuit model, R_S corresponds to the series resistance from the lead wires and platinum electrodes, R_{PEM} is the resistance of the PEM, and C_{PEM} is the capacitance of the PEM. The diameter of the semicircle, R_{PEM}, is the value that is used in Equation 1-7, along with the geometry of the conductivity cell and PEM sample, to calculate ionic conductivity. Often when modeling the impedance response of actual PEMs, the capacitor, C_{PEM}, is replaced with a constant phase element to account for non-ideal behavior. Constant phase elements are empirical circuit elements that have phase angles independent of frequency and can therefore model non-ideal impedance response. Also, the low frequency response of the electrochemical impedance measurement is not shown in Figure 1-11. Theoretically, double-layer capacitance should lead to a straight vertical line at $R_S + R_{PEM}$, although this is frequently not observed. Lastly, recent approaches for ensuring the validity of impedance models have been presented and should be taken into account when reporting electrochemical impedance spectroscopy results (see also Figure A-3).[47, 48]

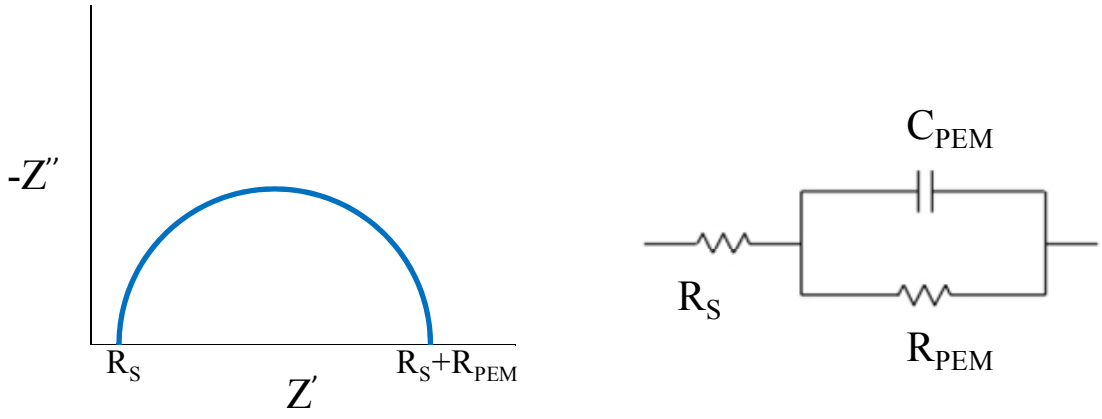

Figure 1-11. A model Nyquist plot for a highly conductive PEM measured in-plane, along with the corresponding equivalent circuit. For the equivalent circuit, R_S corresponds to the series resistance from the lead wires and platinum electrodes, R_{PEM} is the resistance of the PEM, and C_{PEM} is the capacitance of the PEM. The diameter of the semicircle corresponds to R_{PEM}.

1.7 Technical Overview

In Chapter 2, the LbL assembly of a polyphosphazene with ethylene glycol side chains, poly[bis(methoxyethoxyethoxy)-phosphazene] (MEEP), with poly (acrylic acid) (PAA) is explored and compared to previously studied poly(ethylene oxide)/PAA LbL systems. Similar to other hydrogen-bonded LbL films, the growth behavior, ionic conductivity, and other bulk properties are tuned by adjusting the pH of the assembly solutions. MEEP/PAA LbL films assembled at higher pH values (> 3) have improved water uptake and transport causing enhanced ion transport at humidified conditions. At 100% RH, the ionic conductivity of an optimized MEEP/PAA film approaches 10^{-3} S cm^{-1}, which is one order of magnitude higher than previously studied hydrogen-bonded LbL systems. Additionally, the MEEP/PAA films are hydrolytically stable, where

pristine MEEP is water soluble, and the mechanical properties of the LbL films are superior to neat MEEP.

Next, Chapter 3 introduces the sulfonation of an aromatic polyether, poly(2,6-dimethyl 1,4-phenylene oxide) (sPPO), to a degree of sulfonation greater than 75%. The water soluble sPPO is paired with several amine-containing polycations to form highly conductive LbL films. The most promising system is sPPO paired with poly(diallyl dimethyl ammonium chloride) (PDAC). PDAC/sPPO films at optimized assembly conditions have ionic conductivity values of 3.5×10^{-2} S cm^{-1}, which is the highest value ever reported for a LbL system. Additionally, the methanol permeability of all sPPO-based LbL films is over two orders of magnitude lower than traditional fuel cell PEMs. To validate the of high ionic conductivity and methanol resistance of these sPPO-based LbL films, we apply them as coatings on Nafion membranes for use in DMFCs. At a typical operating voltage of 0.3 V, the PDAC/sPPO coated Nafion DMFC produces 53.2% more power than unmodified Nafion. Other aspects of DMFC performance including open circuit voltage, methanol crossover current, and temperature dependent performance are reported for PDAC/sPPO coated Nafion.

Chapter 4 focuses on understanding the basis for the high conductivity of PDAC/sPPO films by studying structure-property relationships of a series of films assembled with different salt concentrations in the assembly solutions. Film growth is modulated from 6.91 nm/bilayer (BL) up to 62.2 nm/BL as the salt concentration of all assembly solutions is increased to 0.5 M. It is shown that the ionic conductivity can be further enhanced by selectively adding 1.0 M salt to only the sPPO assembly solution, giving a maximum value of 7.0×10^{-2} S cm^{-2}. Selectively adding salt to the sPPO

assembly solution decreases the ionic crosslink density of the films and increases the water uptake, yielding high ionic conductivity, especially at high relative humidity values. Interestingly, thermal gravimetric analysis (TGA) and elemental analysis show little compositional variation for films assembled with different salt concentrations in the assembly baths. Using a spray LbL technique, thick PDAC/sPPO films are fabricated to allow for the preliminary characterization of the mechanical properties of free-standing membranes.

Lastly, in Chapter 5 composite membranes of highly conductive LbL films and electrospun fiber mats (EFMs) are investigated for fuel cell applications. The mechanical properties of PDAC/sPPO films are improved by forming the LbL matrix on easily tunable EFM supports. Coating an EFM with the LbL dipping process produces composite membranes with interesting "bridged" morphologies; the ionic conductivity of the composites is similar to pristine PDAC/sPPO films. Spray LbL assembly is studied as a means for the rapid formation of LbL films on the EFMs, while also allowing vacuum to be applied during assembly. At optimized conditions, LbL EFM composites have conformal coatings of the individual fibers throughout the bulk of the EFM. The mechanical properties of the spray coated EMFs are shown to be superior to the pristine PDAC/sPPO LbL system.

2. Ion Conduction and Water Transport in Polyphosphazene Based Multilayers

Portions of this chapter are reproduced from Avni A. Argun, J. Nathan Ashcraft, Marie K. Herring, David K.Y. Lee, Harry R. Allcock, Paula T. Hammond, *Chemistry of Materials*, 2009, submitted.

Abstract

Layer-by-layer (LbL) assembled films of poly[bis(methoxyethoxyethoxy)-phosphazene] (MEEP) and poly (acrylic acid) (PAA) are demonstrated by utilizing the hydrogen bonding between these two polymers. These films show controlled thickness growth, high ionic conductivity, and excellent hydrolytic stability. The ionic conductivity of these films is studied by changing the assembly pH of initial polymer solutions and thereby controlling the hydrogen-bonding characteristics. Despite similar film composition, MEEP/PAA LbL films assembled at higher pH values have enhanced water uptake and transport properties, which play a key role in increasing ion transport within the films. At fully humidified conditions, the ionic conductivity of MEEP/PAA is 7 x 10^{-4} S cm^{-1}, over one order of magnitude higher than previously studied hydrogen-bonded LbL systems. Finally, free standing films are isolated from low-energy surface substrates, which allows for bulk characterization of these thin films.

2.1 Introduction

Many electrochemical energy conversion and storage devices such as fuel cells, batteries and dye-sensitized solar cells rely on electrolytes for ionic transport. Conventional electrolytes consist of a polar liquid capable of solvating ions. The need for a safe and lightweight solid state electrolyte has driven extensive research to replace caustic or flammable liquid electrolytes to circumvent problems associated with leakage. A known compromise in this area is the balance between high ion transport and mechanical integrity. Often high ionic conductivity values are achieved by utilizing polymers with low glass transition temperatures and low degrees of crystallization, at the expense of mechanical durability. Poly(ethylene oxide) (PEO) has been one of the most thoroughly investigated polymer electrolytes because it bears cation-solvating ether groups and a flexible backbone for facile ion mobility.[49-51] However, its crystallinity, and limited chemical stability are major limitations for realistic applications. To minimize crystallization, small molecule plasticizers have been used with PEO in lithium-ion batteries; however, these plasticizers are typically highly flammable and result in a more liquid-like electrolyte system, both of which lead to serious hazards if a device were to be breached. For applications such as fuel cell or flow cell membranes in which the electrolyte is often hydrated, the chemical stability of PEO becomes a greater issue.

To address the above issues, Allcock and coworkers have designed a hybrid organic-inorganic polymer, poly[bis(methoxyethoxyethoxy)phosphazene] (MEEP), by functionalizing a highly versatile polyphosphazene backbone with ethylene oxide chains

(Figure 2-1).[52, 53] The phosphazene backbone has numerous advantages over that of PEO, such as higher chain flexibility and thermo-oxidative stability. The properties of the polymer can be tuned through substitution reactions on the highly versatile parent polymer, poly(dichlorophosphazene). Furthermore, the dry (0% RH) ionic conductivity of MEEP is over two orders of magnitude higher than that of PEO in non-plasticized systems (10^{-3} vs. 10^{-5} S cm^{-1}), an essential property for solid polymer electrolytes to reduce electrical resistance.[54] Due to the highly flexible nature of both its backbone and side chains, MEEP lacks mechanical integrity. Moreover, MEEP is water-soluble, which makes it impractical for use in highly hydrated environments such as fuel cells. A way to address this issue is by exposing the polymer to gamma or UV radiation, which results in a crosslinked MEEP network.[55, 56] Due to the stability of the phosphazene backbone, the crosslink occurs only on the side chain and increases the mechanical stability of MEEP. However, gamma radiation is not easily accessible and the UV radiation method involves sensitizers that need to be removed upon crosslinking process. A better strategy to stabilize MEEP films, as well as providing mechanical robustness, is much needed.

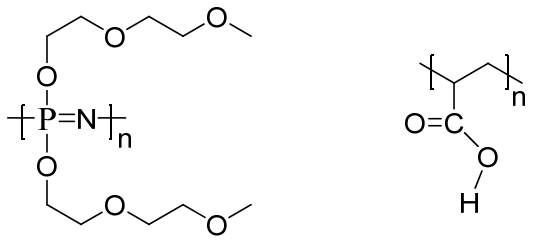

MEEP **PAA**

Figure 2-1. Chemical structures of poly[bis(methoxyethoxyethoxy)phosphazene] (MEEP) and poly (acrylic acid) (PAA). LbL films are made by the hydrogen-bonding interactions between protonated PAA and the ether oxygens on MEEP.

Layer-by-layer (LbL) assembly is a versatile thin-film fabrication method which consists of the repeated, sequential immersion of a substrate into aqueous solutions of complementary functionalized materials.[10, 11] The LbL method provides stable polymer blends and allows for composition, morphology, and property control through the adjustment of assembly parameters such as pH. The tunability, environmentally-benign aqueous processing, and nanoscale blending of materials which are otherwise impossible to construct make this system a significant competitor to create novel solid state electrolytes for various energy applications.[57, 58] In addition to commonly used electrostatic interactions for LbL film growth, secondary interactions such as hydrogen bonding have proven effective in incorporating neutral, water soluble polymers into LbL films.[59, 60]

In this work, we introduce the LbL assembly method to create homogenous blends of MEEP, a hydrogen-bonding acceptor, and poly (acrylic acid) (PAA), a hydrogen-bonding donor, with controlled film growth, high ionic conductivity, and excellent hydrolytic stability. To the best of our knowledge, this is the first incorporation of a phosphazene based polymer into a multilayer structured thin film. These films are promising candidates as truly solid state polymer electrolytes in electrochemical devices such as fuel cells and batteries. We show the relative humidity dependence of conductivity as well as the water transport characteristics of these unique blends. The LbL assembly process allows fine tuning of the desired properties by simple adjustments to the assembly conditions. We also show the isolation of MEEP/PAA LbL assembled films from the substrate, which allows bulk characterization of free-standing films.

2.2 Materials and Methods

Chemicals. MEEP (M_w ~ 264,000 determined by aqueous GPC) was synthesized according to previously published procedures.[53] Poly(acrylic acid) (PAA) (250,000 M_w, Polysciences) was used as received. Both MEEP and PAA were weighed and diluted to the desired concentration using Millipore MilliQ deionized water (18.2 MΩ cm filtered through a 0.22 μm membrane).

LbL Assembly Methods. Assembly of the LbL films was completed by using a programmable ZEISS DS50 slide stainer. To construct LbL films, substrates (glass, patterned ITO, polystyrene, or ZnSe) were first immersed in aqueous MEEP solution (10 mM calculated based on the repeat unit) for 20 minutes, followed by three two minute rinses in water, and then in PAA (10 mM) for 20 minutes followed by three two minute rinses in water. The pH of both polymer solutions and rinse baths were identical and adjusted prior to assembly by adding 1M HCl solution dropwise. The dipping process was repeated numerous times to produce a film of desired thickness. The free-standing films were peeled off from polystyrene substrates.

Ionic Conductivity. For in-plane conductivity measurements, LbL films deposited on microscope slides (VWR) were placed in a conductivity cell with platinum wires as the electrodes, and tested in a humidity and temperature controlled chamber (Electro-tech Systems, Inc.). Relative humidity was controlled down to 10% RH, and dry (0% RH) measurements were performed in a nitrogen-filled glove box with <1 ppm water content. Through-plane conductivity measurements were performed by depositing LbL films on patterned ITO substrates (Delta Technologies), and gold electrodes were thermally evaporated (~100nm) on the multilayers. The active area was 6 mm^2. Ionic conductivity

values were determined by electrochemical impedance spectroscopy with a Solartron 1260 impedance analyzer by sweeping the frequency from 1 MHz down to 1 Hz.

Bulk Characterization. Thickness measurements were made by scoring the films with a razor blade and measuring the step change in height between the film and substrate with a Tencor P16 profilometer (1 mg applied force). FTIR spectra were obtained from thin films deposited on CVD grown, IR transparent ZnSe substrates. Free standing films were analyzed with a TA Instruments Q1000 differential scanning calorimeter. Films were cut to yield samples of ~2-3 mg, and all temperature ramp rates were 10 °C/min. Samples were equilibrated at -90 °C, heated to 150 °C, and cooled back to -90 °C. At least two thermal cycles were repeated for each film. The glass transition temperature was calculated from the inflection point of the sigmoidal portion of the heating curve.

Water Uptake Behavior. A Masscal G1 (quartz crystal microbalance/heat conduction calorimeter) was used for analysis of water uptake and transport properties of LbL films. LbL films were deposited onto 1 inch diameter quartz crystals (5 MHz frequency) with gold electrodes from Masscal Scientific Corp. For all experiments, the temperature of the G1 sample chamber was maintained at 30 °C. Two mass flow controllers supplied nitrogen streams to the G1 sample chamber. One nitrogen stream was kept dry, while the other was humidified to 100% relative humidity (RH). Varying the ratio of these to streams through the G1 software allowed fine control of the sample chamber RH. The total gas flow rate was 50 cm^3 (STP)/min for all experiments. The RH of the G1 samples chamber was monitored using a Sable Systems R300 water vapor analyzer. Films were exposed to a dry nitrogen purge to determine the amount of film

formed on the crystal by comparison with the frequency of the blank crystal before coating. After the films were fully dried, a step change in RH of the sample chamber from 0 to 100% was introduced. The frequency change of the coated crystal caused by water uptake into the films was monitored in real-time. Mass uptake is directly proportional to the frequency change, as given by the Sauerbrey equation (Equation 1-3).[61] Dried films were also exposed to incremental step changes in relative humidity (~15% per step) up to 100% RH to yield a sorption isotherm. To ensure that condensation in the sample chamber did not occur, the frequency change of a blank QCM crystal was observed to be negligible when exposed to a full range of relative humidity conditions.

2.3 Results and Discussion

2.3.1 Multilayer Assembly and Ionic Conductivity

The LbL assembly of the polymers MEEP and PAA is performed by utilizing the hydrogen-bonding interaction between the COOH groups of PAA and ethylene oxide side chains of MEEP (Figure 2-1). The ionization degree of PAA is controlled during thin-film assembly by systematically varying the assembly pH from 3.50 down to 2.00 for all polymer and rinse solutions. In all cases, the MEEP/PAA films grow linearly up to as many as 75 bilayers across the entire assembly pH range. This linearity has also been observed with PEO/PAA multilayers and with other hydrogen-bonded systems.[31, 60] Figure 2-2 shows the bilayer thickness of MEEP/PAA films as a function of assembly pH. The maximum bilayer thickness is greater than 200 nm/bilayer at the lowest

assembly pH values, and is significantly reduced down to 50 nm/bilayer at the assembly pH = 3.5. Large bilayer pair thicknesses are commonly observed in hydrogen-bonded multilayer thin films due to a looser network formed between weakly associative groups; furthermore, the potential for dimerization between PAA side groups increases the chance of greater amounts of film deposited with each cycle.

Because the MEEP/PAA system relies on hydrogen bonding to build the film, the degree of ionization in PAA greatly affects the bond attractions and like-charge repulsion between the polymer chains. At low pH, the ethylene oxide side chains of MEEP paired with the carboxylic acid groups of PAA create enough hydrogen-bond crosslinks between polymer layers to stabilize the resulting film. By changing the pH of the assembly baths, this cross-linking attraction can be varied, thus changing the stability of the film and allowing tuning of the final thickness. At higher pH values, the adsorbed PAA layer becomes increasingly thinner, as hydrogen bonding between PAA side chains (acid-acid dimerization) is decreased. The LbL film growth is suppressed at assembly pH values above pH = 3.5 due to the more highly ionized PAA, which introduces large electrostatic repulsion, and limits the hydrogen-bonding interaction between MEEP and PAA.

Figure 2-2 also shows the tunability of the ionic conductivity of MEEP/PAA films by varying the assembly pH. In-plane conductivity was measured at fully humidified conditions at 25 °C using platinum wires one centimeter apart on the surface of a 50 bilayer MEEP/PAA film. By increasing the assembly pH, the bulk proton conductivity increases from 1×10^{-4} S cm^{-1} at assembly pH = 2.0 up to 7×10^{-4} S cm^{-1} at assembly pH = 3.5. This increase could be partially attributed to the higher ionization of

PAA (more anionic sites for ion transport); however, the effect of ionization on proton conductivity is small as verified by the values obtained from pristine PAA films, and cannot account for the 7-fold increase observed for the LbL assembled films. Therefore, the observed enhancement of conductivity is due to the changes in the effective hydrogen-bond network and/or composition in the films built at higher pH values, and resulting differences in ion and water transport. We hypothesize that the average number of transient hydrogen bonds per unit volume should undergo an overall decrease with these small increases in pH. The observed trend is consistent with the conductivity trend observed for the previously assembled LbL PEO/PAA systems, with MEEP/PAA values consistently being higher than the PEO/PAA values obtained at 100% RH.[31]

To determine the impact of ambient humidity on the ionic conductivity, 25 bilayers of MEEP/PAA films are assembled on patterned ITO/Glass substrates followed by thermal gold evaporation on top of the film to yield an 8-cell ITO | MEEP/PAA | Au configuration. Through-plane conductivity measurements are then carried out by connecting the ITO and gold ends to the impedance analyzer. Figure 2-3 shows the ionic conductivity values of MEEP/PAA multilayers assembled at pH = 2.5 (circles) and pH = 3.0 (triangles) as the relative humidity is decreased from 60% down to 0%. In agreement with conductivity measurements taken at fully humidified conditions, LbL films assembled at high pH values yield higher values, presumably due to a more favorable, loose polymer network for ion and water transport, which would facilitate ion conduction via Grotthuss and carrier mechanisms. On the other hand, it is important to note that the difference in ionic conductivity between these two films becomes systematically less pronounced at drier conditions, namely at relative humidity values less than 20%, and

that the ionic conductivities converge in the dry state to the value of ~ 10^{-9} S cm^{-1}. We attribute this behavior to the crucial role of water in ion transport of hydrated ethylene oxide based systems and the impact of its relative uptake in the films on the mobility of the ionic species, a phenomenon extensively discussed in the following section. As the films approach the dry state, the differences in the hydrogen-bonded network become irrelevant; the rate determining factor for these systems in the dry state is the inherent mobility of the ethylene oxide chain segments in the matrix. The values obtained here at 0% RH can be compared to those reported for PEO/PAA films examined under the same conditions, for which the dry state conductivity for was 3 x 10^{-10} S cm^{-1}.[62]

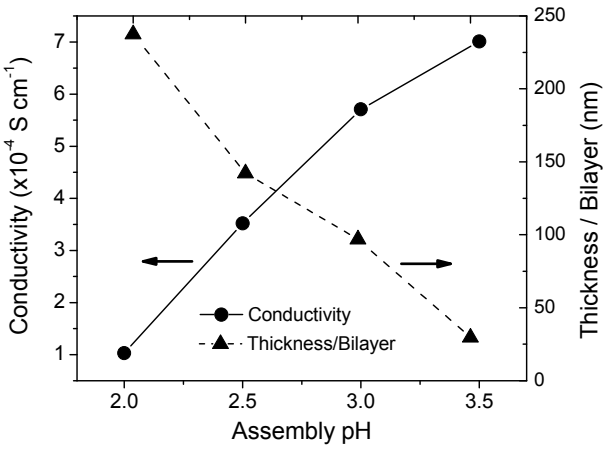

Figure 2-2. The assembly pH dependence of ionic conductivity at 100% RH (circles) and bilayer thickness (triangles). Films assembled at higher pH values grow slower, as PAA becomes increasingly ionized, but these films have higher ionic conductivity values.

Finally, to observe the effect of a small molecule plasticizer in a water-free environment, a drop of propylene carbonate was added onto a dry MEEP/PAA film (assembly pH = 2.5) placed in a glovebox. The ionic conductivity rapidly increased by

three orders of magnitude to reach 1.43 x 10^{-6} S cm^{-1} (Figure 2-3, empty circle) due to the more favorable liquid-like medium for ion transport. However, it is important to note that this value is still much lower than that of a film in fully humidified conditions indicating the crucial impact of water on proton transport through hydrated hydronium ions.[63]

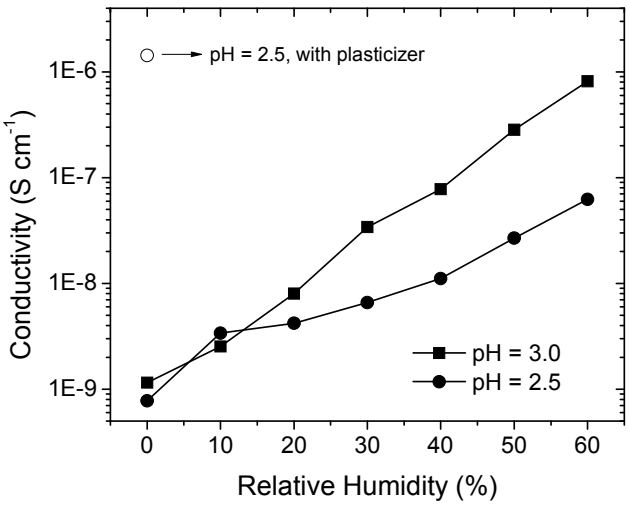

Figure 2-3. The relative humidity dependence of ionic conductivity of MEEP/PAA films assembled at pH = 2.5 and pH = 3.0. Also shown is the conductivity enhancement of a dry film upon addition of a small molecule plasticizer (propylene carbonate).

2.3.2 FTIR Analysis.

In order to better understand the type and extent of hydrogen bonding versus acid ionization at different assembly pH values, we have assembled two MEEP/PAA multilayer films on IR transparent ZnSe substrates at low pH (1.80) and at high pH (3.30), as well as pristine films of MEEP and PAA. Figure 2-4 shows the carboxylic acid region of the FTIR spectra, where the hydrogen-bonding characteristics of LbL films are

investigated. As expected, pristine MEEP does not have any absorption in this region. Pristine PAA, on the other hand, has a strong peak centered at 1711 cm^{-1}, indicative of intra-molecular hydrogen bonding of COOH groups via acid-acid dimerization.[62, 64] For the LbL films of MEEP/PAA, another peak centered at 1740 cm^{-1} is observed in addition to the peak at 1711 cm^{-1}, confirming the partial disruption of PAA's acid-dimerization and the presence of intermolecular hydrogen bonding between the acidic groups of PAA and the ether lone pair electrons of MEEP. The relative intensity of the 1711 cm^{-1} peak decreases as assembly pH increases from 1.80 to 3.30, suggesting a decrease in the extent of COOH groups participating in intra-molecular hydrogen bonding. This is primarily attributed to the higher degree of ionization of PAA, which decreases the number of COOH neighbors available for self-dimerization, and increases hydrogen-bond interactions of remaining COOH groups with MEEP. Also of interest is the COO^- region (~1550 cm^{-1}), which is indicative of changes occurring in the ionization of the carboxylic acid groups in PAA. Differences between the spectra of the PAA and MEEP/PAA films are minimal and difficult to observe in this region, due to the weakness of the ionized acid peak at low pH, and the fact that the degree of ionization varies by a fairly small fraction.

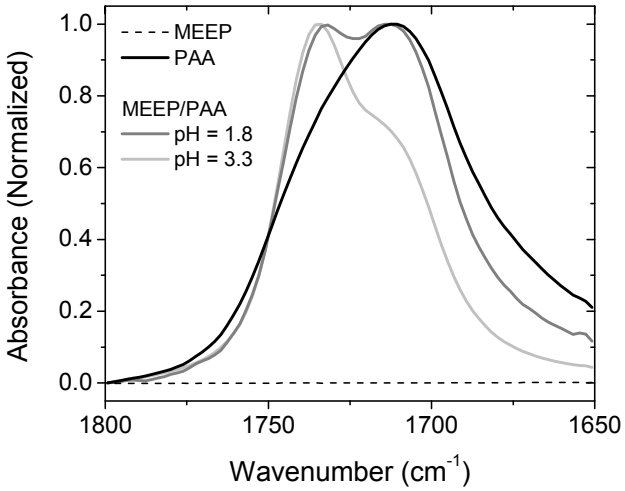

Figure 2-4. FTIR spectra of the carboxylic acid region of MEEP/PAA multilayers assembled at pH 1.8 and 3.3 on IR-transparent ZnSe substrates. The relative intensity of peak at 1710 cm^{-1} appears to decrease as assembly pH increases.

2.3.3 Bulk Characterization of Free-Standing Films.

To analyze the thermal and mechanical characteristics, MEEP/PAA films were deposited on low surface energy polystyrene substrates and gently peeled off with tweezers as previously described by our group.[65] The resulting films appear amber-colored and transparent, indicating a homogenous blend with minimal surface roughness. Figure 2-5 shows a DSC thermogram for a peeled-off MEEP/PAA film assembled at pH = 2.5, along with spun-cast films of neat PAA and MEEP (inset) from water. Multiple heating/cooling cycles are performed on each sample to remove bound water from the film and ensure accurate T_g values are observed. The measured T_g values of pristine PAA and MEEP are found to be 76.0 °C and -80.5 °C, respectively.

All MEEP/PAA LbL films exhibit a single T_g between that of neat MEEP and PAA, which is indicative of a truly homogeneous blended film, and is consistent with

earlier reports of DSC analysis on PEO/PAA LbL films.[62] Interestingly, the observed T_g of MEEP/PAA LbL systems show little or no variation when the pH of the assembly solutions was varied over the range of 1.8 – 3.0. All MEEP/PAA samples assembled at pH values varying from 2.0 to 3.5 exhibited a T_g of -28.0 ± 2.0 °C. For this polymer pair, a T_g of -28.0 °C corresponds to a composition of 52 wt% MEEP or 21 mol% MEEP by use of the Fox equation.[66] The lack of variation between assembly pH and T_g of the resulting LbL blend differs from a similar study on PEO/PAA LbL films, where the T_g of PEO/PAA films varied from ~60 °C when assembled below pH = 2.0 to ~25 °C at assembly pH values ≥ 3.0.[62] The variation in T_g of PEO/PAA films at different assembly pH values were due to different film compositions caused by the degree of ionization of PAA and its ability to form intramolecular versus intermolecular hydrogen bonds, thus leading to decreased adsorption of PAA relative to PEO at higher pH. For the MEEP systems, the changes in intra- versus intermolecular hydrogen bonding also seem to be responsible for changes in conductivity; however, the cause is not due to significant changes in relative MEEP content, which suggests that both the PAA and the MEEP adsorbed layers become thinner with higher pH. This difference between PEO and MEEP may be due in part to structural differences; the ethylene oxide groups attached as side chains to MEEP are very short, and would not undergo significant conformational changes to yield dense, loopy arrangements of high molecular weight PEO during the adsorption cycle, as anticipated with PEO when hydrogen bonding with PAA is optimized. In this case, less PAA adsorbed in the first adsorption cycle of the LbL assembly leads to lowered MEEP adsorption in the second. It is also noted that the relative increase in ionic conductivity with pH is also more moderate than observed with

PEO/PAA, indicative of the smaller differences in the composition and structure of the films with pH. The primary reason for the observed increases in conductivity are therefore likely to be due to the higher number of charged sites available in the film and the decrease in the number of hydrogen bonds acting as effective physical crosslinks in the network, yielding a "looser" network and increased ion mobility.

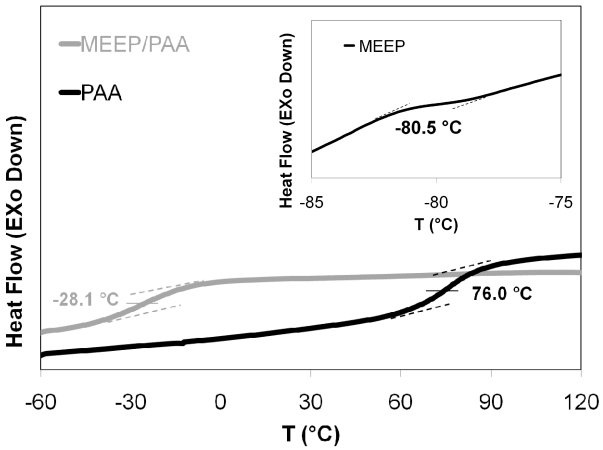

Figure 2-5. DSC thermogram for a free-standing MEEP/PAA film assembled at pH = 2.5, along with neat PAA and MEEP (inset). All MEEP/PAA LbL films displayed one T_g indicative of a homogenous blend. MEEP/PAA films assembled at different pH values showed little change in T_g.

A major concern for polymer electrolytes with low glass transition temperatures is their gum-like nature, which prohibits them from qualifying as truly solid-state electrolytes. To demonstrate the mechanical advantage of LbL assembled systems compared to pristine films of MEEP and PEO, we have tested the indentation response of MEEP/PAA films on glass as well as the pristine MEEP and PAA films for comparison. To minimize the substrate interference, we have assured that the thickness of the polymer

film is at least ten times greater than that of the indentation distance. Preliminary results show that a typical MEEP/PAA film (~6 μm) yields an elastic modulus value of 690 ± 57 MPa at ambient conditions, over an order of magnitude higher than a pristine MEEP film (56 ± 5 MPa). We are currently investigating to verify these values by measuring the tensile strength of free-standing LbL films.

2.3.4 Water Transport

We utilized a recently developed approach to determine the water uptake and transport of MEEP/PAA LbL films with a quartz crystal microbalance (QCM).[42, 43] This QCM method has been used to determine the permeability of various gases through polymer thin films, coatings and powders. QCMs measure the change in mass per unit area of a sample by measuring the variation in frequency of a quartz resonator due to absorption and diffusion of the permeating species, in this case water, in the films. Permeability is define above in Equation 1-4. Analyzing water permeation through a film involves both an equilibrium thermodynamic property, solubility (*S*), and a kinetic property, the diffusion coefficient (*D*). Both parameters, *S* and *D*, can be obtained from mass uptake experiments using the QCM.

To investigate the water uptake characteristics, MEEP/PAA films (5-10 bilayers, 0.5 – 2.1 μm) were assembled on quartz crystals and equilibrated at 30 °C under a dry nitrogen atmosphere until there is no longer a loss in moisture from the film, as determined by QCM. Then, the films were exposed to a step change to 100% RH while monitoring the changes in oscillation frequency. Figure 2-6a shows the water uptake of two MEEP/PAA films upon exposure to a fully humidified environment followed by a

step change back to dry nitrogen and the corresponding water loss. Water uptake as a function of incremental step changes in humidity is shown in Figure 2-6b. The kinetic data from the single step experiment allows for the calculation of the diffusion coefficient through use of a simplified model of one-dimensional diffusion of water into a slab, which has been previously described.[44, 45]

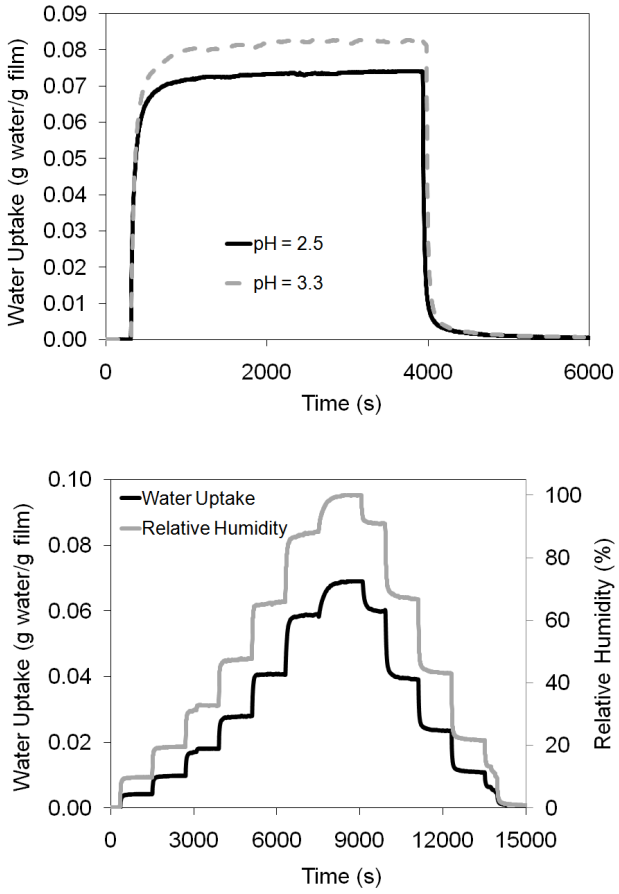

Figure 2-6. Water vapor uptake and desorption as a function of time for MEEP/PAA LbL films assembled at pH = 2.5 and pH = 3.3 at 30°C (top). A step change in the sample chamber relative humidity from 0 to 100% occurs at t=300 s, while a step change from 100 to 0% occurs at t=3900 s. Water vapor sorption isotherm at 30°C for a MEEP/PAA film assembled at pH = 2.5 (bottom).

The linear sorption isotherm from the multi-step experiment yields the films' solubility. The permeability of the film is simply calculated from Equation 1-4 as the product of solubility and the diffusion coefficient. It is important to note that while deviations from the Sauerbrey equation can exist for highly hydrated films, these deviations are minimal for thin films studied at the QCM's fundamental frequency (5 MHz).

The solubility values, diffusion coefficients, and permeability values of water in MEEP/PAA LbL films, along with neat, spun-cast MEEP and PAA films, are given in Table 2-1. PAA has a water uptake value of 0.111 g H_2O/g PAA, which corresponds to 0.32 water molecules per PAA repeat unit, while MEEP uptakes 0.027 g H_2O/g MEEP or 0.38 water molecules per MEEP repeat unit. The water transport properties of PAA are in agreement with literature; however, the water uptake of MEEP is lower than previously reported values and may be attributed to differences in film processing.[43, 67] The water uptake of the MEEP/PAA LbL films is between that of MEEP and PAA, which is expected because the LbL films are homogenous blends of the two polymers. MEEP/PAA films assembled at pH = 3.3 absorb 22.7% more water on a gravimetric basis than pH = 2.5 films, most likely due the increased charge on the incorporated PAA at pH = 3.3. Overall, in the case of MEEP/PAA LbL systems, films assembled at higher pH values have larger diffusion coefficients and solubilities. For example, MEEP/PAA films assembled at pH = 3.3 have diffusion coefficients approximately 30 times larger and solubility values about 25% larger than films assembled at pH = 2.5; thus, films assembled at pH = 3.3 have water permeability values 35 times higher than films assembled at pH = 2.5. The increase in water transport properties at higher pH values is

consistent with the increase in ionic conductivity values of MEEP/PAA films at higher pH values, especially under humidified conditions.[68, 69] Regardless of the mechanism of ion transport through a polymer electrolyte, an increase in the water transport properties will result in higher ionic conductivities when the membrane is humidified.[40] Thus, the increase in ionic conductivity values of MEEP/PAA films assembled at higher pH values is attributed to better water transport, which is improved by a looser hydrogen-bond crosslinked network and the increased presence of some ionized PAA groups.

Table 2-1. Diffusion coefficients, solubilities, and permeabilites of water in MEEP/PAA films assembled at pH = 2.5 and pH = 3.3, along with neat MEEP, PAA and LbL assembled PEO/PAA films (T = 30 °C).

Polymer	**H_2O Uptake** (g H_2O/g film)	**D** (cm^2/s)	**S** (cm^3 H_2O/cm^3 film cmHg)	**P** (Barrer)
MEEP	0.027	1.31E-13	17.5	10.0
PAA	0.111	3.72E-13	70.6	0.03
MEEP/PAA (pH = 2.5)	0.066	1.72E-11	41.7	7.17
MEEP/PAA (pH = 3.3)	0.081	4.84E-10	52.8	255
PEO/PAA (pH = 2.5)[43]	0.090*	1.3E-11	28.1	36

Barrer = 10^{-10} cm^3 (STP) cm cm^{-2} s^{-1} $cmHg^{-1}$, *70% RH

The water transport in MEEP/PAA LbL films and previously assembled PEO/PAA LbL films both assembled at pH = 2.5 compares quite closely, with MEEP/PAA having a slightly higher permeability value, indicating more favorable water transport characteristics.[43] While the functional groups of MEEP and PEO are the same,

the water transport properties might also be influenced by the nature of the hydrogen-bonded network formed in each case by LbL assembly. MEEP, which presents ethylene oxide groups as side chains, may form a relatively stronger LbL hydrogen-bonded network as compared to the ethylene oxide groups contained in the backbone of PEO.

2.4 Conclusion

In conclusion, we have demonstrated the layer-by-layer assembly of MEEP/PAA thin films by utilizing the hydrogen bonding between these two polymers. The ionic conductivity of these films is tuned by changing the assembly pH of initial polymer solutions and thereby controlling the hydrogen-bonding characteristics. The growth rate of these films can be tuned over the range of < 50 nm/bilayer up to > 200 nm/bilayer, which is quite large for a LbL assembled system. At fully humidified conditions, the ionic conductivity of MEEP/PAA is over one order of magnitude higher than previously studied hydrogen-bonded LbL systems (~7 x 10^{-4} S cm^{-1} for MEEP/PAA versus 6 x 10^{-5} S cm^{-1} for PEO/PAA). This improvement in conductivity is attributed to both MEEP's superior ion transport properties and the high water transport of these blends. Using the LbL technique to tune the properties of the film is promising to obtain stable and high performance solid state electrolytes for various electrochemical energy applications. At fully dry conditions, ionic conductivity values of these films show little variation with respect to assembly conditions due to the films' similar morphology and composition, as evidenced by bulk characterization of free-standing films. Free standing films are isolated from low-energy surface substrates, which allowed for bulk characterization of thin films with DSC. Indentation experiments show that the elastic modulus of

MEEP/PAA is over an order of magnitude higher that neat MEEP, which is critical for the applications of solid polymer electrolyte systems. Finally, the water transport characteristics are quantified by gradually changing the environment's relative humidity and monitoring the weight gain/loss of thin films through a QCM technique. The kinetic and thermodynamic data obtained allows for a full characterization of water solubilities, diffusion coefficients, and permeability. MEEP/PAA films assembled at higher pH values have enhanced water uptake and transport properties, which play a key role in increasing ion transport within the films at humidified conditions.

3. Enhanced Direct Methanol Fuel Cell Performance by Methanol Resistant Multilayers

Portions of this chapter are reproduced from Avni A. Argun, J. Nathan Ashcraft, Paula T. Hammond, *Advanced Materials*, 2008, vol. 20, pg. 1539-1543, with permission of Wiley-VCH Verlag GmbH & Co. KGaA.

Abstract

Highly conductive LbL films are fabricated based on sulfonated poly(2,6-dimethyl 1,4-phenylene oxide) (sPPO) that is sulfonated using an improved reaction scheme. We have focused on the application of these LbL systems for use in direct methanol fuel cells (DMFCs), where current state-of-the-art membranes, such as Nafion suffer from high methanol permeability. When methanol permeates across the membrane, it hinders oxygen reduction at the DMFC cathode and significantly reduces the open-circuit voltage of the device. Thus, these LbL films are optimized by tuning the assembly parameters with respect to ionic conductivity (high) and methanol permeability (low). To demonstrate the use of high ionic conductivity and methanol resistance of these sPPO-based LbL films, we apply them as coatings for Nafion membranes in DMFCs. The DMFC performance of a single cell MEA with unmodified Nafion and devices where Nafion membranes are coated with LbL films of linear poly(ethylene imine)/sPPO (LPEI) and poly(diallyl dimethyl ammonium chloride)/sPPO (PDAC) are compared. The best performing LbL coated Nafion system, had a peak power of 11.3 mW cm^{-2}, which is 31.4% higher than plain Nafion. At a typical operating voltage of 0.3 V, the PDAC/sPPO coated Nafion DMFC produces 53.2% more power than unmodified Nafion.

3.1 Introduction

The worldwide need for clean and sustainable energy is ever increasing and electrochemical devices such as batteries, fuel cells, and dye-sensitized photovoltaic cells offer the most promising solutions.[70-73] At the core of these devices is an electrolyte which facilitates charge transport between electrodes. Commonly used liquid or gel electrolytes prohibit widespread use of these devices due to processing difficulties and safety concerns. However, polymer ionic conductors offer high mechanical strength and more fabrication flexibility compared to traditional electrolytes, as well as better physical separation of electrodes. Polymer electrolytes are generally thin films that facilitate the transport of a given ion or ions at predetermined operating conditions. Although the desired properties of solid polymer electrolytes depend on the device application, fast ion conduction is essential to reduce electrical resistance.

Layer-by-layer (LbL) assembly is a versatile thin-film fabrication technique which consists of the repeated, sequential immersion of a substrate into aqueous solutions of complementary functionalized materials.[11, 57] Utilizing electrostatic forces or secondary interactions such as hydrogen bonding, LbL processing provides nanoscale blending of polymers and other organic/inorganic materials which are otherwise impossible to construct. The composition, morphology, and bulk properties are controlled by adjusting assembly parameters such as pH and ionic strength. This technique has been adapted to many other platforms such as spraying, spin-assisted assembly, and roll-to-roll processing.[74] The high versatility, tunability, and ease of processing from the ability to use aqueous solutions make this system a great competitor

to traditionally assembled solid state conductors. Previously, our group has focused on LbL assembled systems that show promise as thin film conductors for photovoltaics, electrochromic devices, and fuel cells, but they were limited in scope of application due to low ion conductivity values. [39, 75, 76] To illustrate, the highest conductivity values achieved in a LbL film to date have been on the order of 10^{-5} S cm^{-1}, while typical values for fully hydrated LbL films are in the 10^{-7} to 10^{-9} S cm^{-1} range.[31, 77]

Here we report the highest ionic conductivity ever obtained from a LbL assembled thin film, 3.5 x 10^{-2} S cm^{-1} at 98% RH and 25 °C, which is an increase of three orders of magnitude in conductivity from previously reported systems and is the same order of magnitude as commercially relevant membranes such as Nafion. Furthermore, these multilayer systems exhibit low liquid methanol permeability, which permits fabrication to be at least one or two orders of magnitude thinner than Nafion. This combination of properties provides a direct application of these films as proton-exchange membranes in direct methanol fuel cells (DMFCs). In this report, we demonstrate that simply coating a Nafion membrane with 3 to 5 bilayers of a multilayer system can lead to significant increases in power output of over 50%. We describe the systematic materials design approach used to assemble these systems, the high stability achieved with these films in fuel cells, and their resulting physical properties.

3.2 Materials and Methods

Materials. PPO (M_w = 23,000), poly(allylamine hydrochloride) (PAH, M_w = 65,000), poly(4-vinylpyridine) (P4VP, M_w = 160,000), 1,2-dichloroethane (DCE), and trimethylsilyl chlorosulfonate (TMSCS) were obtained from Sigma-Aldrich, Inc. LPEI

(M_w = 250,000) and PDAC (M_w = 240,000) were obtained from Polysciences, Inc. Nafion 1135 membranes were generously provided by DuPont.

Synthesis of sPPO. PPO was sulfonated in anhydrous DCE at 85°C (reflux) for four days using TMSCS as the sulfonating agent (TMSCS:PPO molar ratio is 4:1). Dry nitrogen was bubbled throughout the reaction to remove the hydrochloric acid generated. Highly sulfonated PPO precipitate was filtered, rinsed with chloroform, dissolved in methanol and stirred overnight with 1 molar equivalent of sodium methoxide to deprotect the TMSCS group. The sodium form of sPPO (sPPO-Na) was obtained by precipitation into cold acetone followed by filtration. This polymer was then converted to the protonated form (sPPO-H) by dialyzing against 2% HCl for two days and stored until use. FTIR spectra of both the PPO and sPPO are obtained using Nicolet Magna-IR 550 spectrometer.

Layer-by-layer Assembly. Film deposition occurred by using a programmable ZEISS DS50 slide stainer. To construct LbL films, substrates were immersed in a polycation solution (LPEI, PDAC, PAH, or P4VP) for 20 minutes, followed by three two minute rinses in water, and then in sPPO for 20 minutes followed by three two minute rinses in water. The process was repeated numerous times to produce a film of desired thickness. For in-plane measurements, LbL films deposited on glass slides were placed in a conductivity cell with platinum wires as the electrodes, and tested in a humidity and temperature controlled chamber (Electro-tech Systems, Inc.). Through-plane conductivity measurements were performed by depositing 30 bilayers on patterned ITO substrates (Delta Technologies), and gold electrodes were thermally evaporated (Edwards 306, ~100nm) on the multilayers. The active area was 6 mm^2. Ionic conductivity values were

determined by impedance spectroscopy with a Solartron 1260 impedance analyzer by sweeping the frequency from 100 kHz down to 10 Hz. Thickness measurements were made by scoring the films with a razor blade and measuring the step change in height between the film and substrate with a Tencor P10 profilometer. The cross-sectional SEM of Nafion films coated with PDAC/sPPO layers are performed using JEOL 5910 SEM.

Methanol Permeation. Methanol permeability values were determined by use of a dual-chamber apparatus, where the membrane separates a methanol solution from a pure water solution. The increase in methanol concentration as a function of time is determined by the changes in the refractive index of the solution using Waters 2414 Refractive Index Detector.

Membrane Electrode Assembly (MEA) and Fuel Cells. The Nafion 1135 membrane (89.9 μm dry thickness) was treated with 3M nitric acid for two hours and stored in Milli-Q water (Millipore, 18.2 MΩ-cm) until use. MEAs were made by sandwiching either a Nafion membrane or a Nafion membrane coated with a LbL film between gas-diffusion electrodes obtained from E-Tek Inc. The anode contained unsupported Pt–Ru alloy (1:1) and the cathode contained Pt–C (60% Pt). The loading of Pt or Pt-Ru in the catalyst layer was 4 mg cm^{-2} for both anode and cathode layers. The MEA was hot-pressed at 135°C under 240 atm for 5 minutes and tested using DMFC hardware obtained from Fuel Cell Technologies, Inc. Methanol (10% v/v) was fed to the anode at a flow rate of 4 mL min^{-1} using a peristaltic pump and humidified air was supplied to the cathode at 60 mL min^{-1}. Polarization curves were generated from a Gamry PCI750 potentiostat connected to the DMFC hardware.

3.3 Results and Discussion

As mentioned above, the high methanol permeability and high processing costs of Nafion has prohibited wide-spread commercial use of DMFCs.[78] When methanol permeates across the membrane, it hinders oxygen reduction at the DMFC cathode and significantly reduces the open-circuit voltage (OCV) of the device.[79, 80] Some approaches to reduce the methanol permeability of Nafion include composite membranes with methanol barrier layers, introducing inorganic particles into the Nafion membrane, and coating Nafion with thin polyelectrolyte films.[81-84] Aromatic polyethers offer low methanol permeability and high mechanical and chemical stability that make them promising candidates for use in direct methanol fuel cells (DMFCs).[85] A survey of polymers used thus far in the literature indicate that methanol permeability is lowest in polymers containing basic groups such as amine, imine, and imidazole, and sulfur or oxygen containing aromatic polymers.[86] One of the key polymers of interest in methanol fuel cells is sulfonic or phosphonic acid-doped polybenzimidazole (PBI); however, acid doped PBI in its charged form is only accessible by dissolving PBI in highly acidic ($[H^+]$ ~ 10M) solutions, which is unfavorable for use in the LbL assembly process.[87, 88] On the other hand, more readily processed materials are accessible, and many of these have exhibited high conductivity and permselective properties toward methanol.

3.3.1 Sulfonatation of Poly(phenylene oxide)

Poly(2,6-dimethyl 1,4-phenylene oxide) (PPO) is a thermally and mechanically stable aromatic polyether with excellent chemical resistance. Sulfonated forms of PPO (sPPO) can be obtained by dissolving PPO in a common organic solvent and directly

sulfonating the aromatic ring through electrophilic aromatic substitution.[89, 90] It is expected that the increased ionic content within the sPPO matrix may ultimately result in the solubility of the polymer in water and methanol, leading to swelling and ultimately dissolution of neat sPPO cast membranes in methanol/water solutions used in fuel cells; for this reason, the degree of sulfonation reported in the literature for fuel cell applications is rarely above 40%.[91, 92] However, when highly sulfonated sPPO is ionically crosslinked in a LbL film as a polyelectrolyte complex with the corresponding polycation, the resulting film is mechanically stable, insoluble in water, and has lower affinity for methanol. A similar effect has actually been reported by Walker et al. in experiments studying the methanol permeability of ionically crosslinked blends of aminated and sulfonated aromatic polymers where the polyacid/polybase pairs exhibited higher methanol perm-resistance than the homopolymers alone.[93] An anticipated trade-off would be a loss in ionic conductivity; however, the LbL approach allows a systematic examination of the effect of different polycationic backbones ranging in hydrophilic/hydrophobic character and basicity, as well as the impact of pH and ionic strength during assembly. Here we show that by incorporating highly sulfonated PPO into LbL films and tuning the assembly parameters, we can produce robust, stable membranes assembled from aqueous solutions with high ion conduction and low methanol permeation.

PPO is soluble in most chlorinated solvents which allows for introduction of ionic carriers via postsulfonation. The sulfonation is achieved using trimethylsilyl chlorosulfonate (TMSCS) as the sulfonation agent as shown in the reaction scheme given in Figure 3-1a. Unlike harsher reagents such as chlorosulfonic acid, TMSCS allows

better control on sulfonation and prevents chain scission. It also yields a higher degree of sulfonation as the TMS groups maintain a homogeneous reaction with enough protection to screen charged sulfonated groups.[94] With conditions given in Figure 3-1a, it is possible to obtain a water soluble polymer in its sodium form with a high degree of sulfonation (>70%) determined by titration and elemental analysis. This sodium salt is converted to its protonated form by dialyzing against acidic water. FTIR spectra obtained from the KBr pellet confirmed the successful sulfonation of PPO. Two peaks at 1075 cm^{-1} and 677 cm^{-1} appeared after sulfonation, indicative of the $-SO_3$ bands. Concurrently, two peaks (823 cm^{-1} and 753 cm^{-1}) disappeared, showing the change of aromatic substitution from 1,2,4,6 to 1,2,3,4,6.[95] A thin film of sPPO is spun cast onto a glass slide to determine the ionic conductivity of the pristine polymer prior to LbL assembly. Using a two-probe conductivity cell connected to an AC impedance analyzer, the ionic conductivity is measured to be 0.34 S cm^{-1} (25 °C, 98% relative humidity) with low hydrolytic stability due to its solubility in water.

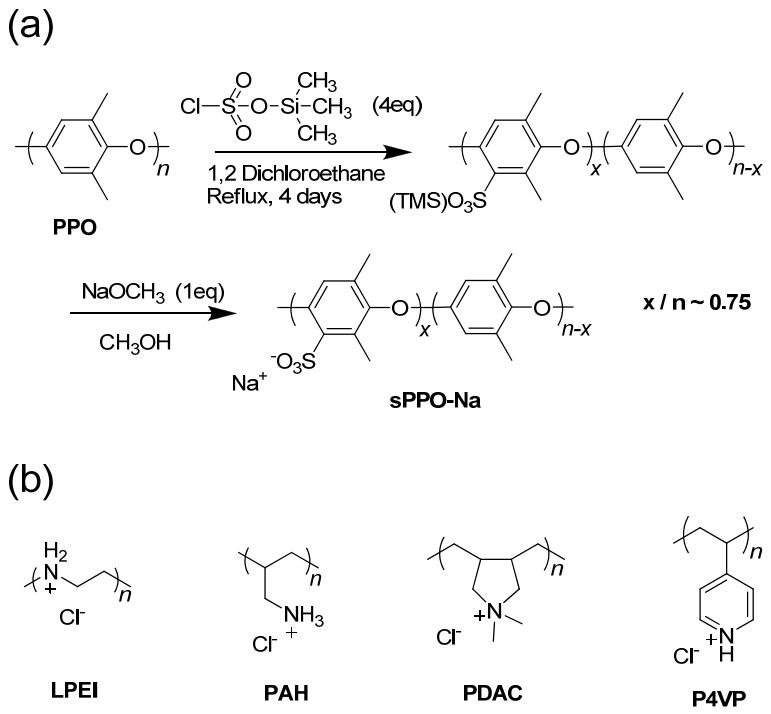

Figure 3-1. Chemical structures of polyelectrolytes used to assemble multilayer films. (a) Controlled sulfonation of PPO with TMSCS as the sulfonating agent. Highly sulfonated sodium form (sPPO-Na) is water soluble and can be converted to the proton form (sPPO-H) by dialysis against acidic water. (b) Various polycations used for LbL assembly. While the ionization of LPEI, PAH, and P4VP is pH dependent, PDAC is permanently charged in water.

3.3.2 Layer-by-Layer Films Based on Sulfonated Poly(phenylene oxide)

Figure 3-1b shows the structures of the water-soluble polycations that are paired with sPPO for the construction of LbL films. These polymers provide different degrees of hydrophilicity and basicity ranging from linear poly(ethylene imine) (LPEI) to poly(allylamine hydrochloride) (PAH), poly(diallyl dimethyl ammonium chloride) (PDAC), and poly(4-vinylpyridine) (P4VP). In order to determine the effect of assembly

parameters on conductivity, 30 bilayers of sPPO and LPEI are deposited on glass slides and placed in a humidity controlled chamber. While sPPO is a strong polyacid, the ionization degree of LPEI is controlled by systematically varying the assembly pH from 5.0 down to 1.5 for all polymer and rinse solutions. For LbL films assembled at pH = 3.0, the conductivity measurement is performed both in-plane (parallel to the substrate) and through-plane (orthogonal to the substrate) to confirm the proton conductivity is isotropic in the LbL film. Below assembly pH = 3.0, the conductivity is measured only in-plane, as the through-plane resistance of the LbL thin film is too low to accurately measure. Figure 3-2 shows the assembly pH dependence of proton conductivity for these films measured in-plane (assembly pH $\leq$ 3,) and through-plane (assembly pH $\geq$ 3). The conductivity increases from 2.00 x 10^{-5} S cm^{-1} to 2.12 x 10^{-3} S cm^{-1} by simply lowering the assembly pH from 5.0 down to 1.5. This value is already two orders of magnitude higher than the best reported value of a LbL system. Increasing the charge of a polymer results in an extended chain conformation in solution; this leads to decreases in its composition in the LbL film. Therefore, at lower assembly pH values, when LPEI becomes almost fully charged, we can maximize the amount of sPPO in the film. It is also important to note that the values obtained from through-plane and in-plane experiments match well, demonstrating that proton conduction is isotropic in these blends.

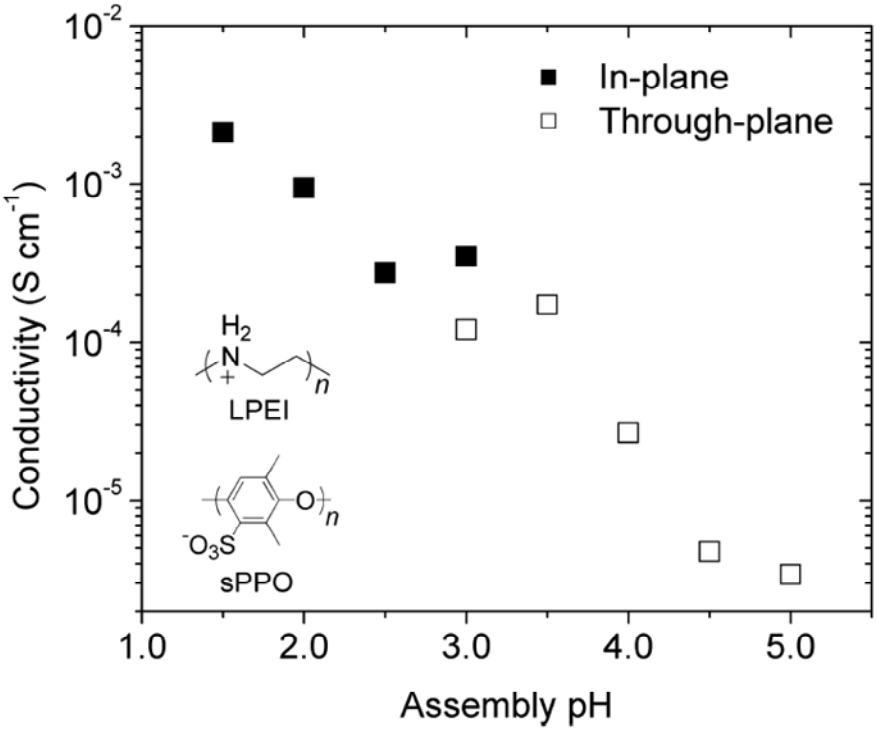

Figure 3-2. Assembly pH dependence of the ionic conductivity of 30 bilayer LPEI/sPPO films measured both in-plane and through-plane. The maximum ionic conductivity obtained from this pair is 2.12 x 10^{-3} S cm^{-1} at assembly pH = 1.5. At low assembly pH values, increased charge of LPEI results in an extended chain conformation in solution that leads to decreases in its composition; therefore maximizing the amount of sPPO in the LbL film.

To demonstrate the effect of the polycation on the resulting nanolayered polymer blends, we have paired sPPO with a more hydrophobic polycation, PDAC. In this case, both polymers are strong polyelectrolytes, permanently charged in solution independent of pH. For this reason, the control of polymer conformation is possible by screening these charges by increasing the ionic strength. With 0.5M NaCl added to the sPPO

solution only, PDAC/sPPO yields the highest conductivity value of 3.53 x 10^{-2} S cm^{-1}, approaching the fuel cell standard Nafion, which is a perfluorosulfonated ionomer that relies on conducting pores within its morphology to achieve ion transport. To the best of our knowledge, this is the highest ionic conductivity reported from a LbL assembled film. We have also used PAH and P4VP, two other pH dependent polycations, to make LbL films paired with sPPO. Table 3-1 lists the conductivity values obtained from LbL films of sPPO complexed with these polycations along with the values of Nafion. Differences in conductivity values of sPPO-containing LbL films are possibly due to variances of the relative amount of sPPO in the blends. Other factors that may impact ionic conductivity are the films' morphology, ionic crosslinking density, and secondary interactions between the PPO backbone and amine groups. For all the LbL systems studied, the conductivity is independent of film thickness, a parameter controlled by varying the number of bilayers. These new solid state ionic conductors will be of interest for a range of electrochemical applications such as fuel cells, solar conversion of water, and photovoltaics.

Table 3-1. Ionic (proton) conductivity and methanol permeability values of various electrostatic LbL films along with the values obtained from a Nafion 1135 film. The permeability values of the LbL films are calculated by incorporating the composite permeability and permeability of the substrate ($P_{Nucleopore}$ = 2.6 x 10^9 cm^2 s^{-1}) into Equation 3-1.

Membrane	Conductivity [a] [S cm^{-1} x 10^3]	MeOH Permeability (P x 10^8) [cm^2 s^{-1}]	Performance Ratio
Nafion 1135	98.0	282	0.35
PDAC/sPPO	35.3 [b]	2.18	16.0
PAH/sPPO	4.23 [c]	0.57	7.42
LPEI/sPPO	2.12 [d]	1.38	1.54
P4VP/sPPO	1.65 [c]	0.84	1.96
LPEI/PAA	0.01 [77]	N/A	N/A

[a] At 98% relative humidity [b] 0.5M NaCl in the sPPO solution [c] Assembly pH = 2 [d] Assembly pH = 1.5

With high conductivity values established, the methanol permeability of the various LbL systems is studied to determine their potential for DMFC application. A dual chamber apparatus is used, where the membrane sample, a substrate coated on both sides with a LbL film, is the separator between a 90% methanol/water (v/v) and pure water.[96] A schematic of the methanol permeation apparatus is shown in Figure 3-3. The increase in methanol concentration in the initially pure water side is monitored as a function of

time, and the following equation is used to calculate of the methanol permeability through the membrane:

$$c_B(t) = \frac{A}{V_B} \cdot \frac{P}{L} \cdot c_A(t - t_0) \qquad \text{Equation 3-1}$$

where c_B is the methanol concentration of the initially pure water solution, A is the exposed membrane area, V_B is the volume of initially pure water, P is the methanol permeability of the membrane, L is the thickness of the membrane, and c_A is the concentration of the methanol solution. A porous Nucleopore membrane was used as the substrate material for determining the permeability of LbL films. The values shown in Table 3-1, P_{LBL}, are calculated from the following series resistance model (also referred to as the ideal laminate theory) for a composite tri-layer membrane with LbL film coating both sides of the Nucleopore® membrane:[97]

$$P_{composite} = \left[\frac{\phi_{LBL}}{P_{LBL}} + \frac{\phi_{Nucleopore}}{P_{Nucleopore}} + \frac{\phi_{LBL}}{P_{LBL}} \right]^{-1} \qquad \text{Equation 3-2}$$

where ϕ_i corresponds to the thickness fraction of component i and P_i is permeability of component i. After measuring the composite membrane permeability, the permeability of the LbL film, P_{LBL}, is calculated from the measured permeability of the substrate and the thickness fraction of all components in Equation 3-2. All of the sPPO-based LbL systems have methanol permeability values at least two orders of magnitude lower than Nafion, as shown in Table 3-1. A common way to screen potential materials for use as the PEM in DMFCs is to look at the ration of ionic conductivity to methanol permeability, which is here referred to as the "performance ratio." Materials with a high conductivity to permeability ratio are the most interesting for commercial DMFC application. In fact,

among fuel cell researchers, it is acceptable to trade-off lower conductivity for reduced methanol crossover for improved DMFC performance. The last column in Table 3-1 lists the performance ratios for all of the sPPO LbL films along with Nafion. Nafion has a performance ratio of 0.35 stemming from its high ionic conductivity but relatively high methanol permeability. All sPPO-based LbL films have performance ratios above 1.5 due to significantly lower methanol permeability values. PDAC/sPPO has the highest performance ratio of 16.0 indicating this is the most promising PEM system and its performance in DMFCs is studies below.

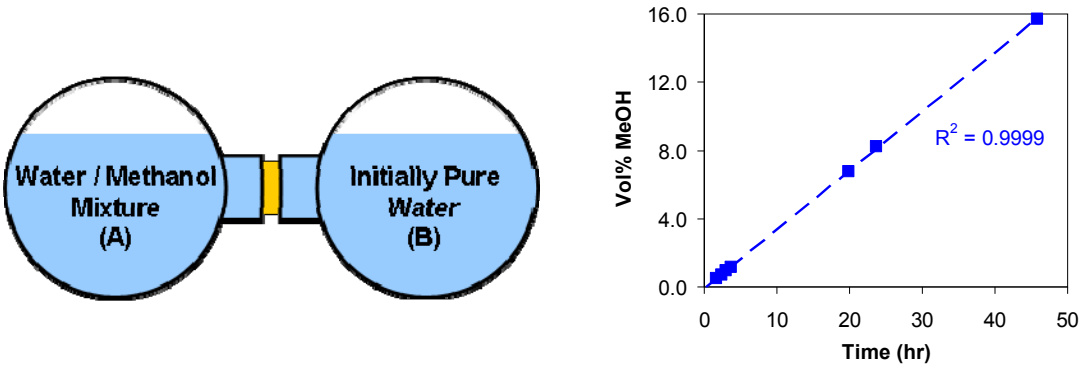

Figure 3-3. Schematic of the dual chamber apparatus used for methanol permeation measurements (left). The composite LbL membrane separates a 90% methanol/water (v/v) (side A) from pure water (side B). The increase in methanol concentration in the initially pure water side (B) is monitored versus time (right), and methanol permeability values are determined from Equations 3-1 and 3-2.

In general, the more sulfonated the PPO systems are, the more permeable they are to methanol, thus eliminating any advantage with respect to Nafion when used in the solid state. However, by introducing various polycations lightly crosslinked with sPPO, it

is possible to lower methanol permeability without sacrificing the ionic conductivity. For example, while the ionic conductivity of PDAC/sPPO is ~3-fold lower than Nafion, having methanol permeability values over two orders of magnitude less than Nafion provides a window where coating Nafion with a thin layer of this LbL material can enhance fuel cell performance. To ensure that Nafion is uniformly coated in the LbL assembly process, a cross-sectional SEM image of Nafion coated with 50 bilayers of PDAC/sPPO is shown in Figure 3-4. The same film deposited onto glass is 2.5 μm thick, and Figure 3-4 confirms that this amount of film is also deposited onto Nafion during the LbL assembly process. Figure 3-4 also shows that there is a sharp transition between the amorphous Nafion on the right and the lighter shaded band of LbL film, which further confirms that the LbL film conformally coats and does not penetrate into the Nafion membrane.

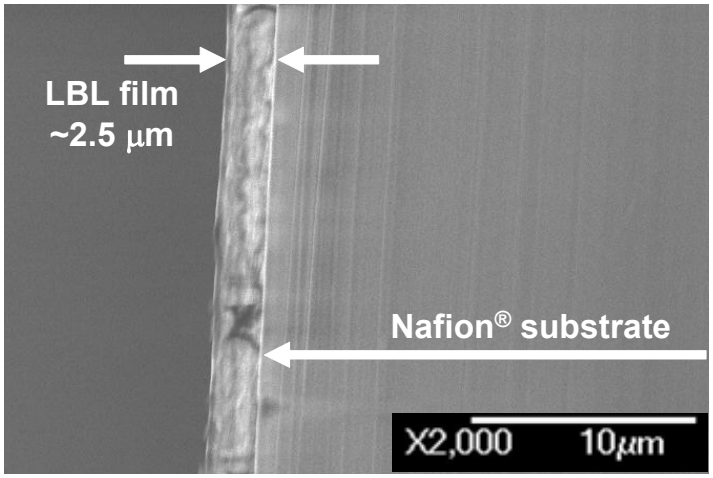

Figure 3-4. SEM cross-sectional image of Nafion 1135 coated with 50 bilayers of PDAC/sPPO. Nafion 1135 is the amorphous region on the right side, and the LbL film is the lighter band adhered to the surface of the Nafion membrane. Note the sharp transition at the Nafion/LbL film interface.

3.3.3 Direct Methanol Fuel Cell Performance

To demonstrate the use of high ionic conductivity and methanol resistance of sPPO based LbL films, we report their utilization as coatings for Nafion membranes in DMFCs. The DMFC performance of a single cell MEA with unmodified Nafion and devices where Nafion membranes are coated with LbL films of LPEI/sPPO and PDAC/sPPO are shown in Figure 3-5. All three devices were tested at the same conditions with 10% methanol/water (v/v) fed to the anode and air to the cathode at 25°C. We found that for each LbL system used, there are an optimal number of bilayers that result in the best DMFC performance for coating Nafion. The best performing system, PDAC/sPPO coated Nafion, had a peak power of 11.3 mW cm^{-2}, which is 31.4% higher than plain Nafion. The LPEI/sPPO coating had a more modest improvement in peak power of 22.1% above plain Nafion. At a typical operating voltage of 0.3 V, the PDAC/sPPO coated Nafion DMFC produced 53.2% more power than unmodified Nafion, while the LPEI/sPPO coated device improved 36.2% in power output. Also, the OCV for both Nafion coated devices improved to 493 mV, which is almost 40 mV higher than plain Nafion. We attribute the higher OCV of the coated membranes to the fact that the LbL systems have lower methanol permeability values than Nafion.

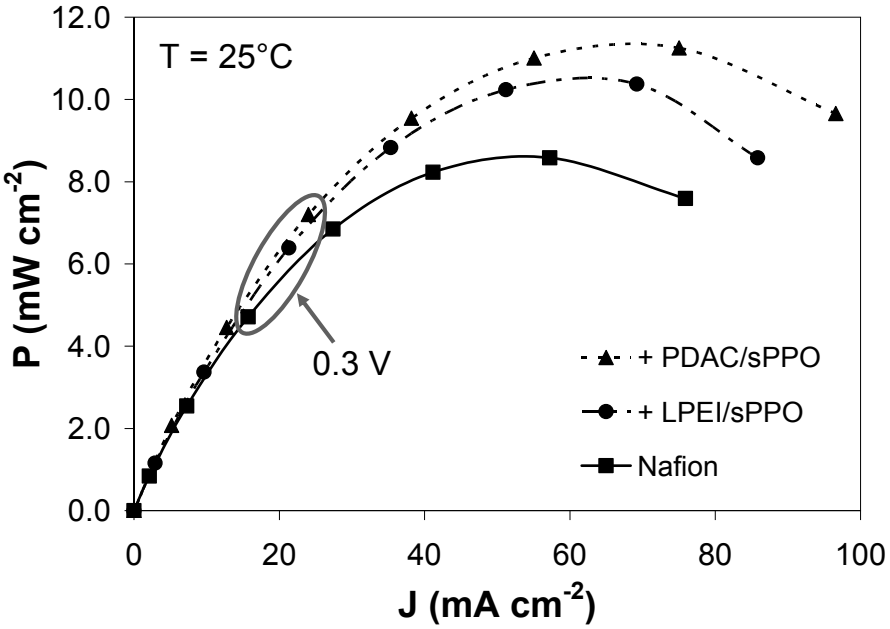

Figure 3-5. Power curves of single MEA DMFCs comparing unmodified Nafion devices with Nafion membranes coated with LbL films of LPEI/sPPO and PDAC/sPPO. For each LbL pair, there are an optimum number of bilayers to maximize the power output. At a typical operating voltage of 0.3 V, the PDAC/sPPO coated Nafion DMFC produced over 50% more power than unmodified Nafion, while the LPEI/sPPO coated device improved 36.2% in power output. Also, the OCV of both Nafion coated devices improved by 40mV as a result of lower methanol permeability.

However, since the LbL systems have lower proton conductivity values, we observed a trade-off between reduced methanol permeability and decreased conductivity as we increase the thickness of the LbL coatings. For LPEI/sPPO, the optimal coating was ten bilayers corresponding to a 0.15 μm thick film on both sides of Nafion, while three bilayers of PDAC/sPPO, which is 0.13 μm of film, is the optimum for this LbL system. Devices with thinner LbL coatings than shown in Figure 3-5 had improved

performance over Nafion, but not as significant as in Figure 3-5. Increasing the thickness of the LbL coating above what is shown in Figure 3-5 resulted in decreased fuel cell performance. Therefore, below the optimal coating thickness, the reduced methanol permeability of the composite membrane outweighs the decrease in ionic conductivity, and above the optimal coating, the reduction in ionic conductivity dominates, causing a decrease in device performance. For PDAC/sPPO coated Nafion PEMs, the power output at 0.3 V of DMFCs where Nafion is coated with 0, 6, 9, or 12 bilayers is shown in Figure 3-6. The DMFCs are tested at three different operating temperatures to observe any trends in performance at temperatures above ambient temperatures. The performance drop-off for Nafion with more than 6 bilayers of PDAC/sPPO coating is significant, especially considering the high ionic conductivity and low methanol permeability of PDAC/sPPO detailed in Table 3-1. Based on the growth of PDAC/sPPO LbL films and its ionic conductivity (and a 1 cm^2 active fuel cell area), the ohmic resistances for a 6 bilayer and 12 bilayer film are 4.1 mΩ and 8.2 mΩ, respectively. Thus, the increase in 4.1 mΩ of resistance from 6 bilayers to 12 bilayers of coating cannot account for the decrease in performance. However, the ohmic resistances of the DMFCs, measured fitting the linear part of the polarization curves on the assembled MEAs, increased from 1.55 Ω for the 6 bilayer coated Nafion to 9.10 Ω for the 9 bilayer coated Nafion. So the increased resistance and decreased power for coatings above 6 bilayers likely comes from when the MEA is fabricated and could be due to contact resistances between the commercial gas diffusion electrodes (design specifically for Nafion) and the composite Nafion PDAC/sPPO PEM. Additionally, since PDAC/sPPO imparts reduced methanol

permeability for the PEM, the additional 6 bilayers should only increase DMFC performance.

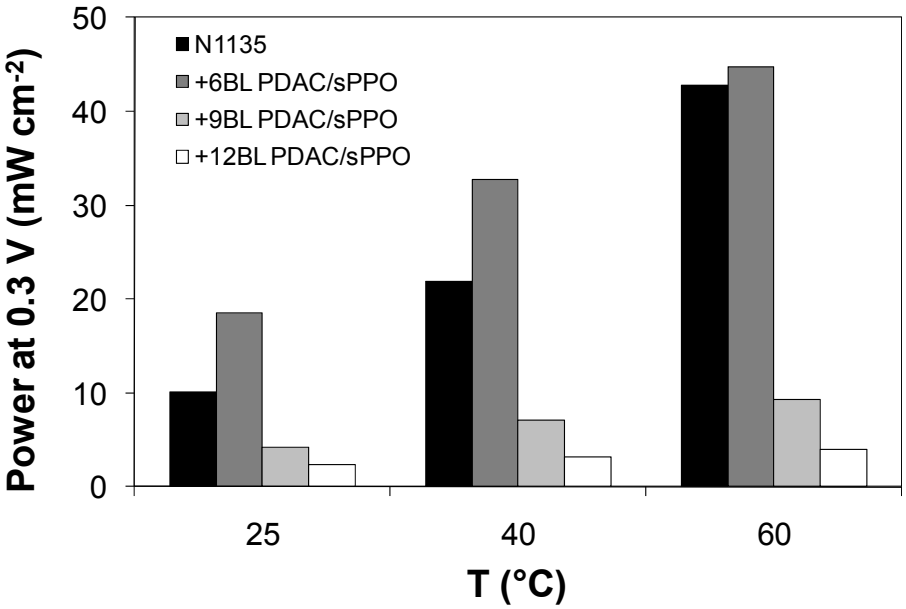

Figure 3-6. Power output at 0.3 V of single MEA DMFCs where the PEM is Nafion or Nafion coated with 6, 9, or 12 bilayers of PDAC/sPPO. The DMFCs are tested at three different operating temperatures. The performance drop-off for Nafion with more than 6 bilayers of PDAC/sPPO coating is striking based on the high ionic conductivity and low methanol permeability of PDAC/sPPO.

To further probe the performance of DMFCs using composite LbL coated Nafion PEMs, the OCV of same series of DMFCs shown above is presented in Figure 3-7. The OCV, as described above, is a measure of the DMFC's voltage when no current is drawn through the system. The OCV of the coated Nafion follows a similar trend to the power output values seen in Figure 3-6, namely the OCV increases when 6 bilayers of

PDAC/sPPO is applied to Nafion, but the OCV decreases for thicker LbL coatings. Normally, a comparison of OCV values for similar PEMs and MEAs could provide insight into the fuel crossover of the different systems, but in this case the high ohmic resistance values noted above factor into the OCV values shown here. Taken together, the OCV values in Figure 3-7 along with the power output values in Figure 3-6, corroborate that the high contact resistance between the PEM and gas diffusion electrodes prevent the benefits of the LbL coated Nafion PEMs from being observed. An electrochemical methanol crossover technique, shown in Figure A-4, is also employed, but suffers from the same contact resistance errors observed in the power output values and OCV values. The gas diffusion electrodes used in this study are optimized for Nafion membranes, as the catalyst particles are applied from a Nafion dispersion. The development of catalyst dispersions and MEAs better suited for PDAC/sPPO, although outside the scope of this thesis, could show the true promise of PDAC/sPPO PEMs for DMFCs.

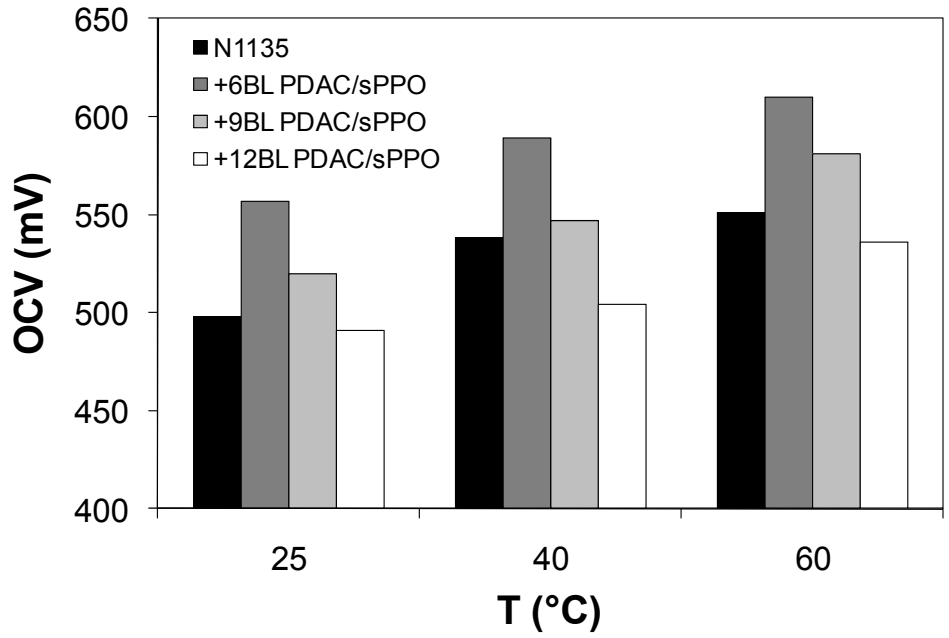

Figure 3-7. OCV of single MEA DMFCs where the PEM is Nafion or Nafion coated with 6, 9, or 12 bilayers of PDAC/sPPO. The DMFCs are tested at three different operating temperatures. The decrease in OCV above 6 bilayers is consistent with the decreased power output for the same DMFCs.

3.4 Conclusion

In summary, using the LbL technique, we have generated a novel solid state thin film with conductivity values over three orders of magnitude higher than the previous best performing multilayer films, making the LbL system a competitor for fuel cell and other solid state electrolyte applications. By pairing sPPO with PDAC in a LbL film and optimizing the assembly conditions, we achieved ionic conductivity values up to 3.53 x 10^{-2} S cm^{-1}. In addition, the studied LbL films are highly methanol resistant with permeability values two orders of magnitude lower than Nafion. The performance ratio

of PDAC/sPPO is 16.0 and is substantially higher than Nafion at 0.35. Coating Nafion membranes with PDAC/sPPO improved DMFC performance by over 50% compared to unmodified Nafion. Due to the trade-off between ionic conductivity and methanol permeability in PDAC/sPPO films as compared to Nafion and the contact resistances between PDAC/sPPO and the gas diffusion electrodes used, an optimal coating thickness of less than 10 bilayers is seen for all LbL systems coated onto Nafion. The development of catalyst dispersions and MEAs better suited for PDAC/sPPO could allow PDAC/sPPO PEMs to be fully realized in DMFCs. Currently, we are developing LbL free standing films from these materials as a way of eliminating the need for a substrate. Since the LbL process involves water soluble processing with a highly controlled film composition, we anticipate that these highly conducting films have great potential to be used in other electrochemical systems requiring highly conductive solid state electrolytes such as batteries, dye-sensitized photovoltaic cells, electrochromic devices, and sensors.

4. Structure-Property Studies of Highly Conductive Layer-by-Layer Assembled Membranes

Abstract

Layer-by-layer (LbL) films composed of poly(diallyl dimethyl ammonium chloride) (PDAC) and sulfonated poly(2,6-dimethyl 1,4-phenylene oxide) (sPPO) (PDAC/sPPO) are studied while varying the ionic strength of assembly solutions to determine the nature of the exceptionally high ionic conductivity of this system. Film growth is modulated from 6.91 nm/bilayer (BL) when assembled with no salt to 62.2 nm/BL when assembled with 0.5 M salt in all assembly solutions. However, at optimized assembly conditions of 1.0 M salt in only the sPPO assembly solution, fully humidified PDAC/sPPO films have ionic conductivity values of 7.00×10^{-2} S cm^{-2} at 25 °C, which is the highest value reported for any LbL system. Selectively adding salt to the sPPO assembly solution decreases the ionic crosslink density of the films and increases the water uptake, yielding high ionic conductivity. Thermal gravimetric analysis (TGA) and elemental analysis interestingly show little compositional variation as films are assembled with different salt concentrations in the assembly baths. Additionally, PDAC/sPPO films fabricated using a recently developed spraying technique allows for the preliminary characterization of the mechanical properties of free-standing membranes.

4.1 Introduction

The development of solid polymer electrolytes with improved performance is critical for the advancement of electrochemical energy devices including hydrogen and direct methanol fuel cells (DMFCs), batteries, dye-sensitized solar cells, and electrochromic systems. An essential property for polymer electrolytes in these applications is high ionic conductivity, which reduces internal resistances, thus improving overall device and system efficiencies. Depending on the specific application, the polymer electrolyte must maintain high ion transport at the required operating conditions (i.e. temperature and humidity) while also exhibiting mechanical durability and chemical stability.[38] For hydrogen and DMFCs, membranes comprised of perfluorosulfonic acid polymers such as Nafion are most commonly used because of superior protonic conductivity at humidified conditions coupled with high mechanical integrity and chemical stability.[5, 98] For hydrogen fuel cells, proton exchange membranes (PEMs) capable of operating at higher temperatures (> 100 °C) and lower humidity (< 50 % RH) are needed to take advantage of improved catalyst kinetics at higher temperature, minimize catalyst poisoning and allow use of less pure fuel streams, and to reduce system complexity associated with external humidification.[99, 100] Current membranes for DMFCs suffer from high fuel cross-over, a phenomena where methanol permeates across the fuel cell from the anode to the cathode causing reduced power output.[101] Methanol cross-over decreases the fuel utilization of the DMFC and polarizes the oxygen electrode, significantly reducing DMFC efficiency.[102, 103]

To minimize the impact of methanol crossover, DMFCs are typically operated with diluted methanol feed solutions of 2 M methanol or lower at the expense of lower system energy densities. Thus, significant effort has been undertaken to develop membranes with reduced methanol permeability, commonly by synthesizing alternative polymer materials or by modifying existing membranes. Some of the alternatives to perfluorosulfonic acid modified polymers include acid-functionalized or -doped polysulfones, poly(ether sulfone)s, poly(ether ketone)s, polybenzimidazoles, polyimides, and polyphosphazenes.[86, 104] Examples of Nafion modifications include impregnation with additional polymers, insertion of metal and metal oxide particles, exposure to irradiation, doping with alternative cations, and applying methanol barrier surface coatings.[105-111] Efforts to reduce the methanol crossover of Nafion by modification often result in decreased ionic conductivity or reduced mechanical properties of the composite membrane. However, we recently reported a layer-by-layer (LbL) assembled system of poly(diallyl dimethyl ammonium chloride) (PDAC) and highly sulfonated poly(2,6-dimethyl 1,4-phenylene oxide) (sPPO) with high ionic conductivity (3.5×10^{-2} S cm^{-1}) and methanol permeability values two orders of magnitude lower than Nafion.[112] When applied as a coating to a Nafion 1135 membrane, DMFC power output improved by 53.2% when tested at 25 °C with 10% methanol as the fuel and air supplied to the cathode.

LbL assembly is a rapidly growing technique for producing functional thin films containing two or more functional materials.[10, 11] The fabrication process consists of alternately submerging a substrate into solutions of materials with complementary functional groups, such as solutions of polycation and polyanion, and repeating until a

film of desired thickness is formed. LbL assembly typically produces homogenous polymer blends that can be tuned with respect to morphology, composition, and thickness by adjusting the assembly bath conditions such as ionic strength for strong polyelectrolytes or pH for weak polyelectrolytes. The relative simplicity and tremendous versatility of the LbL assembly technique has allowed for the exploration of LbL assembly in numerous solid state electrolyte and electrochemical energy applications.[57] Farhat and Hammond first reported using a LbL assembled system in a fuel cell by creating a composite membrane of poly(ethylene oxide)/poly(acrylic acid) (PEO/PAA) multilayers coated on a porous support and testing in a hydrogen fuel cell.[39] Despite suffering from low power output, this work has inspired the application of LbL to other fuel cell systems, with the most promising results being methanol barrier coatings for Nafion in DMFCs.[81, 113]

To further advance this growing field of application for electrostatically assembled thin films in electrochemical systems, there is a need to understand the mechanisms of ion transport in polyelectrolyte multilayers. Durstock and Rubner first studied the ionic conductivity of LbL films where they observed a maximum conductivity of 1×10^{-7} S cm^{-1} for a poly(allylamine hydrochloride)/poly(sodium 4-styrenesulfonate) (PAH/SPS) films, noting the importance that assembly conditions, ionic strength in this case, and plasticization by water have on ion transport in these polyelectrolyte blends.[114] A subsequent study by Farhat and Schlenoff demonstrated that ion transport in multilayer films is improved by doping the film with additional ions after assembly, and Delongchamp and Hammond showed that LbL films that were less ionically crosslinked, achieved by shielding the polymers' charged functional groups

with salt during assembly, yield LbL films with significantly improved ionic conductivity values.[34, 37] Other studies on ion transport in multilayer systems have examined the preferential transport of monovalent ions over divalent ions for certain LbL systems.[35, 36] Lastly, the incorporation of Nafion as a component of LbL films has been attempted, but the ionic conductivity of these films are several orders of magnitude lower than Nafion, likely caused by the disruption of the ionic pathways present in the nanoporous morphology of commercially processed Nafion films.[37, 115]

Here we report the characterization of highly conducting PDAC/sPPO LbL films and seek to understand structure-property relationships by analyzing this system at different assembly conditions. By varying the assembly conditions, primarily the ionic strength of the deposition solutions, an understanding of the nature of the high ionic conductivity of this system is obtained and understood with respect to film growth, morphology, composition, and water uptake and transport. The addition of salt to the assembly baths impacts the growth rate and ionic crosslink density, which results in changes in the ionic conductivity and water management of these films. The addition of salt to all assembly solutions, and the selective addition of salt to only sPPO during fabrication are studied. Transmission electron microscopy (TEM) is employed to analyze the homogeneity of these LbL blends. While the composition of LbL films can be difficult to ascertain, thermal gravimetric analysis (TGA) and elemental analysis are used to probe the composition of PDAC/sPPO films assembled at varying conditions. A quartz crystal microbalance (QCM) technique allows for the precise measurement of the water uptake and permeability in these films. We also utilize a newly developed spraying technique as a way to rapidly assemble free-standing LbL membranes for direct use in

DMFCs; large scale thin films created using this processing method have enabled the measurement of mechanical properties of these systems.

4.2 Materials and Methods

Chemicals. PPO (Mw = 23,000), 1,2-dichloroethane (DCE), and trimethylsilyl chlorosulfonate (TMSCS) were obtained from Sigma-Aldrich, Inc. PDAC (Mw = 240,000) was obtained from Polysciences, Inc. PPO was sulfonated by a previously reported technique to obtain highly sulfonated (> 70% degree of sulfonation), water soluble sPPO.[112]

Dip-Assisted LbL Assembly. Film deposition occurred by using a programmable ZEISS DS50 slide stainer. For LbL film fabrication, substrates were immersed in PDAC for 20 minutes, followed by three two minute rinses in water, and then in sPPO for 20 minutes followed by three two minute rinses in water. The concentration of the polymer solutions was 10 mM for both PDAC and sPPO solutions based on the molecular weight of repeat units. The process was repeated numerous times to produce a film of desired thickness. After assembly, films were rinsed in slightly acidic (~ pH = 2) water to remove any excess salt ions and to ensure that the film is protonated.

Spray-Assisted LbL Assembly. Sprayed films were deposited using the same polymer and rinse solutions mentioned above. Using a home-built automated spraying setup, three airbrushes were pressurized with air at 30 psi and the spray nozzles were directed towards a vertically-mounted substrate rotating at 12 rpm (substrate diameter ~ 7.5 cm).[116] The automated program was then run by a logic relay, spraying the PDAC and sPPO solutions for 3 seconds, with 10 seconds of rinse water spray in between the

polymer sprays to obtain one bilayer. This cycle was repeated to obtain the desired number of bilayers.

Characterization. For ionic conductivity measurements, LbL films were deposited on glass slides and placed in a conductivity cell with two platinum wires as the electrodes, and tested in a humidity and temperature controlled chamber (Electro-tech Systems, Inc.). Impedance values were determined by impedance spectroscopy with a Solartron 1260 impedance analyzer by sweeping the frequency from 100 kHz down to 10 Hz. Thickness measurements were made by scoring the films with a razor blade and measuring the step change in height between the film and substrate with a Tencor P10 profilometer. For bulk characterization, LbL films were also assembled on Teflon substrates and gently peeled off after assembly, similar to a previous report.[117] For thermal analysis, samples were thoroughly dried, and placed in a TA Instruments Q50 Thermogravimetric Analyzer. Under a constant nitrogen purge, samples were heated from 50 °C up to 900 °C at a rate of 10 °C/min. Elemental analysis of the LbL assembled polymers were performed by Midwest Microlab, LLC (duplicate analysis for the atoms C, H, N, and S). FTIR measurements were performed using a Nicolet Magna 860 infrared spectrometer. Films were assembled as free-standing films or on IR-transparent silicon substrates and examined in transmission mode. Uniaxial cyclic tensile tests were conducted on rectangular specimens of films, performed at ambient conditions with an EnduraTEC Electroforce 3200. TEM images were generated on a JEOL 200 CX operated at 200 kV. Ultrathin cross sections were microtomed for at room temperature with a diamond knife and collected on copper grids.

QCM/Water Uptake. A Masscal G1 (quartz crystal microbalance/heat conduction calorimeter, QCM/HCC) was used for analysis of water uptake and transport in LbL films.[118, 119] LbL films were deposited onto 1 inch diameter quartz crystals (5 MHz frequency) with gold electrodes from Masscal Scientific Corp. For all experiments, the temperature of the G1 sample chamber was maintained at 30 °C. Two mass flow controllers supply nitrogen streams to the G1 sample chamber. One nitrogen stream is kept dry, while the other is humidified to 100% relative humidity (RH). Varying the ratio of these to streams through the G1 software allows fine control of the sample chamber RH. The total gas flow rate was 50 cm3(STP)/min for all experiments. The RH of the G1 samples chamber is monitored using a Sable Systems R300 water vapor analyzer. Films were exposed to a dry nitrogen purge to determine the amount of film formed on the crystal by comparison with the frequency of the blank crystal before coating. After the films were fully dried, a step change in RH of the sample chamber from 0 to 100% is introduced. The frequency change of the coated crystal caused by water uptake into the films was monitored in real-time. Mass uptake is directly proportional to the frequency change, as given by the Sauerbrey equation.[120] Dried films were also exposed to incremental step changes in relative humidity up to 100% RH to yield a sorption isotherm. To ensure that condensation in the sample chamber did not occur, the frequency change of a blank QCM crystal was observed to be negligible when exposed to a full range of relative humidity conditions.

4.3 Results and Discussion

4.3.1 Layer-by-Layer Film Growth

The LbL system investigated, PDAC/sPPO, was recently reported to have the highest ionic conductivity of any LbL assembled film and was shown to improve the power output of DMFCs when coated onto a traditional Nafion fuel cell PEM by blocking methanol permeation while maintaining ion conductivity.[112] A previous report briefly described this system's high conductivity at optimized assembly conditions, but did not explore the changes in film properties induced by adjusting the assembly conditions, primarily changing the ionic strength in one or more assembly baths. In addition to changes in ionic conductivity, other properties, including LbL film growth and thickness, thermal decomposition, and water transport are studied at varying assembly conditions. The chemical structures of both PDAC and sPPO are shown in Figure 4-1 along with the LbL growth curves with increasing amounts of NaCl in the assembly solutions for films assembled on glass slides. At all assembly conditions, a delay in the linear LbL growth is observed in the first few deposition cycles, which has previously been reported for dipped LbL systems.[121-123] In this delayed growth regime (< 10 BL), the substrate surface impacts film growth as polymers deposit on nucleation sites on the substrate and form LbL "islands" that coalesce together within the first 3-10 BL.[124] For solid polymer electrolytes, relatively thick films (several microns or more) are needed, so the initial growth regime of this polymer pair is less relevant compared to the bulk film's growth, morphology, and properties.

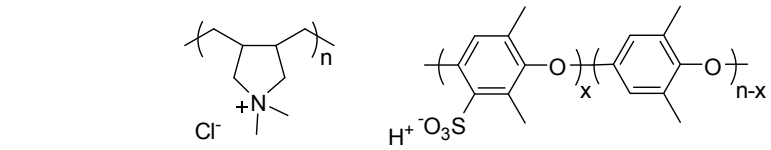

PDAC sPPO

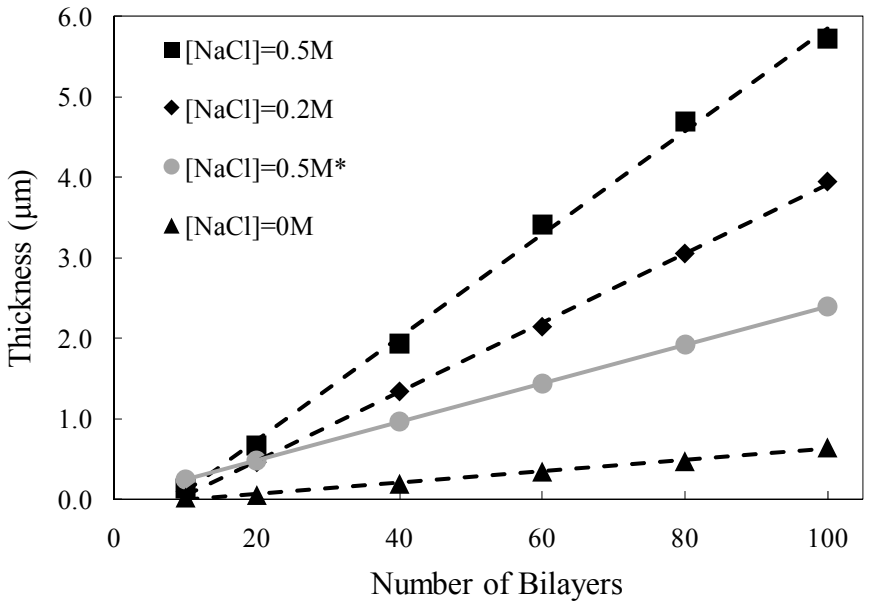

Figure 4-1. Chemical structures of PDAC and sPPO (top). Growth curves for PDAC/sPPO at several different assembly conditions (bottom). The salt concentration given is for all assembly baths, both polymer solutions and all rinse water, except for one film made with only salt in the sPPO solution (*). All films exhibit linear growth after a delayed growth period of 5-10 bilayers.

The growth rate of PDAC/sPPO films can be tuned from 6.91 nm/bilayer (BL) when assembled with no salt in either assembly solution up to 62.2 nm/BL when assembled with 0.5 M salt in all assembly solutions, including the rinse solutions. Films assembled with 0.2 M salt in all assembly baths have a growth rate of 42.9 nm/BL, in

between that of the no salt and 0.5 M salt conditions, showing the tunability of the growth of this system through modulation of the ionic strength of the assembly baths. The growth behavior of PDAC and sPPO, both strong polyelectrolytes, is consistent with previous studies of PDAC/SPS films.[12, 125, 126] As the LbL film is fabricated, the surface charge of the film alternates between positive (PDAC) and negative (sPPO), and this phenomena of overcompensation allows the film to grow.[10] The addition of salt to the assembly solutions shields charge on the surface of the LbL film and on the polymers depositing onto the film, resulting in thicker bilayers and increased growth rates. These thicker, loopier layers are also understood to have lower ionic crosslinking densities.[37] We also investigated the growth of PDAC/sPPO films when salt is only added to the sPPO assembly solution and not to the PDAC solution or any rinse baths. As is also shown in Figure 4-1b, when 0.5 M NaCl is added to only the sPPO assembly solution, PDAC/sPPO films grow at 24.0 nm/BL, which is higher than films with no salt in any assembly bath but lower than when 0.2 or 0.5 M NaCl is present in all solutions. Thus, the same trend of forming thicker films with the addition of salt to assembly solutions is observed when salt is only added to one of the polymer deposition baths. The impacts of selectively adding salt to only sPPO during assembly as compared to adding salt to all assembly baths will be discussed below with respect to film composition, morphology, ionic conductivity, and water transport.

To determine whether there is a specific morphology characteristic of the PDAC/sPPO coating on the substrate, we have obtained a cross-sectional TEM image of a Nafion substrate coated with 12 bilayers of PDAC/sPPO thin film (Figure 4-2). The image confirms that the thickness is consistent with the growth rates obtained above

(~180 nm for 12 bilayers) and the resulting film is uniform and continuous. The LbL film has a darker overall contrast than the substrate, which is likely due to a higher electron density of the aromatic sPPO in contrast to the fluorinated copolymer, and the higher sulfur and oxygen content of the LbL film in general. The multilayer film does not show any signs of a stratified morphology, which is a good indication of intimate blending of the polycation and polyanion due to the chain interpenetration that is characteristic of the electrostatic assembly of polyelectrolytes. In Figure 4-2, it is possible to detect a nanoporous morphology in the Nafion film which corresponds to the sulfonic acid lined pores generated in the film via a form of nanophase segregation with acidic treatment.

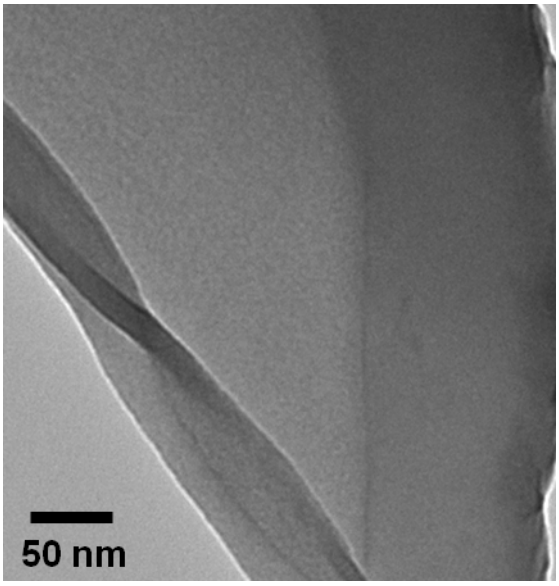

Figure 4-2. Cross-sectional TEM images of a 12 bilayers PDAC/sPPO film coated on a Nafion substrate. The LbL film (right side, top) has a darker overall contrast than the underlying Nafion substrate (left side).

There are no such features present in the PDAC/sPPO multilayers, which appear as featureless thin films with uniform composition. Figure 4-2 also shows that there is a sharp transition between the underlying membrane substrates and the darker band of the LbL film, further confirming that the coating is conformal and does not penetrate into the underlying substrate.

4.3.2 Ionic Conductivity

Figure 4-3 shows the relative humidity dependence of in-plane proton conductivity for PDAC/sPPO films assembled at various ionic strengths. Since LbL assembly yields homogenous blends of polymers rather than stratified layers, the proton conductivity is isotropic and in-plane (parallel to the substrate) measurements yield accurate bulk conductivity values. Both PDAC and sPPO are strong polyelectrolytes, permanently charged in solution, and thus the control of LbL film layer thickness is possible by screening these charges with salt as discussed above. All films show similar humidity dependence; the proton conductivity improves approximately 5-7 fold with every 20% increase in humidity. The dependence is also similar to that of pristine sPPO films (not shown here), indicating that the proton conduction mechanism of the LbL films is analogous to the charge transport mechanism of sulfonate groups in sPPO. With no charge screening (no salt added during assembly), the conductivity of PDAC/sPPO is 1.29×10^{-3} S cm^{-1} at fully humidified conditions. As the ionic strength of the assembly baths is increased, the proton conductivity benefits from relaxed chain conformation and lighter crosslinking density between polyelectrolytes, consistent with increased growth rates in Figure 4-1. This has also improved the water uptake properties as discussed

below. Furthermore, when 1.0 M NaCl is added to the sPPO assembly solution only, PDAC/sPPO yields the highest conductivity value of any LbL system, 7.0 x 10^{-2} S cm^{-1}, approaching the values of industry standard PEMs such as Nafion. We believe that the increased conductivity is a synergistic combination of both better water transport and greater free volume due to a lower effective crosslinking density. The extensive list of conductivity values for PDAC/sPPO at various assembly conditions is summarized in Table 4-1, which demonstrates the tunability of ionic conductivity by simply varying the conditions during the LbL assembly. It is important to note that the salt ions added during the assembly step act to shield the polymer backbones; however, they are rapidly rinsed away during the rinsing steps, and small counterions do not remain within the films in high concentrations following polyion assembly.

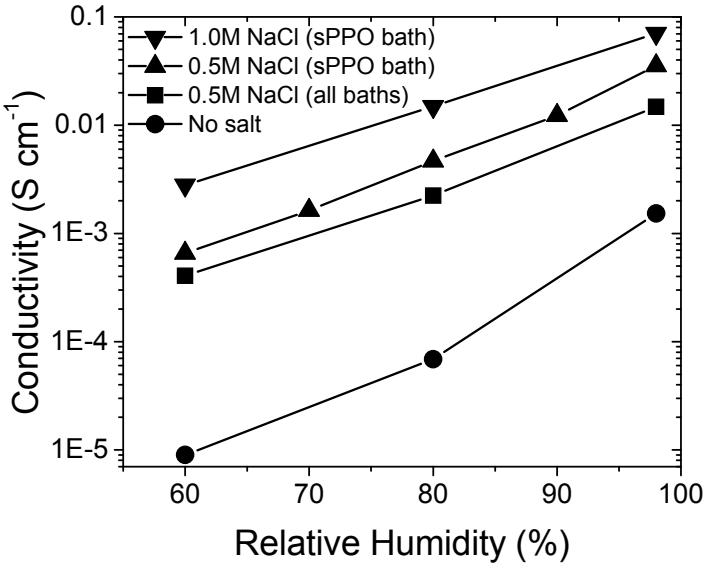

Figure 4-3. Relative humidity dependence of ionic conductivity of PDAC/sPPO films assembled at various ionic strengths. Note that the selective addition of NaCl in sPPO baths result in higher ionic conductivity values.

Table 4-1. The assembly condition dependence of proton conductivity for PDAC/sPPO films. Data are averages over 50 points.

Assembly Condition / Ionic Strength	Proton Conductivity at 98% RH (S cm^{-1})
No salt	1.29×10^{-3}
0.2 M NaCl (All baths)	5.60×10^{-3}
0.5 M NaCl (All baths)	7.09×10^{-3}
1.0 M NaCl (All baths)	2.40×10^{-2}
0.2 M NaCl (sPPO bath only)	1.12×10^{-2}
0.5 M NaCl (sPPO bath only)	3.51×10^{-2}
1.0 M NaCl (sPPO bath only)	7.00×10^{-2}

For comparison, the proton conductivity of pristine sPPO at 98% RH is 3.35×10^{-1} S cm^{-1}

In sulfonated PEMs, proton conduction is generally accepted to be through the Grotthuss mechanism, where the protons hop between ionized sulfonate groups. The temperature dependence of conductivity of LbL films when immersed in deionized water is investigated to verify the mechanism of conduction.[127] A free-standing PDAC/sPPO film (~ 9 μm thick) is prepared on a polystyrene substrate followed by careful removal from the substrate via lift-off and thoroughly rinsing in deionized water. The proton conductivity dramatically increases from 2.5×10^{-2} S cm^{-1} at 30 °C to 9.0×10^{-2} S cm^{-1} at 80 °C. An Arrhenius type dependency is observed (see supporting information) with activation energy of about 25.6 kJ mol^{-1}, which is lower than that of pristine sPPO films reported in literature (~40 kJ mol^{-1}), suggesting a more favorable medium for proton transport.[126, 128] For comparison, the temperature dependent conductivity of an 89.9 μm

thick Nafion film (Nafion 1135) is tested in water over the same temperature range to yield an activation energy of 11.7 kJ mol^{-1}. It is also worth mentioning that the activation energy value observed for the PDAC/sPPO film is much lower than the sPPO films measured at low humidity conditions (~70 kJ mol^{-1}).[129, 130]

4.3.3 Bulk Film Analysis

TGA was performed on PDAC/sPPO films peeled off of polystyrene substrates. Since the films were thoroughly dried before TGA, there is negligible mass loss before 200 °C, as no water was present in the films initially. Figure 4-4 shows the thermal decomposition of PDAC/sPPO LbL films, along with pristine PDAC and sPPO films prepared by drop-casting from aqueous solutions. PDAC has two sharp thermal decomposition steps at ~350 °C and ~450 °C, after which the mass remaining is less than 5%. The TGA curve for sPPO shows two main decomposition steps, a sharp mass loss at ~325 °C and a broader loss starting at ~425 °C, in agreement with previous reports.[131] The mass loss at ~325 °C is attributed to the loss of sulfonate groups, and the decomposition starting at ~425 °C is caused by the degradation of the PPO backbone. Interestingly, there is significant mass remaining in the sPPO sample, even above 800 °C, indicating that there may be salt ions present in the sPPO solution. A representative TGA curve for a PDAC/sPPO film assembled with 0.5 M NaCl in all assembly solutions shows that the decomposition closely follows PDAC, except there is more remaining mass above 500 °C. The large amount of salt or other impurities present in the sPPO sample prevents an accurate calculation of the composition of the PDAC/sPPO films; however films assembled with different salt concentrations yield nearly identical TGA

curves, which implies the composition of the film does not vary significantly with changes in ionic strength in the assembly solutions. The lack of compositional change in PDAC/sPPO films is further confirmed by the results of elemental analysis, where all the PDAC/sPPO films prepared from varying assembly conditions yield similar PDAC content monitored by the weight percentage of nitrogen in the LbL films.

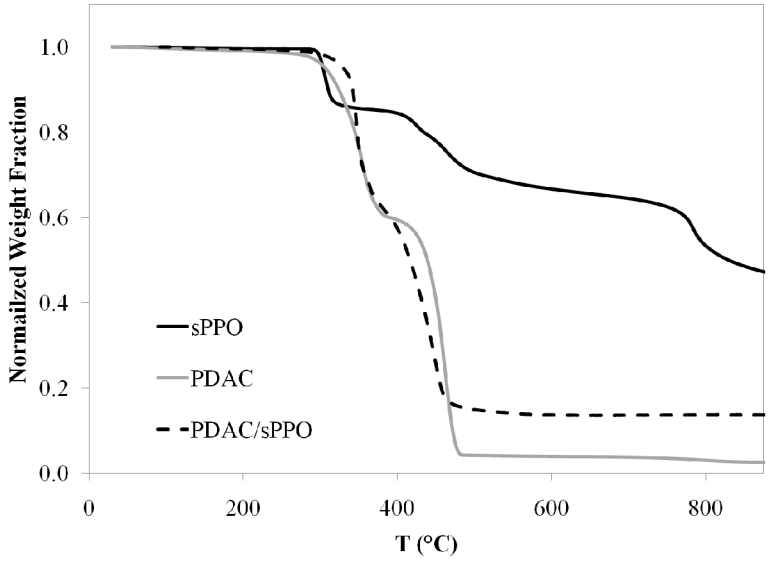

Figure 4-4. TGA of sPPO, PDAC, and a 60 bilayer PDAC/sPPO film assembled with 0.5 M NaCl in all assembly solutions. PDAC/sPPO films assembled with different ionic strength solutions produced films with similar thermal decomposition curves.

To further understand the growth behavior and composition of the PDAC/sPPO films, the thickness of films in increments of 0.5 BL is studied for LBL films assembled from selectively salted and fully salted assembly solutions (Figure 4-5). For a film assembled at pH = 2 with 0.2 M NaCl in only the sPPO assembly solution, the additional film thickness from PDAC deposition from 19.0 BL to 19.5 BL and from 20.0 BL to

20.5 BL is ~ 1 nm, while the film growth due to sPPO absorption from 19.5 BL to 20.0 BL is 8.6 nm. This difference in deposition for PDAC and sPPO could imply that the majority component of the PDAC/sPPO film is sPPO; however it is improbable that the composition of the film matches the 0.5 BL thickness increments, which are an 8.6:1 ratio in favor of sPPO. More importantly, the 0.5 BL data verifies that the sPPO deposits in a thicker, loopier conformation and confirms that the selective addition of salt to sPPO enhances ion transport, especially when considered with the water uptake and transport results below. Additionally, there is potential for the sPPO layer to be thinner than observed, as it is exposed to salt free rinses after deposition. However, for a film assembled with 0.2 M NaCl in all the solutions (both polymer solutions and all rinse baths), the deposition of PDAC and sPPO is more uniform, only slightly favoring the PDAC growth (5:6).

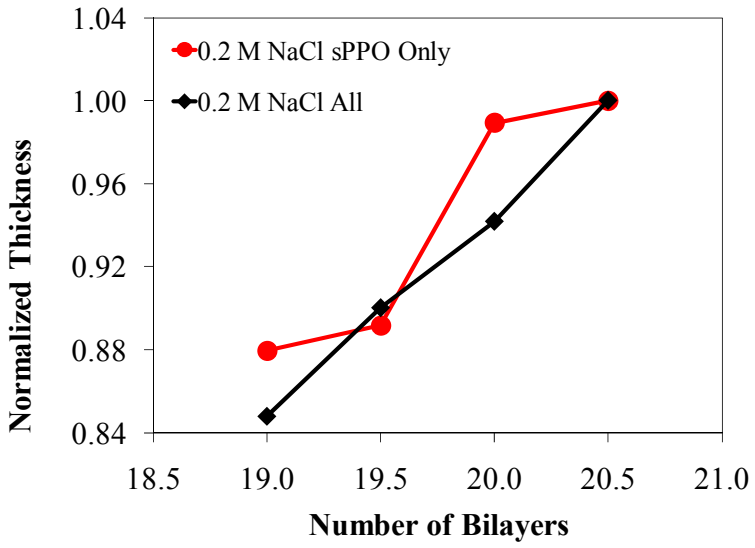

Figure 4-5. Step growth curves for LbL assembly of PDAC/sPPO films on glass assembled at pH = 2 with 0.2 M NaCl in only the sPPO assembly solution and 0.2M NaCl in all assembly baths.

4.3.4 Water Management

To analyze the water uptake and transport of PDAC/sPPO LbL films, we employ a newly developed quartz crystal microbalance (QCM) technique.[43, 118] This QCM technique allows for the measurement of solubility (S) of water in a thin film, a thermodynamic property, and for the diffusion coefficient (D), a kinetic property. Solubility and diffusion coefficients are both determined from water uptake experiments using the QCM and permit the calculation of the permeability of water in the LbL films, and permeability is defined above in Equation 1-4.

To analyze water uptake, PDAC/sPPO films were assembled on quartz crystals and equilibrated at 30 °C under a dry nitrogen atmosphere until there is no longer a loss in moisture from the film, as evidenced by a constant frequency response from the QCM. The PDAC/sPPO films are subsequently exposed to a series of step changes in humidity from 0% to 100%. The linear sorption isotherm from these multi-step experiments yields the solubility of water in the film. It must be noted that deviations from the Sauerbrey equation can exist for highly hydrated, compliant films, but these deviations are minimal for thin films studied at the QCM's fundamental frequency. Understanding the water transport properties of fuel cell PEMs is critical for the development of highly conductive membranes and for the reduction of balance of plant humidification systems.[40] Membranes comprised of polymers with strong acid functionalities, such as sulfonic acid groups, have highly humidity dependent ionic conductivity values.[41] In hydrated PEMs, protons migrate by the Grotthuss "hopping" mechanism; increased water in the PEM allows for better proton transport.[129] Additionally, for PDAC/sPPO films, water uptake at

different assembly conditions provides insight to the degree of crosslinking and thus availability of charged groups within the LbL films.

Figure 4-6 shows the gravimetric water uptake of PDAC/sPPO films assembled with sodium chloride concentrations in the sPPO solution ranging from 0 M to 1.0 M. It is clear that films assembled with higher salt concentrations in the sPPO assembly bath absorb more water; films made with 1.0 M sodium chloride in sPPO absorb 19.1% more water (0.260 g water/g film) than films assembled with no salt in the sPPO deposition bath (0.218 g water/g film). As a reference, PDAC and sPPO, both water soluble polymers, uptake 0.440 g water/g film and 0.502 g water/g film at 100%, respectively. The blended LbL systems absorbs less than either pristine PDAC or sPPO, which is to be expected as many of the charged functional groups from both polymers participate in the ionic crosslinking that stabilizes the film. Also, a film assembled with 0.5 M NaCl in all assembly baths absorbs 0.273 g water/g film, which is more than any condition with salt only in sPPO. The increased water uptake of the film assembled with 0.5 M salt in all assembly baths implies a looser crosslinking density, consistent with the growth rates shown in Figure 4-1, as more charged groups on PDAC and sPPO are left available to interact with water molecules. However, increased water uptake alone does not directly translate into higher ionic conductivity values for this LbL system, as the film assembled with only 0.5 M NaCl in sPPO only has a conductivity value ~5x higher than the film assembled with 0.5 M NaCl in all solutions. Thus, while selectively adding salt to the sPPO assembly bath does not appear to impact film composition significantly, it appears that water uptake and ionic conductivity are improved as sPPO maintains more available charge groups, and likelier takes on a loopier, more favorable conformation within the

film. The permeability of water in PDAC/sPPO films follows a similar trend; films assembled with no salt and films assembled with 1.0 M salt in sPPO only had water permeability values of 1.36 Barrer and 5.46 Barrer, respectively (Barrer = 10^{-10} cm^3 cm cm^{-2} s^{-1} $cmHg^{-1}$). Films assembled with salt in all assembly baths had permeabilities at least one order of magnitude higher (> 25 Barrer). Since films with salt in all assembly baths have better water transport properties yet lower ionic conductivities, it indicates that the mobility of protons in the hydrated film determines ionic conductivity, with water transport playing a supporting role. Films assembled with increased salt in sPPO have the best morphology for ion transport coupled with favorable water transport properties and therefore yield superior ionic conductivities.

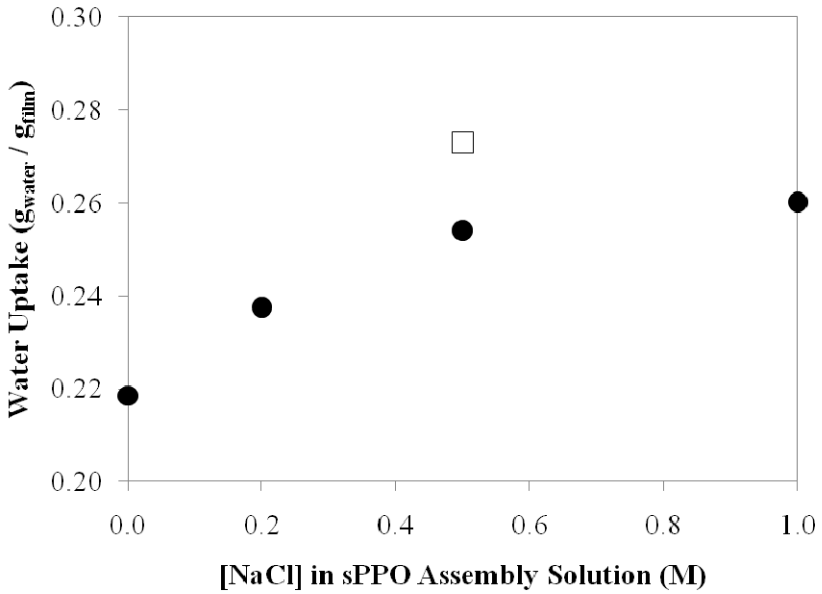

Figure 4-6. Water uptake of PDAC/sPPO LbL films at 100% RH assembled with different concentrations of salt in the sPPO assembly bath (filled circles). All films were assembled at pH = 1.0 with no salt in the PDAC solution, except for one film assembled with 0.5 M salt in both the PDAC and sPPO solution (open square).

4.3.5 Spray-Assisted Layer-by-Layer Films

As shown above, LbL assembly is an effective method to create highly conductive thin film composites. However, dip-assisted LbL assembly often requires long processing times to generate membranes thick enough for mechanical robustness required for free-standing films (~30 minutes per bilayer including rinsing steps). To address this, our group has recently developed an automated sprayer system, which reduces the processing time down to ~50 seconds per bilayer.[116] Spraying also allows for using larger substrates and reduces the contamination probability of the film during assembly since the substrate is never immersed into the polymer solutions. Very similar to the dip-assisted assembly, spraying steps include subsequent misting of polymer and rinse solutions on a substrate rotating at 12 rpm. Rotation allows for quick draining of the misted droplets to yield overall homogenous films. The film growth is linear as a function of number of bilayers allowing for precise thickness control. Increasing the ionic strengths of polymer solutions by adding NaCl results in thicker (and more conductive) films similar to the dip-assisted films. For comparison, the thickness of a LbL film sprayed from solutions comprising 0.2M NaCl (all baths) is monitored up to 100 bilayers yielding ~ 14 nm/BL growth rate, similar to the dip-assisted films shown in Figure 4-1. This film has an ionic conductivity value of 6.22×10^{-3} S cm^{-1}(at 25 °C, 98% RH), very similar to the values given in Table 4-1 from dip assembled films. When 0.2M salt is selectively added to the sPPO assembly solution, the conductivity increases to 11.76×10^{-3} S cm^{-1}, consistent with the trends shown for dip assembled LbL films.

When sprayed on a polystyrene coated silicon substrate from solutions containing higher concentrations of NaCl (0.5M), it is possible to generate LbL films as thick as 10

μm (400 BL) that can be easily peeled off from the substrate as free-standing films, shown in Figure 4-7. When sprayed from ca. 25 cm distance with all three spray nozzles directed at the substrate (PDAC, sPPO and rinse water), the resulting film area is ~40 cm^2. Mechanical properties of a spray assembled 250 BL free-standing film (~ 8 μm thick) were obtained at ambient conditions from stress-strain curves, and compared to the values of pristine sPPO of similar thickness. The PDAC/sPPO film yields a respectable elastic modulus value of 523 MPa, significantly higher than that of pristine sPPO (120 MPa). It also has 9% break strain, 3% higher than sPPO. These suggest that the LbL films stabilized with ionic crosslinking yield more robust films compared to the parent sPPO polymer.

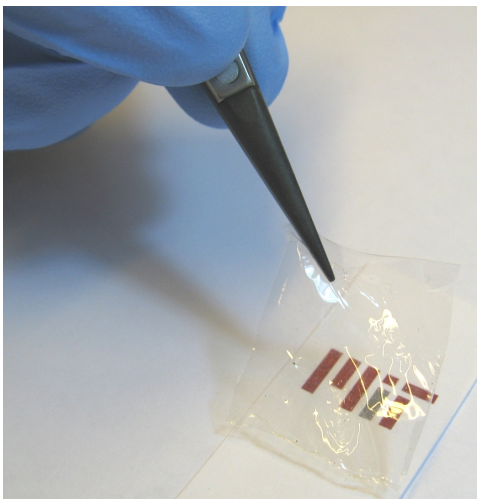

Figure 4-7. A picture of a free-standing PDAC/sPPO film (~10 μm) assembled on polystyrene coated silicon substrate using spray-assisted LbL method. Assembly conditions: pH = 2.0, [PDAC] = 10 mM, [sPPO] = 10 mM, [NaCl] = 0.5 M (all solutions).

4.4 Conclusion

PDAC/sPPO LbL films fabricated with various salt concentrations in the assembly solutions are studied to understand the basis of the high ionic conductivity of this system. Since PDAC and sPPO are both strong polyelectrolytes, adding salt to the assembly solutions shields the charged groups on both polymers, which impacts the formation and properties of these films. The film growth, morphology, composition, and water management of these films is investigated with salt added to all assembly solutions and with salt selectively added to only sPPO. The growth rate of PDAC/sPPO is tuned from 6.91 nm/BL when assembled with no salt up to 62.2 nm/BL when assembled with 0.5 M salt in all assembly solutions. Film growth is also adjusted by selectively adding salt to only sPPO; films grow at 24.0 nm/BL when the sPPO solution contains 0.5 M NaCl. TEM micrographs show that these LbL films are homogenous blends at the conditions studied. The ionic conductivities of PDAC/sPPO films follow a similar trend as growth rates, increasing from 1.29 x 10^{-3} S cm^{-1} when no salt is added during assembly to 2.40 x 10^{-2} S cm^{-1} when 1.0 M salt is added to all deposition baths. However, when salt is selectively added to only the sPPO assembly solution, higher conductivities are observed. For example, with 1.0 M salt in only the sPPO assembly solution, PDAC/sPPO films have ionic conductivity values of 7.00 x 10^{-2} S cm^{-1}, which is the highest value reported for any LbL system. Interestingly, TGA and elemental analysis indicate the composition of these films vary little with changes in the salt concentration of the assembly baths. A QCM technique is used to measure the water uptake and transport in PDAC/sPPO films. Both water uptake and permeability increase with increasing salt in the assembly baths. PDAC/sPPO films with salt in all assembly baths

have larger water uptake and permeability values than films assembled with salt only in sPPO but lower ionic conductivity values. Thus the increase in proton mobility in hydrated PDAC/sPPO membranes comes from reduced ionic crosslinking, which is most favorable for proton transport when the sPPO assembly solution selectively contains salt. Furthermore, PDAC/sPPO films are fabricated using a spraying technique allows thick films to be quickly produced. Thick, free-standing PDAC/sPPO films are analyzed with uniaxial tensile testing to yield an elastic modulus value of 523 MPa.

5. Layer-by-Layer Electrospun Mat Composite Membranes for Fuel Cells

Abstract

Composite membranes of highly conductive layer-by-layer (LbL) films and electrospun fiber mats (EFMs) are investigated for fuel cell applications. The mechanical properties of highly conducting PDAC/sPPO LbL films are improved by forming the LbL matrix on highly tunable EFM support. Free-standing LbL films have moderate mechanical properties when dry, but are mechanically deficient when hydrated. Coating an EFM with the LbL dipping process produces composite membranes with interesting "bridged" morphologies. The ionic conductivity of the composites is similar to the pristine LbL system. The spray LbL assembly method is studied as a means for the rapid formation of LbL films, while also allowing a vacuum to be applied during assembly. At optimized conditions, LbL EFM composites have conformal coatings of the individual fibers throughout the bulk of the EFM and have uniform surface coatings, which is important for electrochemical devices where the membrane acts as a barrier. The mechanical properties of the spray coated EMFs are shown to be superior to the LbL only system.

5.1 Introduction

Hydrogen and methanol fuel cells have the potential to replace traditional electricity generating technologies and provide clean, safe energy in applications such as stationary power generation, distributed power in buildings, and lightweight portable power for transport and portable electronics. Numerous challenges must be overcome to enable wide spread utilization of fuel cells including high materials and system costs, the ability to operate over a wider range of conditions (more extreme temperatures and humidities), improved or simplified water management, and long-term durability.[1] One of the crucial components in hydrogen and methanol fuel cells that limit device lifetime is the proton exchange membrane (PEM), which is at the core of the membrane electrode assembly (MEA). PEMs act as separators between the fuel, hydrogen or methanol, and oxidant, typically air, and must maintain high protonic transport at the fuel cell's operating conditions. However, current membranes are subject to both chemical and mechanical degradation that lead to membrane and thus device failure, limiting the lifetime and application of PEM fuel cells. For hydrogen and DMFCs, membranes comprised of perfluorosulfonic acid polymers such as Nafion are most commonly used because of superior protonic conductivity and water transport at humidified conditions coupled with relatively high mechanical integrity and chemical stability.[5]

There have been many recent publications studying the impacts of PEM durability on fuel cell lifetime.[132-137] Tang et al. show that when Nafion is exposed to higher temperatures and relative humidities its mechanical properties, Young's modulus in this case, can decrease by over 15%.[138] Another report observes a larger decrease in

the Young's modulus of almost an order of magnitude when Nafion is fully hydrated.[139] More importantly, the temperature and humidity cycling that membranes are exposed to in the fuel cell can lead to membrane failure from the repeated swelling/deswelling in a constrained geometry. For example, membrane failure has been observed when only cycling a fuel cell between wet and dry operating conditions without supplying fuel and oxidant.[140] Such cycling was also shown to drastically decrease the strain to failure of the membrane when subjected to uniaxial tensile loading after humidity cycling.[141] A similar study investigating only thermal cycling between -40 °C and 80 °C showed a decrease in the toughness of Nafion after 385 cycles.[142] PEM failure is exacerbated under real-world device operating conditions where chemical degradation is also present. Chemical degradation caused by peroxides, free radicals, and fuel impurities has been extensively been studied.[143-145] Accelerated lifetime tests of membranes, such as Fenton's Test, are commonplace, but the correlation to actual lifetime testing is debated.[146] When membranes fail, pinholes and microcracks propagate until fuel crossover or electrical shorts cause catastrophic device failure. Thus, significant effort has been undertaken to improve the mechanical properties of current PEMs.

The two most common approaches to improving PEM mechanical properties are synthesizing similar perfluorosulfonic acid polymers with differences in the polymers' side chains or backbone and reinforcement with more robust polymers or other additives. An example of a polymer with slight differences in structure verses Nafion is achieved by shortening the length of the sulfonic acid containing side chains. Studies have shown that polymers bearing these shorter side chains have higher glass transition temperatures and also contained some crystallinity, which may further enhance bulk mechanical

properties.[147, 148] A separate study on similar shortened side chain (SSC) Nafion analogues show an improved resistance to tear formation and propagation.[149] Another group working on SSC perfluorosulfonic acid membranes reported higher glass transition temperatures, improved mechanical properties over a range of temperatures, and improved lifetime.[150] The most prevalent means of reinforcing Nafion is through incorporating polytetrafluoroethylene (PTFE) into the Nafion matrix. Porous PTFE membranes are impregnated with Nafion by soaking in Nafion solutions or by gravity filtration.[151-153] Since the PTFE is a large fraction of the composite membrane, these systems have much lower ionic conductivities; much thinner membranes must therefore be used to minimize ohmic losses. Commercial examples of PTFE-reinforced perfluorosulfonic acid membranes have been produced by W.L. Gore and DuPont (Nafion XL series). Other means of reinforcing Nafion have been attempted by incorporating carbon nanotubes, metal oxides, and zirconium phosphates into Nafion matrices.[154-156]

A superior means to fabricate mechanically robust PEMs is much needed. A promising approach is to combine two relatively new processing techniques, layer-by-layer (LbL) assembly of polymer thin films and the electrospinning of nanofiber mats. LbL assembly is an extremely versatile technique that allows for the conformal coating of any substrate with a blended polymer film of two or more polymers possessing complementary interactions, i.e. oppositely charged functional groups.[10, 11, 23] Recent reports from the Hammond group present LbL-based PEMs with high performance in hydrogen and direct methanol fuel cells.[39, 112] Most importantly, the LbL system of composed of poly(diallyl dimethyl ammonium chloride) (PDAC) and sulfonated

poly(2,6-dimethyl 1,4-phenylene oxide) (sPPO), structures shown in Figure 5-1a, obtains the highest ionic conductivity of any LbL assembled system at 7.00 x 10^{-2} S cm^{-1}, which is close to the values of state-of-the-art PEMs. Also, a new spray-assisted LbL process has recently been developed to reduce to fabrication of LbL films by up to a factor of 40.[116] An interesting class of materials for reinforcing LbL membranes is electrospun fiber mats (EFMs). EFMs are non-woven, highly porous materials with high surface to volume ratios. A wide range of polymers can be formed into EFMs, and it has been shown that the resulting fiber diameters can easily be tuned during fabrication.[157] Figure 5-1b shows a representative scanning electron microscopy (SEM) image of an EFM made from polycaprolactone (PCL) with fiber diameters of ~10 μm. By combining mechanically durable EFMs with highly conductive PDAC/sPPO multilayer films, superior PEMs can be generated. Additionally, the combination of these two processes allows for decoupling of the membrane structure and mechanics from the chemical and ion transporting characteristics of the membrane. As an aside, a recent publication from Krogman et al. utilizes LbL-coated EFMs to produce asymmetric composite membranes as protective barriers against toxic gases, thus demonstrating the versatility of combining LbL assembly with EFMs.[158]

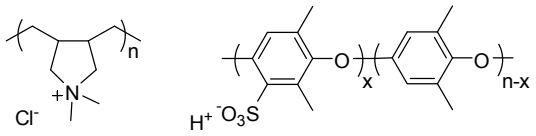

PDAC sPPO

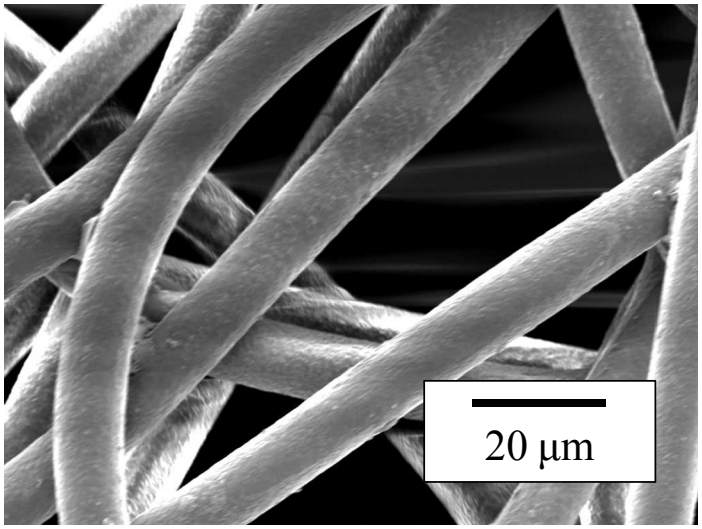

Figure 5-1. Chemical structures of PDAC and sPPO (top). These two polymers are combined in the LbL assembly process to yield highly conductive PEMs. Scanning electron micrograph of PCL EFM with fiber diameters of ~10 μm (bottom). These two systems, LbL films and EFMs, are combined to yield mechanically reinforced, composite PEMs.

Here we report the characterization of the first LbL EFM composite membranes for electrochemical device applications. The mechanical properties of highly conducting PDAC/sPPO LbL films are sought to be improved by forming the LbL matrix on highly tunable EFM supports. Free-standing PDAC/sPPO films have reasonable mechanical properties when dry, but lack mechanical integrity when hydrated. Coating a PCL EFM with PDAC/sPPO by the LbL dipping process produces composite membranes with

interesting “bridged” morphologies. The ionic conductivity of the composites is similar to the pristine LbL system. To further exploit the combination of LbL assembly and EFMs, we use the recently developed spray LbL assembly method to coat PDAC/SPS onto nylon EFMs. The spray assembly permits for the rapid formation of LbL films, while also allowing a vacuum to be applied during assembly. Composites assembled without vacuum yield membranes with coatings that do not penetrate into the bulk of the EFM. Conversely, LbL EFM composites assembled with a mild vacuum during assembly show conformal coatings of the individual fibers throughout the bulk of the EFM. Additionally, the vacuum-assembly composite membranes have uniform surface coatings, which is important for electrochemical devices where the membrane often is required to act as a barrier. The mechanical properties of the spray coated EMFs are shown to be superior to the pristine LbL system previously studied.

5.2 Materials and Methods

Chemicals. PPO (Mw = 23,000), poly(sodium 4-styrenesulfonate) (SPS, Mw ~ 200,000), and PCL (Mw = 80,000) were obtained from Sigma-Aldrich, Inc. PDAC (Mw = 240,000) was obtained from Polysciences, Inc. Nylon 6(3)T was obtained from Scientific Polymer Products, Inc. PPO was sulfonated as previously reported to yield highly sulfonated sPPO.[112]

Electrospun Mats. The electrospinning apparatus, similar to previously reports, consists of two aluminum disks 10 cm in diameter oriented parallel to each other and separated by distance of 35 cm.[159] A 30 vol% solution of Nylon 6(3)T in dimethylformamide is pumped with a syringe pump (Harvard Apparatus PHD 2000) at a

rate of 0.01 mL min^{-1} to a needle in the top aluminum disk. A power supply provides a 34 kV potential to the upper aluminum disk. The process is allowed to run for 2 hours producing an EFM about 100 μm thick, after which the EFM is placed in an oven at 140 °C to anneal for 3 hours. PCL EFMs were made using the same setup from a 10% solution of chloroform and methanol (3:1 by weight).

LbL Dip Assembly. EFM samples about 1" x 2" in size were directly placed into home-built plastic sample holders without any surface treatment to ensure the sample remained planar during assembly. LbL assembly utilized a programmable ZEISS DS50 slide stainer. EFMs were immersed in PDAC for 15 minutes, followed by three two minute rinses in water, and then placed in sPPO for 15 minutes followed by three two minute rinses in water; the process was repeated numerous times to yield thick coatings. PDAC and sPPO solutions were both 10 mM based on the molecular weight of repeat units. The composite membranes were rinsed in deionized water after assembly to remove excess ions from the films.

LbL Spray Assembly. EFM samples about 4" x 4" in size were directly placed onto a 3" diameter plastic funnel fitted with a steel mesh for support. Sprayed films were fabricated using the same polymer and rinse solutions described above, substituting SPS for sPPO. A home-built automated spraying setup, as previously detailed, was used to coat the EFMs.[116] An automated program run by a logic relay controlled the apparatus, spraying the PDAC and sPPO solutions for 3 seconds, with 10 seconds of rinse water spray in between the polymer sprays. The process was repeated numerous times to generate thick coatings. For some samples, a mild vacuum was applied to the back of the EFM using a venturi pump supplied with nitrogen. LbL films were also assembled on

untreated Teflon substrates or polystyrene coated silicon wafers and gently peeled off after assembly, similar to a previous report.[117]

Characterization. SEM images were obtained on a JEOL JSM-6060 scanning electron microscope after coating the composite membranes with 5 nm of Au/Pd. Cross-sectional images were obtained by freeze fracturing composite membranes in liquid nitrogen. Ionic conductivity measurements of the coated EFMs were made by cutting 1 cm x 2cm samples and placing in a conductivity cell with two platinum wires 1cm apart as the electrodes. The total thickness of the composite membrane is used in conductivity calculations. Temperature and humidity were controlled using a chamber from Electro-tech Systems, Inc. Impedance values were determined by electrochemical impedance spectroscopy with a Solartron 1260 impedance analyzer, measuring from 100 kHz down to 10 Hz. The thickness of the composite membrane was measured using cross-sectional imaging on an optical microscope. Uniaxial tensile tests were conducted at constant engineering strain rates on rectangular specimens of coated EFMs at ambient conditions with an EnduraTEC Electroforce 3200 (ELF) in displacement control mode. Strain was measured with a Qimagine Retiga 1300 video extensometer. The force-displacement data as taken from the ELF and the videoextensometer, respectively, were reduced to true stress-true strain results assuming isotropic incompressible behavior. True stress is defined as the ratio of force to current (deformed) cross-sectional area and true strain is defined as the natural logarithm of the ratio of current length to original length (length being the axial distance between video-imaged marks).

5.3 Results and Discussion

5.3.1 Dipped Layer-by-Layer Composite Films

The approach that we are pursuing to enhance the mechanical properties of PDAC/sPPO LbL systems is to use EFMs as a substrate material. LbL assembly is used to generate coatings on EFMs to produce thin, mechanically stable composite fuel cell membranes for high power density power devices. Because these material systems can be greatly modified at the molecular level to alter localized mobility, mechanics, and stability simply by changing the relative compositions of each adsorbed bilayer (BL) of polymer or by altering the nature or composition of the underlying electrospun network, the systems are infinitely tunable and the architectures of the films can be modified across the thickness to achieve highly optimized and readily processable ultrathin fuel cell membranes that rival or exceed the performance of Nafion.

Stress-strain curves of free standing PDAC/sPPO films are shown in Figure 5-2 for both ambient (dry) and fully hydrated (wet) conditions. The free standing films were fabricated as discussed previously (Section 4.3.5) It has previously been shown that PDAC/sPPO films have higher elastic modulus values and break strains than pristine sPPO, an indication that the blended LbL films are more mechanically durable than sPPO. The free standing PDAC/sPPO films exhibit elastic-plastic behavior with elastic modulus values ranging from 250-1100 MPa and yield stress values ranging from 4-40 MPa depending on the processing conditions. In cyclic testing the films are seen to unload linearly at the same slope as the initial loading, recover further during the zero load portion of the cycle, reload at the same slope as the initial loading until the yield

stress is reached, and then roll over to rejoin the initial curve. Films assembled with more salt in the assembly baths, and more specifically salt in all assembly baths, have higher elastic modulus values (> 1000 MPa) and yield stress values (> 20 MPa). These greater mechanical properties are consistent with the water uptake results previously reported for PDAC/sPPO, where films assembled at higher salt concentrations absorb more water due to a looser crosslinked network. Thus, films assembled at higher salt concentrations form a more compliant network, while films assembled with smaller salt concentrations or no salt at all form tightly crosslinked, more rigid materials. Overall, the mechanical values of PDAC/sPPO compare well with the corresponding properties of Nafion, which has an elastic modulus of 300 MPa and a yield stress of 12 MPa.[138, 139, 160] However, the layer-by-layer films tear at quite small strains and are sensitive to edge defects from cutting the sample to size for testing. The average break strain among free-standing PDAC/sPPO films is 0.07, which is quite low compared to Nafion which breaks at a strain greater than 1.0. Under hydrated conditions the PDAC/sPPO films at all assembly conditions become very rubbery and have an elastic modulus of order ~ 1 MPa. At the hydrated operating conditions of a fuel cell, these mechanical values would lead to very short MEA lifetimes due to mechanical failure of the membrane.

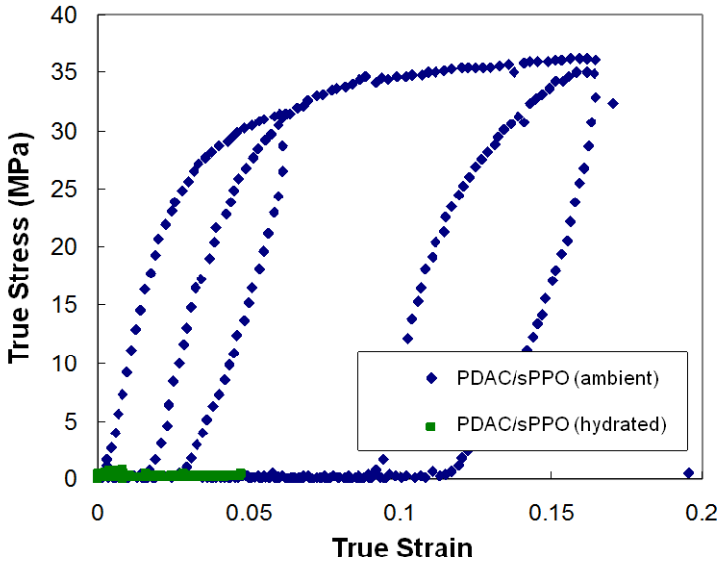

Figure 5-2. Typical cyclic stress-strain curves for free standing PDAC/sPPO films at ambient (dry) and fully humidified (wet) conditions. The PDAC/sPPO films are assembled at pH = 1.0 with 0.5 M NaCl in the sPPO assembly solution. The film is sprayed onto a polystyrene coated silicon wafer and gently removed after assembly.

To improve the mechanical properties of PDAC/sPPO films, especially at hydrated conditions, EMFs are used as reinforcing substrates and coated through the LbL dip assembly process. Figure 5-3 shows SEM images of PCL EFMs coated through the LbL dip assembly process with 0 BL, 50 BL, 125 BL, and 250 BL of PDAC/sPPO. The uncoated PCL EFMs have fiber diameters of ~10 μm as shown in Figure 5-3a. The thickness of the PCL EFMs is ~20 μm. It is clear from Figure 5-3 that as additional bilayers of PDAC/sPPO are coated onto the PCL EFMs, the void space initially present in the PCL EFM is continually reduced. To compare, LbL films of PDAC/sPPO fabricated at the same assembly conditions on a planar glass substrate grow at a rate of 24.0 nm BL^{-1}. Therefore, 50 BL of PDAC/sPPO corresponds to a 1.2 μm film, and a 250

BL PDAC/sPPO corresponds to 6 μm in thickness. From Figure 5-3b (50 BL coating) and Figure 5-3d (250 BL), the amount of PDAC/sPPO film appears to be more than 1.2 μm and 6 μm, respectively, especially where the PCL fibers intersect. As the LbL fim is being applied to the EFM, it is likely that the polymer solutions and rinse solutions do not have sufficient time to drain out of the film. The amount of time that the EFM is exposed to air between assembly steps is approximately five seconds, which would allow for the polymer solutions to be held in place by surface tension in the regions where fibers closely intersect and form thicker films than on planar substrates. This "bridging" phenomenon is quite similar to the behavior recently reported by Krogman et al. where LbL films of PDAC/SPS were sprayed onto EFMs and the interstitial void space between fibers is quickly filled in.[158] This occurs despite the fact that the sprayed polymer droplets are approximately 5 μm in diameter (the hydrodynamic radius of the polymers in solutions are ~50 nm), but are able to fill in regions between fibers that span 10-20 μm. Krogman attributed this to the EFM acting as an "electrostatic net," where the droplets coalesce on the fiber surfaces and begin to span regions where fibers are in close proximity. Comparing the sprayed system from Krogman to the dipped system here, it is likely that a similar growth mechanism causes the "bridged" growth. Another previous study focused on the conformal coating of EFM fibers through chemical vapor deposition.[161] This "bridged" growth may allow for the formation of thick coatings that prevent fuel crossover inside an operating fuel cell, while maintaining high ionic conductivity from the PDAC/sPPO and mechanical reinforcement from the EFM.

The in-plane ionic conductivity values of PCL EFMs coated with 125 BL and 250 BL of PDAC/sPPO are shown in Figure 5-4, along with a PDAC/sPPO film assembled

on a glass slide. The composite membranes have ionic conductivity values similar to the pristine PDAC/sPPO film. It should be noted that for the conductivity calculations of the composite LbL EFM membranes, the total thickness of the membrane is used. As the number of bilayers deposited on the EFMs increases, the ionic conductivity of the composite membrane increases. Since the overall membrane thickness is not changing as the LbL film is applied, and as the void space of the EFM is filled by the LbL film, the

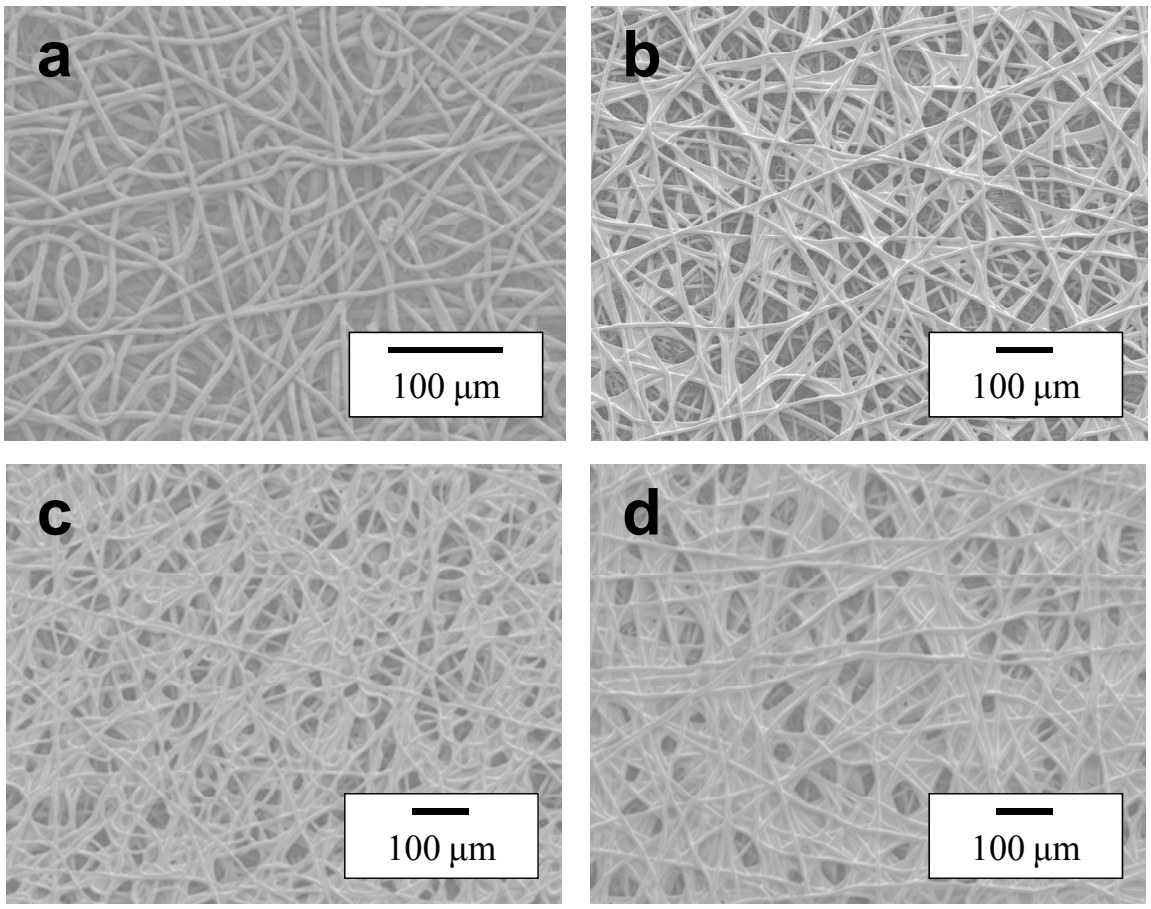

Figure 5-3. SEM images of PCL EFMs coated with 0 BL (a), 50 BL (b), 125 BL (c), and 250 BL of PDAC/sPPO. PCL EFMs have fiber diameters of ~10 μm. PDAC/sPPO deposition conditions are pH = 1.0, 0.5 M NaCl in sPPO, and no salt in PDAC or any rinse solutions.

pathways for ion transport increase to approach that of a pristine LbL film. In fact, it appears that the ionic conductivity of the composite would eventually approach the conductivity of PDAC/sPPO at a large number of bilayers. In theory the conductivity of an EFM completely filled in with PDAC/sPPO would be about 15% less than a pristine PDAC/sPPO film because the EFM would occupy about 15% of the composite membranes volume, which would decrease the effective cross-sectional area of the membrane for ion transport. Also, the slope of the composite membrane is the same as the PDAC/sPPO only film, indicating the mechanism of ion transport through the composite is the same (see Chapter 4).

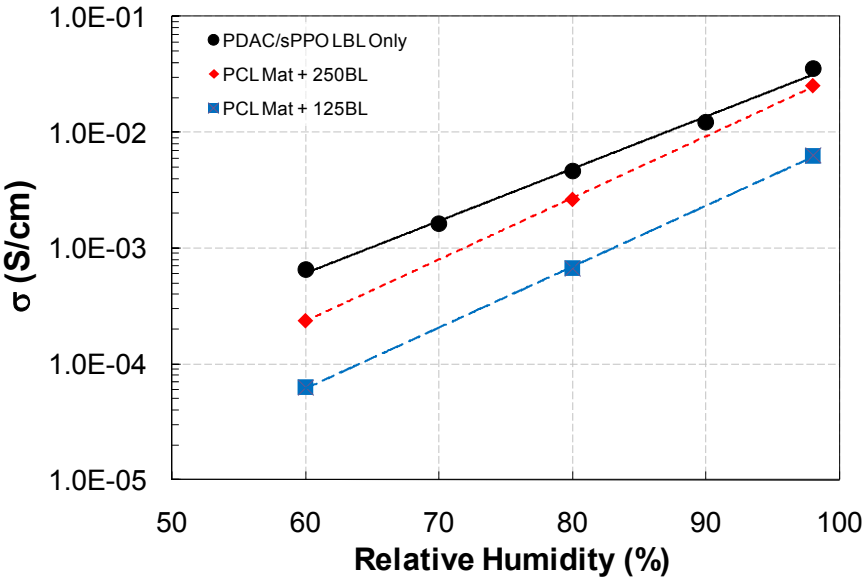

Figure 5-4. Relative humidity dependence of ionic conductivity of PDAC/sPPO films coated on PCL EFMs. PDAC/sPPO deposition conditions are pH = 1.0, 0.5 M NaCl in sPPO, and no salt in PDAC or any rinse solutions. As the number of bilayers deposited on the EFM increases, the void space of the EFM is increasingly filled in with PDAC/sPPO.

5.3.2 Sprayed Layer-by-Layer Composite Films

To further improve the promise of PEMs comprised of EFMs coated with highly conductive LbL films, an improved methodology is needed. A more robust EFM material is needed; PCL is known to be biodegradable and hydrolytically unstable, so a more durable nylon EFM was selected. Nylon 6(3)T is used because it does not require harsh solvents, such as hexafluoroisopropanol, to be used for the electrospinning process. Also, to generate thick coatings on the EFMs, a spray-assisted LbL technique that reduces the LbL deposition time by a factor of up to 40 is used. While the above PDAC/sPPO dip coated mats showed a "bridging" morphology, the LbL film did not penetrate into the interior of the EFM. With spray LbL, it is possible to draw a vacuum on the downstream side of the EFM, effectively coating the thickness of the EFM. It is also possible to coat both side of the EFM by simply flipping the EFM over during the spraying process. Figure 5-5 shows the materials used for the spray coatings. The nylon mat has average fiber diameters of ~ 1.5 μm and is coated with PDAC/SPS. The thickness of the nylon EFMs is ~100 μm. SPS is used as a commercially available analogue to sPPO, as significantly larger quantities of material are needed for the spray LbL process (volumes of sPPO which are not available with the current lab-scale synthesis). Although SPS is somewhat similar to sPPO, LbL films of PDAC/SPS have ionic conductivity values one order of magnitude lower than PDAC/sPPO, preventing a direct conductivity comparison between the dipped films above and sprayed films in this section.

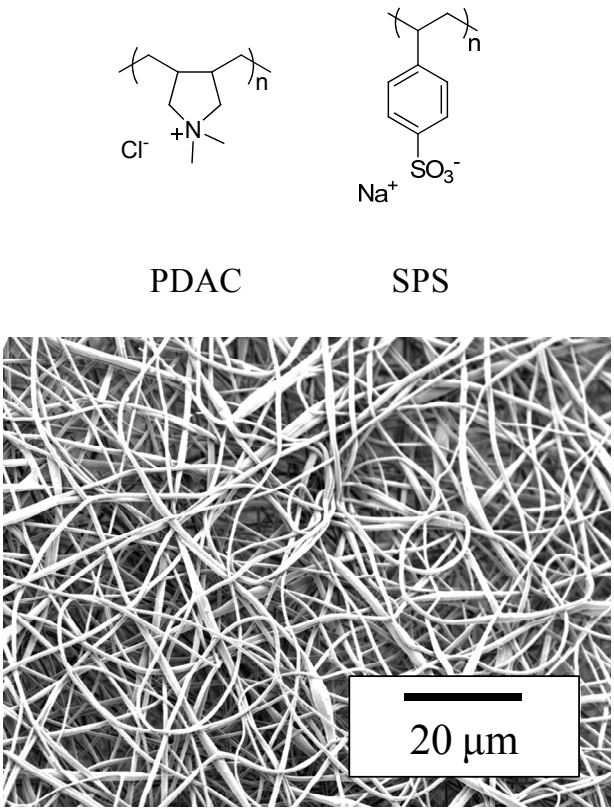

Figure 5-5. Chemical structures of PDAC and SPS (top). Nylon EFMs (bottom) having fiber diameters of ~1.5 μm are used as substrates.

Representative SEM images of the spray coated nylon EFMs are shown in Figure 5-6. Figure 5-6a and 5-6b shows the front and back sides, respectively, of an EFM coated with 175 bilayers of PDAC/SPS. As can be seen in Figure 5-6a, 175 BL of PDAC/SPS almost provides a uniform film that covers the surface of the EFM. However, the coating is less uniform than the dipped films above, evidenced by the almost granular nature of the LbL coating, or any polymeric LbL system sprayed onto a flat surface. It is surprising that the 175 BL film applied to the EFM does not produce a thick, uniform surface coating, as a film assembled at the same conditions on glass would be approximately 4.42 μm thick. The most likely explanation for the lack of film present is the

hydrophobicity of the untreated nylon fibers. The polymer solutions do not wet the fibers well, and the onset of LbL film growth is significantly delayed. The surface of the fibers could be functionalized through plasma etching (applies a negative charge to the EFM surfaces), but this may not penetrate throughout the bulk of the EFM uniformly. Other solution based functionalization routes could be explored as a way to provide better LbL film growth and adhesion to the EFMs. For these spray LbL coatings, the "bridging" appears to form a surface barrier/coating more rapidly than dip coating, as can be seen by comparing Figure 5-6a (175 BL) with Figure 5-3d (250 BL). This is consistent with the fact that the rapid spray technique mists polymer droplets onto the surface for 3 seconds, while the dip technique exposes the EFM to the polymer solutions for 15 minutes. Thus, the spray coatings do not penetrate more than 10 μm into the EFM, but form surface coatings more quickly. It is also expected that both the size and surface functionality of the fibers and the porosity of the EFMs will significantly impact LbL film formation on or within the mat. One downside to the basic spraying technique is that the LbL material is only deposited onto the surface of the EFM, penetrating ~5 μm at most into the film. As an illustration, Figure 5-6b shows the lack of LbL film growth on the back side of the nylon EFM. The apparent surface film in Figure 5-6b is caused by polymer solutions that become trapped in the funnel holding the EFM and collect on the downstream side during the spray process. Thus, these spray coated films would not perform well in a fuel cell due to poor conductivity though the composite and high fuel crossover.

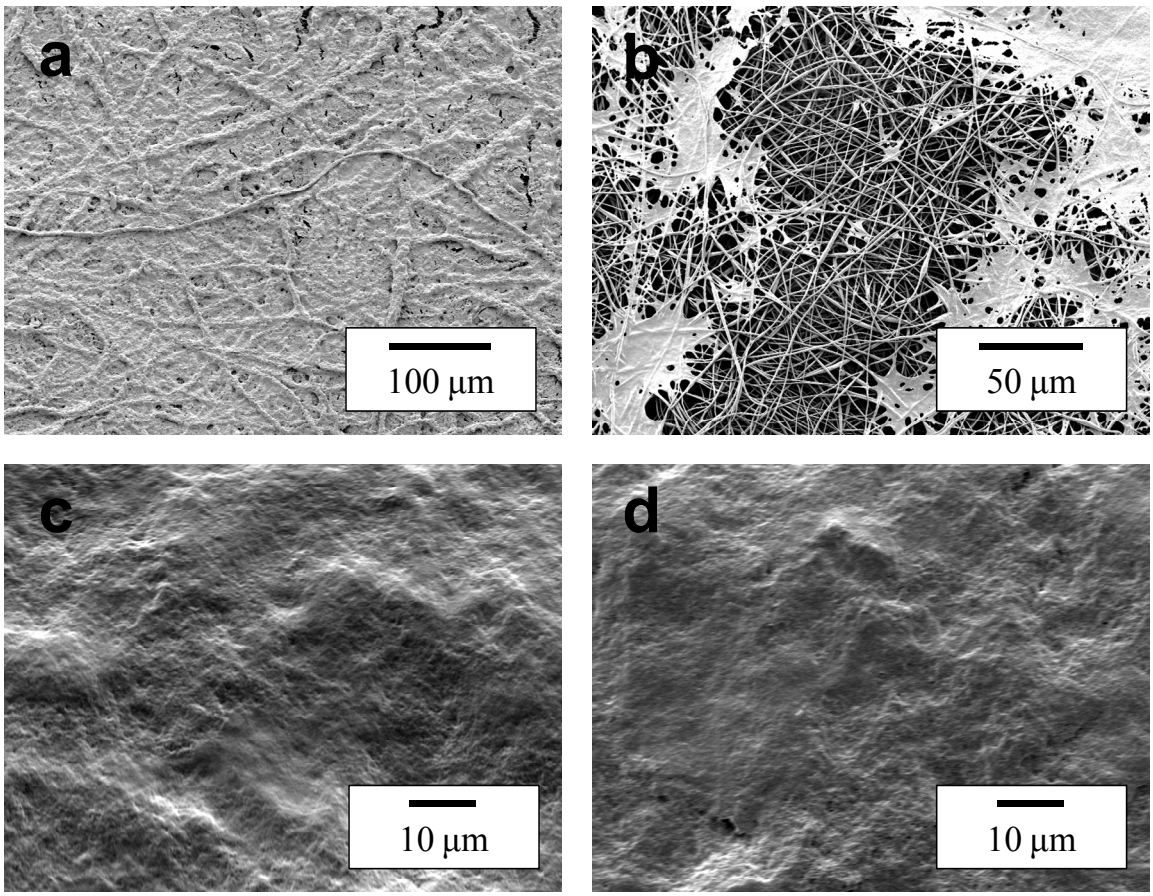

Figure 5-6. SEM images of nylon EFMs (a – front-side, b – back-side) spray coated with 175 BL of PDAC/SPS. The spray coatings provide a less uniform surface coating on the front of the EFM where the underlying fibers are still visible. When a vacuum is applied during the spray deposition more uniform surface films are observed (c). After 150 BL are deposited on the front the EFM is flipped over to produce an identical coating on the backside of the EMF (d).

To further improve the application of these composite membranes for use in fuel cells, a vacuum is applied to the downstream side of the EMF during assembly. Applying a vacuum during the LbL spraying process allows for the polymer mists to penetrate the thickness of the EFM and to potentially provide a highly conductive matrix that will

prevent fuel crossover. Figure 5-6c shows a representative SEM image of the nylon EFM that is coated with 150 BL of PDAC/SPS with a mild vacuum applied to the back of the EFM. Interestingly, the surface of the mat appears to have a more uniform coating when the vacuum is applied during LbL deposition. When a mild vacuum is applied to the EFM, the individual fibers of the EFM are conformally coated, as the deposition occurs below the critical Reynolds number for flow separation from the downstream side of a cylinder.[162] Thus, the LbL films deposit conformally on each fiber, eventually coalescing on the surface into a uniform surface coating. In contrast, the LbL coating applied without vacuum forms only on the exposed parts of the fibers, producing a surface film where the underlying fibers are still visible. Furthermore, the nylon EMF coated with vacuum is flipped and 150 BL are also coated onto the backside, as shown in Figure 5-6d. It is clear that the vacuum is still sufficient to yield the same coating as on the front-side of the EMF.

To probe the interior of the spray coated EFMs, cross-sectional SEM images are obtained by freeze fracturing the composite membranes in liquid nitrogen. Figure 5-7a shows the cross-section of a nylon EFM spray coated with 175 BL of PDAC/SPS without vacuum, and Figure 5-7b shows a spray coated EFM with 150 BL of PDAC/SPS with vacuum. For composite membranes prepared without vacuum, the interior of the EFM remains mostly void space and it appears that the individual fibers are not coated. It is clear that a surface coating comprises most of the LbL film that is deposited during spraying. For samples prepared with vacuum, Figure 5-7b shows that the individual fibers of the EFM are coated up to 50 μm into the film. The enlarged inset shows that the conformal nature of the coating can extend over 1 μm in thickness for this set of

conditions. It is clear that the vacuum spraying produces superior composite membranes and that with further optimization, LbL EFM composite membranes could be produced with minimal, if any, void space.

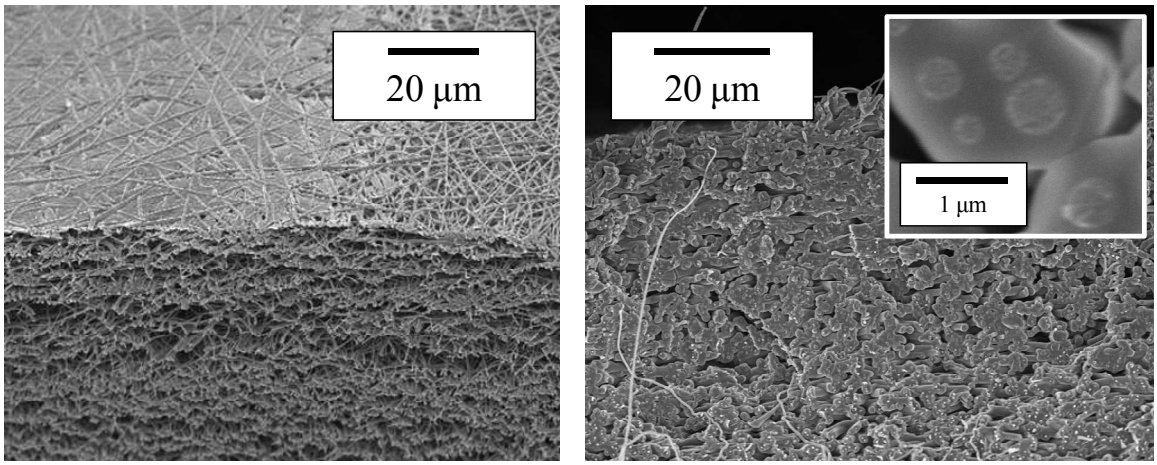

Figure 5-7. Cross-sectional SEM images of nylon EFMs spray coated with 175 BL of PDAC/SPS without vacuum (left) and spray coated with 150 BL of PDAC/SPS with vacuum (right). Without vacuum, the interior of the EFM is uncoated and only a surface film is formed. With vacuum applied, the fibers of the EFMs are conformally coated and a uniform surface is present.

Monotonic and cyclic uniaxial tensile testing is performed on nylon EMFs and nylon EMFs spray coated with PDAC/SPS LbL films to attain the mechanical behavior of these systems (Figure 5-8). Uncoated nylon EFMs exhibit elastic-plastic behavior with an elastic modulus ranging from 8 - 53 MPa and a yield stress ranging from 0.2 - 2 MPa. In cyclic testing the nylon EFMs are seen to unload linearly at the same slope as the initial loading and to reload along nearly the same path as unloading. The variation in modulus and yield stress values are attributed to variations in the relative humidity at the

time of testing, although spraying the specimen with water prior to testing does not induce significant changes in the mechanical behavior as compared to a film tested at 47 % RH. The nylon EFMs are susceptible to necking and break at strains ranging from 0.3 - 1.0. The elastic modulus of the PDAC/SPS spray coated nylon EMFs is equivalent to or slightly greater than the uncoated nylon EFM. However, the failure mode is distinct from either the pristine LbL film or the uncoated EFM. At an intermediate strain, the surface LbL coating of the composite membrane tears, while the rest of the film remains intact and is able to continue to support a significant stress. After this tear initiates, the majority of the deformation will occur at the tear. A specimen that had this tear occur at a strain of 0.02 did not fail completely until a local strain of 0.8 was observed. The mechanical characteristics of the coated mats actually improved when tested after being soaked in water for 5 minutes. The elastic modulus dropped by 50% relative to the dry specimens, but the deformation was uniform and there was no partial tearing up to a strain of 0.15.

Figure 5-9 shows SEM images of the spray coated EFMs after mechanical testing for both the dry and hydrated cases; it is clear that in the dry case cracking occurs all along the surface whereas in the hydrated case the surface layer is able to deform with the rest of the mat without cracking. This results from the more ductile behavior of the LbL coating under hydrated conditions as seen in bare film testing. Consequently, the spray coated mats exhibit superior mechanical properties as compared to the bare films, but are still deficient when compared to commercial PEMs. A summary of the mechanical properties of the materials studied in this chapter is given in Table 5-1.

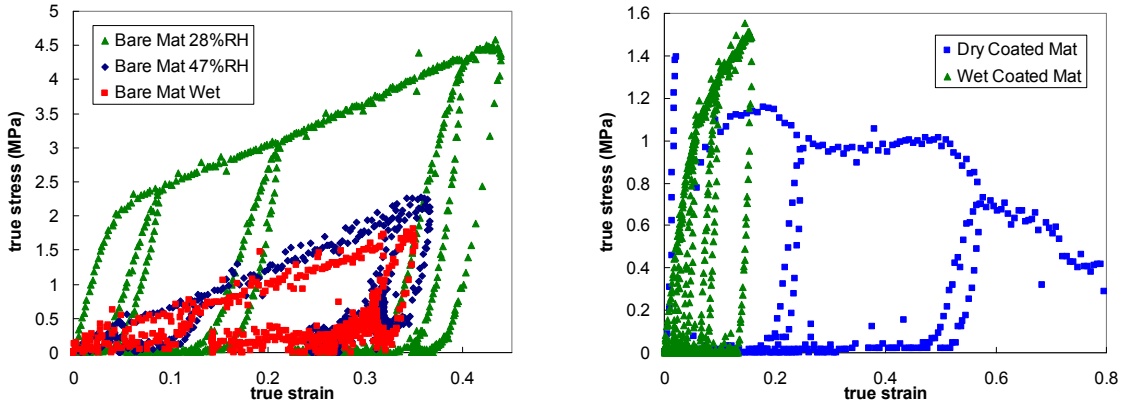

Figure 5-8. Cyclic stress-strain curves for nylon EMFs at several relative humidity values (left). Cyclic stress-strain curves for nylon EMFs spray coated with 175 BL of PDAC/SPS at ambient (dry) and fully humidified (wet) conditions (right). The PDAC/sPPO films are assembled at pH = 1.0 with 0.5 M NaCl in the sPPO assembly solution.

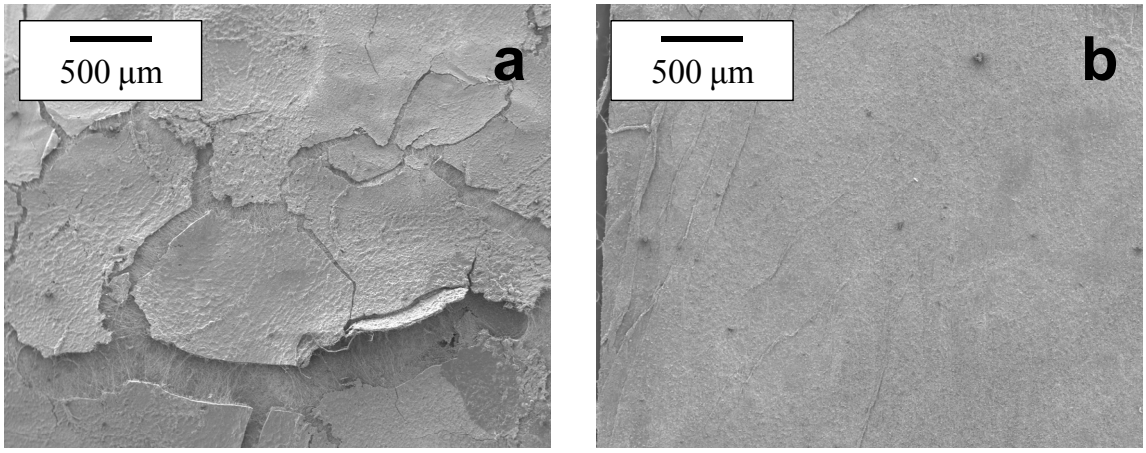

Figure 5-9. SEM images of the spray coated EFMs after mechanical testing at dry (a) and hydrated (b) conditions. When tested at dry conditions, cracking of the LbL coating occurs all along the surface; however at hydrated conditions, the LbL coating is able to deform with the rest of the EFM without cracking or detaching.

Table 5-1. Comparison of the mechanical properties (elastic modulus and break strain) of the LbL films, EFMs, and composite membranes studied in Chapter 5.

Sample	Conditions	Elastic Modulus (MPa)	Break Strain
Nafion	Ambient	300	> 1.0
PDAC/sPPO	Ambient	250 – 1100	~ 0.1
PDAC/sPPO	Hydrated	~ 1	n/a
Nylon EFM	Both	10 – 50	0.3 – 1.0
Nylon Spray Coated	Ambient	60 – 90	~ 0.1
Nylon Spray Coated	Hydrated	30 – 50	> 0.2

5.4 Conclusion

Composite membranes of highly conductive layer-by-layer (LbL) films and electrospun fiber mats (EFMs) are investigated for fuel cell applications. The mechanical properties of highly conducting PDAC/sPPO LbL films are improved by forming the LbL matrix on highly tunable EFM support. Free standing PDAC/sPPO films have an elastic modulus values up to 1100 MPa and maximum yield stress values of 40 MPa. PDAC/sPPO films assembled with more salt in the assembly baths have better mechanical properties due to the more favorable crosslinked network that is formed. The mechanical properties of PDAC/sPPO are on par with commercial PEMs like Nafion at

moderate relative humidity to dry conditions; however, the PDAC/sPPO films break at extremely low strains (~ 0.07) and become very rubbery with low elastic modulus values. Coating a PCL EFM with the LbL dipping process produces composite membranes with interesting "bridged" morphologies that span adjacent fibers. The ionic conductivity of the composite membranes is similar to the pristine LbL system, especially when thick coatings are applied. To increase the thickness of LbL coatings and fill in more of the void space in the EFM, the spray LbL assembly is utilized as a means for the rapid formation of LbL films. When the spray LbL technique is used along with an applied pressure gradient across the EFM during assembly, the resulting LbL EFM composites have conformal coatings of the individual fibers throughout the bulk of the EFM and have uniform surface coatings. The mechanical properties of the spray coated EMFs are shown to be superior to the LbL only system, particularly at hydrated conditions. Future studies are underway to model the mechanical behavior of the LbL EFM composite membranes, and to develop future systems with increased mechanical durability.

Summary and Perspective

In this thesis work, the performance of LbL assembled solid state ion conductors is substantially improved, while structure-property relationships are studied and developed to allow the tuning of the LbL process to produce films with optimal bulk properties. First, LbL assembled films of poly[bis(methoxyethoxyethoxy)-phosphazene] (MEEP) and poly (acrylic acid) (PAA) are investigated, where the hydrogen bonding between these two polymers controls film growth. At fully humidified conditions, the ionic conductivity of MEEP/PAA is over one order of magnitude higher than previously studied hydrogen-bonded LbL systems. Films assembled at optimal pH conditions have enhanced water uptake and transport properties, which play a key role in increasing ion transport within the films.

Next, LbL systems based on a highly sulfonated aromatic polyether (sPPO) are studied. The best performing sPPO system has ionic conductivity values which are the same order of magnitude as commercially relevant PEMs and is the highest ionic conductivity ever obtained from a LbL assembled film. Additionally, these LbL systems have methanol permeability values over two orders of magnitude lower than traditional PEMs. Consequently, the incorporation of sPPO systems into DMFCs results in a 53% improvement in power output. By studying sPPO films assembled over a range of assembly conditions, it is shown that films assembled with salt selectively added to the sPPO assembly bath have the best performance due to a combination of enhanced water uptake and transport, favorable composition, and reduced ionic crosslink density. Lastly, the mechanical properties of highly conducting LbL films are improved by using robust

electrospun fiber mats (EFMs) as supporting substrates. The LbL sPPO systems have poor mechanical properties when hydrated. Coating an EFM with the LbL dipping process produces composite membranes with interesting "bridged" morphologies and maintains the high ionic conductivity values of the neat LbL film. Spray LbL assembly is employed to rapidly fabricate LbL films on EFMs. The mechanical properties of the spray coated EMFs are shown to be superior to the pristine LbL systems, especially at hydrated conditions.

The future success of PEM fuel cells is certainly up for debate. Although significant effort has focused on hydrogen fuel cells for automotive applications, it quite unlikely that widespread adoption of fuel cell powered cars will happen. High costs for the fuel cell system (and thus vehicle) and the required infrastructure almost guarantee we will not see fuel cell vehicles populating our streets. Consumer behavior, safety issues, and governmental policy also pose hurdles to the adoption of fuel cell powered vehicles. However, it is likely that hydrogen fuel cells will succeed in niche markets, which will aid in the development of improved fuel cell technology. Hydrogen fuel cells have found commercial application in warehouse forklifts, stationary backup power for office buildings and data centers, and in residential combined heat and power (CHP) units. In all of these applications, the benefits of rapid startup time, high up-time, high efficiency, and environmental friendliness outweigh the negatives, mainly the high system cost. For DMFCs, the "holy grail" is widespread use in consumer electronics – laptops, cell phones, portable media players, GPS devices, etc. Similar obstacles to hydrogen fuels cells also exist for DMFCs. As compared to the incumbent technology, batteries (especially Li-ion batteries), DMFCs offer the benefits of long lifetime, quick

recharging, and reduced weight; however the increased cost associated with DMFC systems prevent their use in these commercial applications. Again, similar to hydrogen fuel cells, DFMCs have found use in niche applications, with portable power for military being the most promising area. For powering the equipment of soldiers, the benefits DMFCs offer enhance soldier survivability and are thus worth the premium costs. As DMFC systems are refined for military use, advances in technology may allow for the introduction into select consumer devices.

Improved PEMs will allow for the production of fuel cells that are more efficient, reliable, and durable, have longer lifetimes, and are more cost effective. Paired with advanced catalysts, particularly high performing non-precious metal catalysts, and improved MEA fabrication, the future for fuel cells looks promising (with the above caveats for automobiles and consumer electronics properly considered). For almost 50 years, Nafion and other perfluorosulfonated membranes have almost been exclusively used as PEMs, although significant effort over that time has focused on synthesizing polymers that perform better. This thesis work shows that a simpler, better approach to PEM fabrication is found in LbL assembly. The spectrum of materials that can be incorporated into LbL films for solid-state electrolyte applications is only beginning to be explored. Judicious selection of future polymers for LbL assembly, tuned using the guidelines discussed throughout this work, and mechanically reinforced, if necessary, with EFMs or other substrates, will allow for even more compelling PEMs to be developed. Not only will applications in fuel cells be realized, but other systems, such as batteries, solar cells, electrochromic devices, sensors, and photoelectrochemical devices will greatly benefit from these high performing LbL assembled materials.

References

1. de Bruijn, F., The current status of fuel cell technology for mobile and stationary applications. *Green Chemistry* **2005,** 7, (3), 132-150.
2. Institute, C. F. C. What is a fuel cell? http://abruna.chem.cornell.edu/fuelcell/what%20is%20a%20fuel%20cell.html.
3. Hockaday, R.; Navas, C., Proceedings of the Conference on Portable Fuel Cells. **1999**, 45.
4. Kho, B. K.; Bae, B.; Scibioh, M. A.; Lee, J.; Ha, H. Y., On the consequences of methanol crossover in passive air-breathing direct methanol fuel cells. *Journal of Power Sources* **2005,** 142, (1-2), 50-55.
5. Doyle, M.; Rajendran, G., Perfluorinated Membranes. In *Handbook of Fuel Cells: Fundamentals, Technology and Applications*, Vielstich, W.; Lamm, A.; Gasteiger, H. A., Eds. John Wiley & Sons Ltd.: Chichester, England, 2003; Vol. 1, pp 351-411.
6. Srinivasan, S.; Dave, B. B.; Murugesamoorthi, K. A.; Parthasarathy, A.; Appleby, A. J., Overview of Fuel Cell Technology. In *Fuel Cell Systems*, Blomen, L. J. M. J.; Mugerwa, M. N., Eds. Plenum Press: New York, NY, 1993; pp 37-72.
7. Alkire, R. C.; Gerischer, H.; Kolb, D. M.; Tobias, C. W., Advances in Electrochemical Science and Engineering. **1997,** 5, 195-301.
8. Curtin, D. E.; Lousenberg, R. D.; Henry, T. J.; Tangeman, P. C.; Tisack, M. E., Advanced materials for improved PEMFC performance and life. *Journal of Power Sources* **2004,** 131, (1-2), 41-48.
9. Vielstich, W., Ideal and effective efficiencies of cell reactions and comparison to carnot cycyles. In *Handbook of Fuel Cells: Fundamentals, Technology and Applications*, Vielstich, W.; Lamm, A.; Gasteiger, H. A., Eds. John Wiley & Sons Ltd.: Chichester, England, 2003; Vol. 1, pp 26-30.
10. Decher, G.; Hong, J. D.; Schmitt, J., Buildup of Ultrathin Multilayer Films by a Self-Assembly Process .3. Consecutively Alternating Adsorption of Anionic and Cationic Polyelectrolytes on Charged Surfaces. *Thin Solid Films* **1992,** 210, (1-2), 831-835.
11. Decher, G., Fuzzy nanoassemblies: toward layered polymeric multicomposites. *Science* **1997,** 277, (5330), 1232-1237.
12. Schlenoff, J. B.; Dubas, S. T., Mechanism of Polyelectrolyte Multilayer Growth: Charge Overcompensation and Distribution. *Macromolecules* **2001,** 34, (3), 592-598.
13. Clark, S. L.; Montague, M. F.; Hammond, P. T., The effect of ion type and ionic content on templating patterned ionic multilayers. In *Organic Thin Films*, 1998; Vol. 695, pp 206-219.
14. Shiratori, S. S.; Rubner, M. F., pH-Dependent Thickness Behavior of Sequentially Adsorbed Layers of Weak Polyelectrolytes. *Macromolecules* **2000,** 33, (11), 4213-4219.
15. Berg, M. C. Biological Applications of Weak Polyelectrolyte Multilayers. Massachusetts Institute of Technology, Cambridge, MA, 2005.

16. Eckle, M.; Decher, G., Tuning the Performance of Layer-by-Layer Assembled Organic Light Emitting Diodes by Controlling the Position of Isolating Clay Barrier Sheets. *Nano Letters* **2001,** 1, (1), 45-49.
17. Yamada, M.; Shiratori, S. S., Smoke sensor using mass controlled layer-by-layer self-assembly of polyelectrolytes films. *Sensors and Actuators B: Chemical* **2000,** 64, (1-3), 124-127.
18. DeLongchamp, D.; Hammond, P. T., Layer-by-layer assembly of PEDOT/polyaniline electrochromic devices. *Advanced Materials* **2001,** 13, (19), 1455-+.
19. Brust, M.; Bethell, D.; Kiely, C. J.; Schiffrin, D. J., Self-Assembled Gold Nanoparticle Thin Films with Nonmetallic Optical and Electronic Properties. *Langmuir* **1998,** 14, (19), 5425-5429.
20. Hua, F.; Shi, J.; Lvov, Y.; Cui, T., Patterning of Layer-by-Layer Self-Assembled Multiple Types of Nanoparticle Thin Films by Lithographic Technique. *Nano Letters* **2002,** 2, (11), 1219-1222.
21. Kotov, N. A.; Magonov, S.; Tropsha, E., Layer-by-Layer Self-Assembly of Alumosilicate-Polyelectrolyte Composites: Mechanism of Deposition, Crack Resistance, and Perspectives for Novel Membrane Materials. *Chemistry of Materials* **1998,** 10, (3), 886-895.
22. Liu, Y.; Wang, A.; Claus, R. O., Layer-by-layer electrostatic self-assembly of nanoscale Fe3O4 particles and polyimide precursor on silicon and silica surfaces. *Applied Physics Letters* **1997,** 71, (16), 2265-2267.
23. Hammond, P. T., Form and Function in Multilayer Assembly: New Applications at the Nanoscale. *Advanced Materials* **2004,** 16, (15), 1271-1293.
24. Sukhorukov, G. B.; Donath, E.; Lichtenfeld, H.; Knippel, E.; Knippel, M.; Budde, A.; Möhwald, H., Layer-by-layer self assembly of polyelectrolytes on colloidal particles. *Colloids and Surfaces A: Physicochemical and Engineering Aspects* **1998,** 137, (1-3), 253-266.
25. Lvov, Y. M.; Lu, Z.; Schenkman, J. B.; Zu, X.; Rusling, J. F., Direct Electrochemistry of Myoglobin and Cytochrome P450cam in Alternate Layer-by-Layer Films with DNA and Other Polyions. *Journal of the American Chemical Society* **1998,** 120, (17), 4073-4080.
26. Decher, G.; Schlenoff, J. B., *Multilayer thin films : sequential assembly of nanocomposite materials*. Wiley-VCH: Weinheim, 2003; p xix, 524 p.
27. Wang, L.; Wang, Z.; Zhang, X.; Shen, J.; Chi, L.; Fuchs, H., A new approach for the fabrication of an alternating multilayer film of poly(4-vinylpyridine) and poly(acrylic acid) based on hydrogen bonding. *Macromolecular Rapid Communications* **1997,** 18, (6), 509-514.
28. Stockton, W. B.; Rubner, M. F., Molecular-Level Processing of Conjugated Polymers. 4. Layer-by-Layer Manipulation of Polyaniline via Hydrogen-Bonding Interactions. *Macromolecules* **1997,** 30, (9), 2717-2725.
29. Quinn, J. F.; Caruso, F., Facile Tailoring of Film Morphology and Release Properties Using Layer-by-Layer Assembly of Thermoresponsive Materials. *Langmuir* **2004,** 20, (1), 20-22.
30. Sukhishvili, S. A.; Granick, S., Layered, Erasable, Ultrathin Polymer Films. *J. Am. Chem. Soc.* **2000,** 122, (39), 9550-9551.

31. DeLongchamp, D. M.; Hammond, P. T., Highly Ion Conductive Poly(ethylene oxide)-Based Solid Polymer Electrolytes from Hydrogen Bonding Layer-by-Layer Assembly. *Langmuir* **2004,** 20, (13), 5403-5411.
32. Zhang, H. Y.; Wang, Z. Q.; Zhang, Y. Q.; Zhang, X., Hydrogen-bonding-directed layer-by-layer assembly of poly(4-vinylpyridine) and poly(4-vinylphenol): Effect of solvent composition on multilayer buildup. *Langmuir* **2004,** 20, (21), 9366-9370.
33. Michaels, A. C., Polyelectrolyte Complexes. *Industrial and Engineering Chemistry* **1965,** 57, (10), 32-40.
34. Farhat, T. R.; Schlenoff, J. B., Ion Transport and Equilibria in Polyelectrolyte Multilayers. *Langmuir* **2001,** 17, (4), 1184-1192.
35. Krasemann, L.; Tieke, B., Selective ion transport across self-assembled alternating multilayers of cationic and anionic polyelectrolytes. *Langmuir* **2000,** 16, (2), 287-290.
36. Harris, J. J.; Stair, J. L.; Bruening, M. L., Layered Polyelectrolyte Films as Selective, Ultrathin Barriers for Anion Transport. *Chemistry of Materials* **2000,** 12, (7), 1941-1946.
37. DeLongchamp, D. M.; Hammond, P. T., Fast Ion Conduction in Layer-By-Layer Polymer Films. *Chem. Mater.* **2003,** 15, (5), 1165-1173.
38. Gray, F. M., *Polymer Electrolytes*. Royal Society of Chemistry: Cambridge, England, 1997.
39. Farhat, T. R.; Hammond, P. T., Designing a new generation of proton-exchange membranes using layer-by-layer deposition of polyelectrolytes. *Advanced Functional Materials* **2005,** 15, (6), 945-954.
40. Pivovar, B. S., An overview of electro-osmosis in fuel cell polymer electrolytes. *Polymer* **2006,** 47, (11), 4194-4202.
41. Zawodzinski, J. T. A.; Derouin, C.; Radzinski, S.; Sherman, R. J.; Smith, V. T.; Springer, T. E.; Gottesfeld, S., Water Uptake by and Transport Through Nafion 117 Membranes. *Journal of The Electrochemical Society* **1993,** 140, (4), 1041-1047.
42. Vogt, B. D.; Soles, C. L.; Lee, H. J.; Lin, E. K.; Wu, W., Moisture absorption into ultrathin hydrophilic polymer films on different substrate surfaces. *Polymer* **2005,** 46, (5), 1635-1642.
43. Smith, A. L.; Ashcraft, J. N.; Hammond, P. T., Sorption isotherms, sorption enthalpies, diffusion coefficients and permeabilities of water in a multilayer PEO/PAA polymer film using the quartz crystal microbalance/heat conduction calorimeter. *Thermochimica Acta* **2006,** 450, (1-2), 118-125.
44. Crank, J., *The Mathematics of Diffusion*. Oxford University Press: Oxford, 1979.
45. Hernandez-Munoz, P.; Gavara, R.; Hernandez, R. J., Evaluation of solubility and diffusion coefficients in polymer film-vapor systems by sorption experiments. *Journal of Membrane Science* **1999,** 154, (2), 195-204.
46. Bard, A.; Faulkner, L., *Electrochemical Methods: Fundamentals and Applications*. Second ed.; John Wiley and Sons, Inc.: Hoboken, 2001.
47. Shukla, P. K.; Orazem, M. E.; Crisalle, O. D., Validation of the measurement model concept for error structure identification. *Electrochimica Acta* **2004,** 49, (17-18), 2881-2889.

48. Orazem, M. E., A systematic approach toward error structure identification for impedance spectroscopy. *Journal of Electroanalytical Chemistry* **2004,** 572, (2), 317-327.
49. Wright, P. V., Polymer electrolytes - the early days. *Electrochimica Acta* **1998,** 43, (10-11), 1137-1143.
50. Mendolia, M. S.; Farrington, G. C., High-conductivity, solid polymeric electrolytes. *Adv. Chem. Ser.* **1995,** 245, (Materials Chemistry), 107-30.
51. Murata, K.; Izuchi, S.; Yoshihisa, Y., An overview of the research and development of solid polymer electrolyte batteries. *Electrochimica Acta* **2000,** 45, (8-9), 1501-1508.
52. Blonsky, P. M.; Shriver, D. F.; Austin, P.; Allcock, H. R., Polyphosphazene Solid Electrolytes. *Journal of the American Chemical Society* **1984,** 106, (22), 6854-6855.
53. Allcock, H. R.; Austin, P. E.; Neenan, T. X.; Sisko, J. T.; Blonsky, P. M.; Shriver, D. F., Polyphosphazenes with etheric side groups: prospective biomedical and solid electrolyte polymers. *Macromolecules* **1986,** 19, (6), 1508-12.
54. Blonsky, P. M.; Shriver, D. F.; Austin, P.; Allcock, H. R., Complex-Formation and Ionic-Conductivity of Polyphosphazene Solid Electrolytes. *Solid State Ionics* **1986,** 18-9, 258-264.
55. Bennett, J. L.; Dembek, A. A.; Allcock, H. R.; Heyen, B. J.; Shriver, D. F., Radiation crosslinking of poly[bis(2-(2-methoxyethoxy)ethoxy)phosphazene]: effect on solid-state ionic conductivity. *Chemistry of Materials* **1989,** 1, (1), 14-16.
56. Nelson, C. J.; Coggio, W. D.; Allcock, H. R., Ultraviolet Radiation-Induced Cross-Linking of Poly[Bis(2-(2-Methoxyethoxy)Ethoxy)Phosphazene]. *Chemistry of Materials* **1991,** 3, (5), 786-787.
57. Lutkenhaus, J. L.; Hammond, P. T., Electrochemically enabled polyelectrolyte multilayer devices: from fuel cells to sensors. *Soft Matter* **2007,** 3, (7), 804-816.
58. Argun, A. A.; Ashcraft, J. N.; Hammond, P. T., Highly Conductive, Methanol Resistant Polyelectrolyte Multilayers. *Advanced Materials* **2008,** 20, 1539-1543.
59. Sukhishvili, S. A.; Granick, S., Layered, Erasable, Ultrathin Polymer Films. *Journal of the American Chemical Society* **2000,** 122, (39), 9550-9551.
60. Kharlampieva, E.; Sukhishvili, S. A., Hydrogen-bonded layer-by-layer polymer films. *Polymer Reviews* **2006,** 46, (4), 377-395.
61. Sauerbrey, G., The use of quartz oscillators for weighing thin layers and for microweighing. *Z. Phys.* **1959,** 155, 206-222.
62. Lutkenhaus, J. L.; McEnnis, K.; Hammond, P. T., Tuning the Glass Transition of and Ion Transport within Hydrogen-Bonded Layer-by-Layer Assemblies. *Macromolecules* **2007,** 40, (23), 8367-8373.
63. Paddison, S. J., Proton conduction mechanisms at low degrees of hydration in sulfonic acid-based polymer electrolyte membranes. *Annual Review of Materials Research* **2003,** 33, 289-319.
64. Wang, L. Y.; Fu, Y.; Wang, Z. Q.; Fan, Y. G.; Zhang, X., Investigation into an alternating multilayer film of poly(4-vinylpyridine) and poly(acrylic acid) based on hydrogen bonding. *Langmuir* **1999,** 15, (4), 1360-1363.

65. Lutkenhaus, J. L.; Hrabak, K. D.; McEnnis, K.; Hammond, P. T., Elastomeric flexible free-standing hydrogen-bonded nanoscale assemblies. *Journal of the American Chemical Society* **2005,** 127, (49), 17228-17234.
66. Fox, T. G., Bulletin of the American Physical Society **1956,** 1, 123.
67. Arce, A.; Fornasiero, F.; Rodriguez, O.; Radke, C. J.; Prausnitz, J. M., Sorption and transport of water vapor in thin polymer films at 35 degrees C. *Physical Chemistry Chemical Physics* **2004,** 6, (1), 103-108.
68. Pourcelly, G.; Oikonomou, A.; Gavach, C.; Hurwitz, H. D., Influence of the Water-Content on the Kinetics of Counterion Transport in Perfluorosulfonic Membranes. *Journal of Electroanalytical Chemistry* **1990,** 287, (1), 43-59.
69. Zawodzinski, T. A.; Derouin, C.; Radzinski, S.; Sherman, R. J.; Smith, V. T.; Springer, T. E.; Gottesfeld, S., Water-Uptake by and Transport through Nafion(R) 117 Membranes. *Journal of the Electrochemical Society* **1993,** 140, (4), 1041-1047.
70. Smitha, B.; Sridhar, S.; Khan, A. A., Solid polymer electrolyte membranes for fuel cell applications - a review. *Journal of Membrane Science* **2005,** 259, (1-2), 10-26.
71. Wegner, G., Polymers as functional components in batteries and fuel cells. *Polymers for Advanced Technologies* **2006,** 17, (9-10), 705-708.
72. Rajendran, R. G., Polymer electrolyte membrane technology for fuel cells. *MRS Bulletin* **2005,** 30, (8), 587-590.
73. Vielstich, W.; Lamm, A.; Gasteiger, H. A., *Handbook of Fuel Cells : Fundamentals, Technology, and Applications*. Wiley: Chichester, England ; New York, 2003.
74. Cho, J.; Char, K.; Hong, J. D.; Lee, K. B., Fabrication of highly ordered multilayer films using a spin self-assembly method. *Advanced Materials* **2001,** 13, (14), 1076-1078.
75. Lowman, G. M.; Hammond, P. T., Solid-state dye-sensitized solar cells combining a porous TiO2 film and a layer-by-layer composite electrolyte. *Small* **2005,** 1, (11), 1070-1073.
76. DeLongchamp, D. M.; Kastantin, M.; Hammond, P. T., High-Contrast Electrochromism from Layer-By-Layer Polymer Films. *Chemistry of Materials* **2003,** 15, (8), 1575-1586.
77. DeLongchamp, D. M.; Hammond, P. T., Fast Ion Conduction in Layer-By-Layer Polymer Films. *Chemistry of Materials* **2003,** 15, (5), 1165-1173.
78. Arico, A. S.; Srinivasan, S.; Antonucci, V., DMFCs: from fundamental aspects to technology development. *Fuel Cells* **2001,** 1, (2), 133-161.
79. Vielstich, W.; Lamm, A.; Gasteiger, H. A., *Handbook of Fuel Cells : Fundamentals, Technology, and Applications*. Wiley: Chichester, England ; New York, 2003; p 4 v.
80. Qi, Z.; Kaufman, A., Open circuit voltage and methanol crossover in DMFCs. *Journal of Power Sources* **2002,** 110, (1), 177-185.
81. Jiang, S. P.; Liu, Z.; Tian, Z. Q., Layer-by-Layer Self-Assembly of Composite Polyelectrolyte-Nafion Membranes for Direct Methanol Fuel Cells. *Advanced Materials* **2006,** 18, (8), 1068-1072.

82. Si, Y. C.; Lin, J. C.; Kunz, H. R.; Fenton, J. M., Trilayer membranes with a methanol-barrier layer for DMFCs. *Journal of the Electrochemical Society* **2004,** 151, (3), A463-A469.
83. Miyake, N.; Wainright, J. S.; Savinell, R. F., Evaluation of a sol-gel derived Nafion/silica hybrid membrane for polymer electrolyte membrane fuel cell applications - II. Methanol uptake and methanol permeability. *Journal of the Electrochemical Society* **2001,** 148, (8), A905-A909.
84. Yang, B.; Manthiram, A., Multilayered membranes with suppressed fuel crossover for direct methanol fuel cells. *Electrochemistry Communications* **2004,** 6, (3), 231-236.
85. Hickner, M. A.; Ghassemi, H.; Kim, Y. S.; Einsla, B. R.; McGrath, J. E., Alternative Polymer Systems for Proton Exchange Membranes (PEMs). *Chemical Reviews* **2004,** 104, (10), 4587-4611.
86. Roziere, J.; Jones, D. J., Non-fluorinated polymer materials for proton exchange membrane fuel cells. *Annual Review of Materials Research* **2003,** 33, 503-555.
87. Wainright, J. S.; Wang, J. T.; Weng, D.; Savinell, R. F.; Litt, M., Acid-doped polybenzimidazoles: a new polymer electrolyte. *Journal of the Electrochemical Society* **1995,** 142, (7), L121-L123.
88. Pu, H.; Meyer, W. H.; Wegner, G., Proton transport in polybenzimidazole blended with H3PO4 or H2SO4. *Journal of Polymer Science, Part B: Polymer Physics* **2002,** 40, (7), 663-669.
89. Bouzek, K.; Moravcova, S.; Samec, Z.; Schauer, J., H+ and Na+ ion transport properties of sulfonated poly(2,6-dimethyl-1,4-phenyleneoxide) membranes. *Journal of the Electrochemical Society* **2003,** 150, (6), E329-E336.
90. Yang, S.; Gong, C.; Guan, R.; Zou, H.; Dai, H., Sulfonated poly(phenylene oxide) membranes as promising materials for new proton exchange membranes. *Polymers for Advanced Technologies* **2006,** 17, (5), 360-365.
91. Jung, B.; Kim, B.; Yang, J. M., Transport of methanol and protons through partially sulfonated polymer blend membranes for direct methanol fuel cell. *Journal of Membrane Science* **2004,** 245, (1-2), 61-69.
92. Kim, B.; Jung, B., Partially sulfonated polystyrene and poly(2,6-dimethyl-1,4-phenylene oxide) blend membranes for fuel cells. *Macromolecular Rapid Communications* **2004,** 25, (13), 1263-1267.
93. Walker, M.; Baumgartner, K. M.; Kaiser, M.; Kerres, J.; Ullrich, A.; Rauchle, E., Proton-conducting polymers with reduced methanol permeation. *Journal of Applied Polymer Science* **1999,** 74, (1), 67-73.
94. Iojoiu, C.; Marechal, M.; Chabert, F.; Sanchez, J. Y., Mastering sulfonation of aromatic polysulfones: Crucial for membranes for fuel cell application. *Fuel Cells* **2005,** 5, (3), 344-354.
95. Huang, R. Y. M.; Kim, J. J., Synthesis and Transport Properties of Thin Film Composite Membranes. I. Synthesis of Poly(phenylene Oxide) Polymer and Its Sulfonation. *Journal of Applied Polymer Science* **1984,** 29, 4017.
96. Pivovar, B. S.; Wang, Y. X.; Cussler, E. L., Pervaporation membranes in direct methanol fuel cells. *Journal of Membrane Science* **1999,** 154, (2), 155-162.
97. Rossi, G.; Nulman, M., Effect of Local Flaws in Polymeric Permeation Reducing Barriers. *Journal of Applied Physics* **1993,** 74, (9), 5471-5475.

98. Mauritz, K. A.; Moore, R. B., State of Understanding of Nafion. *Chem. Rev.* **2004,** 104, (10), 4535-4586.
99. Savinell, R.; Yeager, E.; Tryk, D.; Landau, U.; Wainright, J.; Weng, D.; Lux, K.; Litt, M.; Rogers, C., A Polymer Electrolyte for Operation at Temperatures up to 200 C. *Journal of The Electrochemical Society* **1994,** 141, (4), L46-L48.
100. Li, Q.; He, R.; Jensen, J. O.; Bjerrum, N. J., Approaches and Recent Development of Polymer Electrolyte Membranes for Fuel Cells Operating above 100 C. *Chemistry of Materials* **2003,** 15, (26), 4896-4915.
101. Ren, X.; Zawodzinski, T. A.; Uribe, F.; Dai, H.; Gottesfield, S., Methanol Cross-over in Direct Methanol Fuel Cells. *Electrochemical Society Proceedings* **1995,** 95-23, 284-298.
102. Heinzel, A.; Barragan, V. M., A review of the state-of-the-art of the methanol crossover in direct methanol fuel cells. *Journal of Power Sources* **1999,** 84, (1), 70-74.
103. Wang, J. T.; Wainright, J. S.; Savinell, R. F.; Litt, M., A direct methanol fuel cell using acid-doped polybenzimidazole as polymer electrolyte. *Journal of Applied Electrochemistry* **1996,** 26, (7), 751-756.
104. Hickner, M. A.; Ghassemi, H.; Kim, Y. S.; Einsla, B. R.; McGrath, J. E., Alternative Polymer Systems for Proton Exchange Membranes (PEMs). *Chemical Reviews* **2004,** 104, (10), 4587-4612.
105. Jia, N.; Lefebvre, M. C.; Halfyard, J.; Qi, Z.; Pickup, P. G., Modification of Nafion Proton Exchange Membranes to Reduce Methanol Crossover in PEM Fuel Cells. *Electrochemical and Solid-State Letters* **2000,** 3, (12), 529-531.
106. Shao, Z.-G.; Wang, X.; Hsing, I. M., Composite Nafion/polyvinyl alcohol membranes for the direct methanol fuel cell. *Journal of Membrane Science* **2002,** 210, (1), 147-153.
107. Ma, Z. Q.; Cheng, P.; Zhao, T. S., A palladium-alloy deposited Nafion membrane for direct methanol fuel cells. *Journal of Membrane Science* **2003,** 215, (1-2), 327-336.
108. Hobson, L. J.; Ozu, H.; Yamaguchi, M.; Hayase, S., Modified Nafion 117 as an Improved Polymer Electrolyte Membrane for Direct Methanol Fuel Cells. *Journal of The Electrochemical Society* **2001,** 148, (10), A1185-A1190.
109. Uchida, H.; Ueno, Y.; Hagihara, H.; Watanabe, M., Self-Humidifying Electrolyte Membranes for Fuel Cells. *Journal of The Electrochemical Society* **2003,** 150, (1), A57-A62.
110. Shao, P. L.; Mauritz, K. A.; Moore, R. B., [Perfluorosulfonate Ionomer]/[Mixed Inorganic Oxide] Nanocomposites via Polymer-in Situ Sol-Gel Chemistry. *Chemistry of Materials* **2002,** 7, (1), 192-200.
111. Tricoli, V., Proton and Methanol Transport in Poly(perfluorosulfonate) Membranes Containing Cs+ and H+ Cations. *Journal of The Electrochemical Society* **1998,** 145, (11), 3798-3801.
112. Argun, A. A.; Ashcraft, J. N.; Hammond, P. T., Highly Conductive, Methanol Resistant Polyelectrolyte Multilayers. *Advanced Materials* **2008,** 20, (8), 1539-1543.
113. Deligöz, H.; Yilmaztürk, S.; Karaca, T.; Özdemir, H.; Koç, S. N.; Öksüzömer, F.; Durmus, A.; Gürkaynak, M. A., Self-assembled polyelectrolyte multilayered

films on Nafion with lowered methanol cross-over for DMFC applications. *Journal of Membrane Science* **2009,** 326, (2), 643-649.
114. Durstock, M. F.; Rubner, M. F., Dielectric Properties of Polyelectrolyte Multilayers. *Langmuir* **2001,** 17, (25), 7865-7872.
115. Daiko, Y.; Katagiri, K.; Matsuda, A., Proton Conduction in Thickness-Controlled Ultrathin Polycation/Nafion Multilayers Prepared via Layer-by-Layer Assembly. *Chemistry of Materials* **2008,** 20, (20), 6405-6409.
116. Krogman, K. C.; Zacharia, N. S.; Schroeder, S.; Hammond, P. T., Automated Process for Improved Uniformity and Versatility of Layer-by-Layer Deposition. *Langmuir* **2007,** 23, (6), 3137-3141.
117. Lutkenhaus, J. L.; Hrabak, K. D.; McEnnis, K.; Hammond, P. T., Elastomeric Flexible Free-Standing Hydrogen-Bonded Nanoscale Assemblies. *J. Am. Chem. Soc.* **2005**.
118. Vogt, B. D.; Soles, C. L.; Lee, H.-J.; Lin, E. K.; Wu, W.-l., Moisture absorption into ultrathin hydrophilic polymer films on different substrate surfaces. *Polymer* **2005,** 46, (5), 1635-1642.
119. Smith, A. L.; Shirazi, H. M., Principles of quartz crystal microbalance/heat conduction calorimetry: Measurement of the sorption enthalpy of hydrogen in palladium. *Thermochimica Acta* **2005,** 432, (2), 202-211.
120. Sauerbrey, G., Verwendung von Schwingquarzen zur Wägung dünner Schichten und zur Mikrowägung. *Zeitschrift für Physik A Hadrons and Nuclei* **1959,** 155, (2), 206-222.
121. Tsukruk, V. V.; Bliznyuk, V. N.; Visser, D.; Campbell, A. L.; Bunning, T. J.; Adams, W. W., Electrostatic Deposition of Polyionic Monolayers on Charged Surfaces. *Macromolecules* **1997,** 30, (21), 6615-6625.
122. Losche, M.; Schmitt, J.; Decher, G.; Bouwman, W. G.; Kjaer, K., Detailed Structure of Molecularly Thin Polyelectrolyte Multilayer Films on Solid Substrates as Revealed by Neutron Reflectometry. *Macromolecules* **1998,** 31, (25), 8893-8906.
123. Ladam, G.; Schaad, P.; Voegel, J. C.; Schaaf, P.; Decher, G.; Cuisinier, F., In Situ Determination of the Structural Properties of Initially Deposited Polyelectrolyte Multilayers. *Langmuir* **1999,** 16, (3), 1249-1255.
124. Schmitt, J.; Gruenewald, T.; Decher, G.; Pershan, P. S.; Kjaer, K.; Loesche, M., Internal structure of layer-by-layer adsorbed polyelectrolyte films: a neutron and x-ray reflectivity study. *Macromolecules* **2002,** 26, (25), 7058-7063.
125. Dubas, S. T.; Schlenoff, J. B., Factors Controlling the Growth of Polyelectrolyte Multilayers. *Macromolecules* **1999,** 32, (24), 8153-8160.
126. Guzman, E.; Ritacco, H.; Rubio, J. E. F.; Rubio, R. G.; Ortega, F., Salt-induced changes in the growth of polyelectrolyte layers of poly(diallyl-dimethylammonium chloride) and poly(4-styrene sulfonate of sodium). *Soft Matter* **2009,** 5, (10), 2130-2142.
127. Springer, T. E.; Zawodzinski, T. A.; Gottesfeld, S., Polymer Electrolyte Fuel Cell Model. *Journal of The Electrochemical Society* **1991,** 138, (8), 2334-2342.
128. Chuanqing, W.; Yuhui, H.; Guangmin, C.; Guo, L.; Shulu, Z., Single-ion conducting polymeric electrolytes based on sulfonated poly(phenylene oxide). *Journal of Applied Polymer Science* **1997,** 63, (5), 559-563.

129. Kreuer, K.-D., Proton Conductivity: Materials and Applications. *Chemistry of Materials* **1996,** 8, (3), 610-641.
130. Liu, Y.; Yu, Q.; Yuan, J.; Ma, L.; Wu, Y., Brønsted acid-base polymer electrolyte membrane based on sulfonated poly(phenylene oxide) and imidazole. *European Polymer Journal* **2006,** 42, (9), 2199-2203.
131. Fu, H.; Jia, L.; Xu, J., Studies on the sulfonation of poly(phenylene oxide) (PPO) and permeation behavior of gases and water vapor through sulfonated PPO membranes. I. Sulfonation of PPO and characterization of the products. *Journal of Applied Polymer Science* **1994,** 51, (8), 1399-1404.
132. Weber, A. Z.; Newman, J., A theoretical study of membrane constraint in polymer-electrolyte fuel cells. *AIChE Journal* **2004,** 50, (12), 3215-3226.
133. Majsztrik, P. W.; Bocarsly, A. B.; Benziger, J. B., Viscoelastic Response of Nafion. Effects of Temperature and Hydration on Tensile Creep. *Macromolecules* **2008,** 41, (24), 9849-9862.
134. Solasi, R.; Zou, Y.; Huang, X.; Reifsnider, K.; Condit, D., On mechanical behavior and in-plane modeling of constrained PEM fuel cell membranes subjected to hydration and temperature cycles. *Journal of Power Sources* **2007,** 167, (2), 366-377.
135. Kusoglu, A.; Karlsson, A. M.; Santare, M. H.; Cleghorn, S.; Johnson, W. B., Mechanical response of fuel cell membranes subjected to a hygro-thermal cycle. *Journal of Power Sources* **2006,** 161, (2), 987-996.
136. Bauer, F.; Denneler, S.; Willert-Porada, M., Influence of temperature and humidity on the mechanical properties of Nafion® 117 polymer electrolyte membrane. *Journal of Polymer Science Part B: Polymer Physics* **2005,** 43, (7), 786-795.
137. Liu, W.; Ruth, K.; Rusch, G., Membrane durability in PEM fuel cells. *Journal of New Materials for Electrochemical Systems* **2001,** 4, (4), 227-232.
138. Tang, Y.; Karlsson, A. M.; Santare, M. H.; Gilbert, M.; Cleghorn, S.; Johnson, W. B., An experimental investigation of humidity and temperature effects on the mechanical properties of perfluorosulfonic acid membrane. *Materials Science and Engineering: A* **2006,** 425, (1-2), 297-304.
139. Kundu, S.; Simon, L. C.; Fowler, M.; Grot, S., Mechanical properties of Nafion(TM) electrolyte membranes under hydrated conditions. *Polymer* **2005,** 46, (25), 11707-11715.
140. Lai, Y.-H.; Mittelsteadt, C. K.; Gittleman, C. S.; Dillard, D. A., Viscoelastic Stress Model and Mechanical Characterization of Perfluorosulfonic Acid (PFSA) Polymer Electrolyte Membranes. *ASME Conference Proceedings* **2005,** 2005, (37645), 161-167.
141. Xinyu, H.; Roham, S.; Yue, Z.; Matthew, F.; Kenneth, R.; David, C.; Sergei, B.; Thomas, M., Mechanical endurance of polymer electrolyte membrane and PEM fuel cell durability. *Journal of Polymer Science Part B: Polymer Physics* **2006,** 44, (16), 2346-2357.
142. McDonald, R. C.; Mittelsteadt, C. K.; Thompson, E. L., Effects of Deep Temperature Cycling on Nafion® 112 Membranes and Membrane Electrode Assemblies. *Fuel Cells* **2004,** 4, (3), 208-213.

143. Inaba, M.; Kinumoto, T.; Kiriake, M.; Umebayashi, R.; Tasaka, A.; Ogumi, Z., Gas crossover and membrane degradation in polymer electrolyte fuel cells. *Electrochimica Acta* **2006,** 51, (26), 5746-5753.
144. Hubner, G.; Roduner, E., EPR investigation of OH radical initiated degradation reactions of sulfonated aromatics as model compounds for fuel cell proton conducting membranes. *Journal of Materials Chemistry* **1999,** 9, (2), 409-418.
145. Borup, R.; Meyers, J.; Pivovar, B.; Kim, Y. S.; Mukundan, R.; Garland, N.; Myers, D.; Wilson, M.; Garzon, F.; Wood, D.; Zelenay, P.; More, K.; Stroh, K.; Zawodzinski, T.; Boncella, J.; McGrath, J. E.; Inaba, M.; Miyatake, K.; Hori, M.; Ota, K.; Ogumi, Z.; Miyata, S.; Nishikata, A.; Siroma, Z.; Uchimoto, Y.; Yasuda, K.; Kimijima, K. I.; Iwashita, N., Scientific aspects of polymer electrolyte fuel cell durability and degradation. *Chemical Reviews* **2007,** 107, (10), 3904-3951.
146. Healy, J.; Hayden, C.; Xie, T.; Olson, K.; Waldo, R.; Brundage, M.; Gasteiger, H.; Abbott, J., Aspects of the Chemical Degradation of PFSA Ionomers used in PEM Fuel Cells. *Fuel Cells* **2005,** 5, (2), 302-308.
147. Tant, M. R.; Darst, K. P.; Lee, K. D.; Martin, C. W., Structure and properties of short-side-chain perfluorosulfonate ionomers. *ACS Symposium Series* **1989,** 395, 370-400.
148. Moore, R. B.; Martin, C. R., Morphology and chemical properties of the Dow perfluorosulfonate ionomers. *Macromolecules* **1989,** 22, (9), 3594-3599.
149. Ghielmi, A.; Vaccarono, P.; Troglia, C.; Arcella, V., Proton exchange membranes based on the short-side-chain perfluorinated ionomer. *Journal of Power Sources* **2005,** 145, (2), 108-115.
150. Rivard, L.; Pierpont, D.; Freemyer, H.; Thaler, A.; Hamrock, S. In Fuel Cell Seminar, Miami Beach, FL, 2003; Miami Beach, FL, 2003; p 73.
151. Liu, F.; Yi, B.; Xing, D.; Yu, J.; Zhang, H., Nafion/PTFE composite membranes for fuel cell applications. *Journal of Membrane Science* **2003,** 212, (1-2), 213-223.
152. Nouel, K. M.; Fedkiw, P. S., Nafion®-based composite polymer electrolyte membranes. *Electrochimica Acta* **1998,** 43, (16-17), 2381-2387.
153. Yu, T. L.; Lin, H.-L.; Shen, K.-S.; Huang, L.-N.; Chang, Y.-C.; Jung, G.-B.; Huang, J. C., Nafion/PTFE Composite Membranes for Fuel Cell Applications. *Journal of Polymer Research* **2004,** 11, (3), 217-224.
154. Liu, Y.-H.; Yi, B.; Shao, Z.-G.; Xing, D.; Zhang, H., Carbon Nanotubes Reinforced Nafion Composite Membrane for Fuel Cell Applications. *Electrochemical and Solid-State Letters* **2006,** 9, (7), A356-A359.
155. Chalkova, E.; Fedkin, M. V.; Wesolowski, D. J.; Lvov, S. N., Effect of TiO2 Surface Properties on Performance of Nafion-Based Composite Membranes in High Temperature and Low Relative Humidity PEM Fuel Cells. *Journal of The Electrochemical Society* **2005,** 152, (9), A1742-A1747.
156. Yang, C.; Costamagna, P.; Srinivasan, S.; Benziger, J.; Bocarsly, A. B., Approaches and technical challenges to high temperature operation of proton exchange membrane fuel cells. *Journal of Power Sources* **2001,** 103, (1), 1-9.
157. Fridrikh, S. V.; Yu, J. H.; Brenner, M. P.; Rutledge, G. C., Controlling the Fiber Diameter during Electrospinning. *Physical Review Letters* **2003,** 90, (14), 144502.

158. Krogman, K. C.; Lowery, J. L.; Zacharia, N. S.; Rutledge, G. C.; Hammond, P. T., Spraying asymmetry into functional membranes layer-by-layer. *Nature Materials* **2009,** 8, (6), 512-518.
159. Shin, Y. M.; Hohman, M. M.; Brenner, M. P.; Rutledge, G. C., Experimental characterization of electrospinning: the electrically forced jet and instabilities. *Polymer* **2001,** 42, (25), 09955-09967.
160. Yeo, S. C.; Eisenberg, A., Physical-Properties and Supermolecular Structure of Perfluorinated Ion-Containing (Nafion) Polymers. *Journal of Applied Polymer Science* **1977,** 21, (4), 875-898.
161. Ma, M.; Mao, Y.; Gupta, M.; Gleason, K. K.; Rutledge, G. C., Superhydrophobic Fabrics Produced by Electrospinning and Chemical Vapor Deposition. *Macromolecules* **2005,** 38, (23), 9742-9748.
162. Deen, W. M., *Analysis of Transport Phenomena*. 6th ed.; Oxford Univeristy Press: 1998.

Appendix

The Masscal G1 is the first commercial instrument for performing quartz crystal microbalance/heat conduction calorimetry (QCM/HCC). QCM/HCC provides simultaneous isothermal gravimetric and calorimetric measurements of mass change, thermal power, and viscoelastic loss of thin films exposed to gas mixtures under carefully controlled conditions.

In the Masscal G1, the mass measurement sensor is a 5.00 MHz quartz plate resonator oscillating in the transverse shear mode – often called a quartz crystal microbalance, or QCM. In the G1's normal operation, a thin solid film of sample is deposited directly on a QCM crystal plate and the plate is then placed in the sample chamber of the G1 and the system is equilibrated to the temperature selected for the experiment.

Measurements are made of the mass change, heat flow and motional resistance of the sample in real time during interaction with gases introduced through the G1 gas ports. Changes in the QCM frequency are proportional to the change in mass per unit area of the sample film, permitting high precision mass determinations. A second electrical property of the quartz resonator is also measured – the change in motional resistance, which is proportional to the loss compliance of the film. The QCM is also thermally coupled to a heat sink through a Peltier thermocouple plate in the sample chamber. Any thermal power (heat flow) generated by chemical or biological processes in the thin film on the QCM surface is detected as a voltage change by the thermocouple plate – the heat conduction calorimetry (HCC) principle.

Three quantities – mass, motional resistance, and thermal power – are measured in real time as the film is exposed to atmospheric pressure gas mixtures with varying partial pressures of adsorbing or reacting gases in a carrier gas. Data reduction yields the sorption enthalpy, the sorption isotherm, and the change in loss compliance on gas sorption for the gas/film combination, with sufficient sensitivities for detection of changes in samples as small as monolayer films.

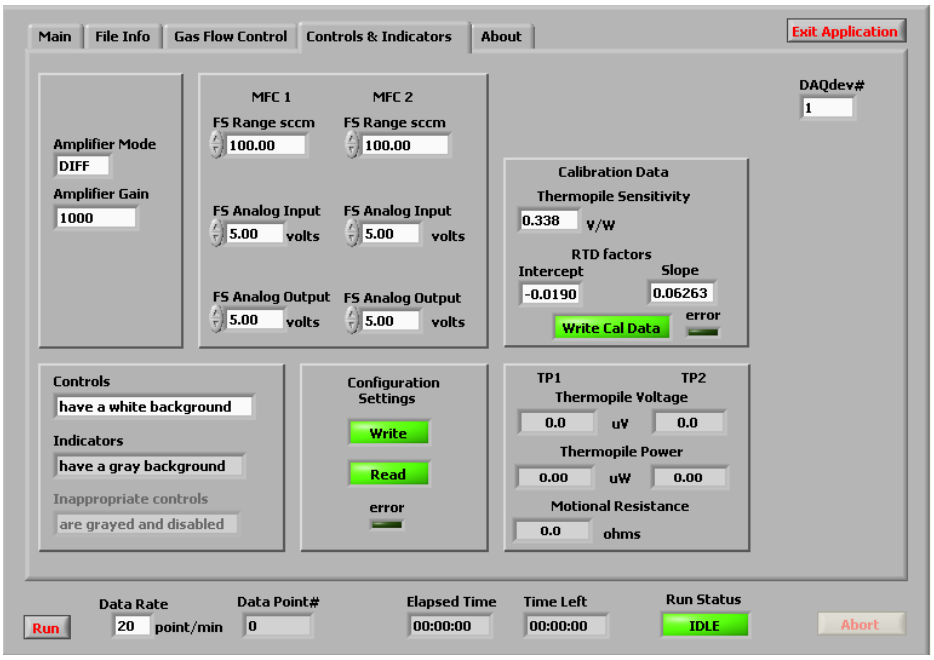

Figure A-1. Calibration settings for the Masscal G1.

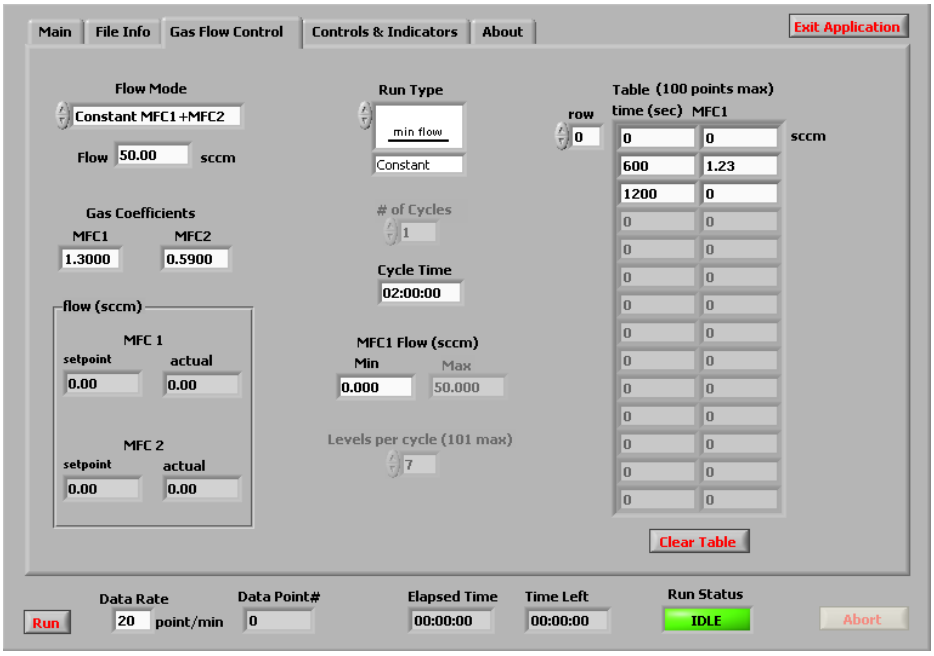

Figure A-2. Representative settings for the operation of the Masscal G1.

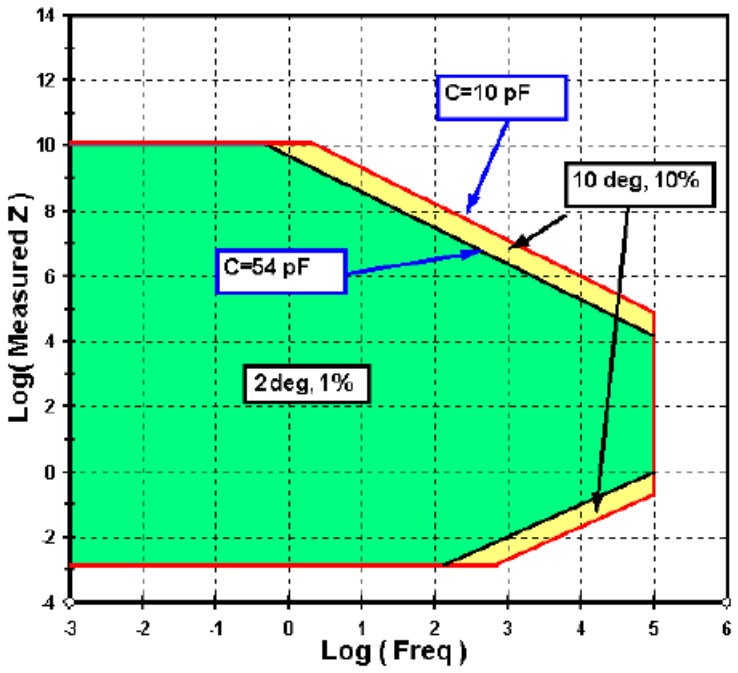

Figure A-3. Electrochemical impedance spectroscopy accuracy plot. Data points in the green shaded area have errors of less than 1%.

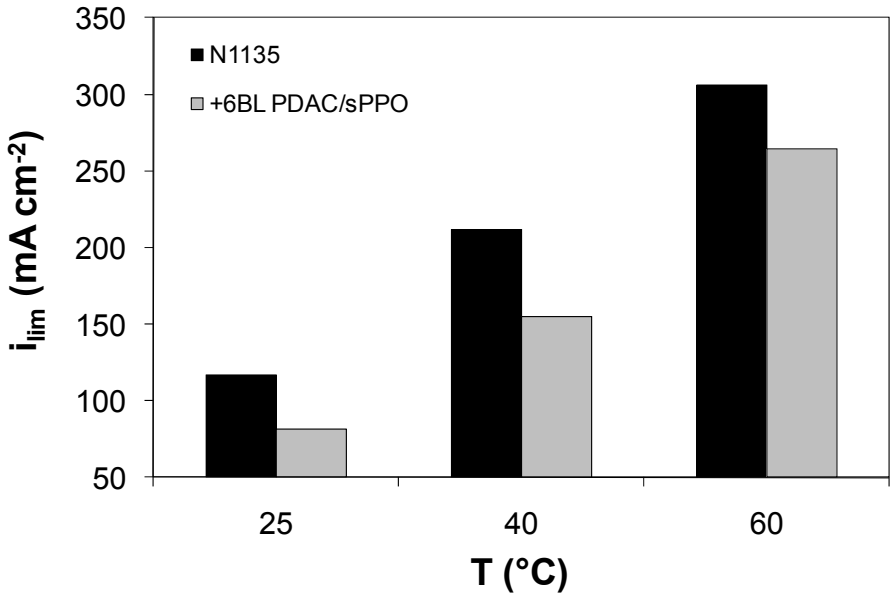

Figure A-4. An electrochemical methanol crossover technique, where pure nitrogen is fed to the cathode instead of air. The measured current is only due to methanol that reaches the cathode and gets oxidized. Coating Nafion with 6 BL of PDAC/sPPO reduces the amount of methanol that crosses the PEM.